The Impact Of Crystal Growth , Oxygenation And Microstructure On The Physics Of The Rare Earth (123) Superconductors

Thèse d'habilitation

présentée à la Faculté des Sciences de

l'Université de Genève

par

Andreas Erb

Département de Physique de la Matière Condensée

Université de Genève

Avril 1999

The Impact Of Crystal Growth , Oxygenation And Microstructure On The Physics Of The Rare Earth (123) Superconductors

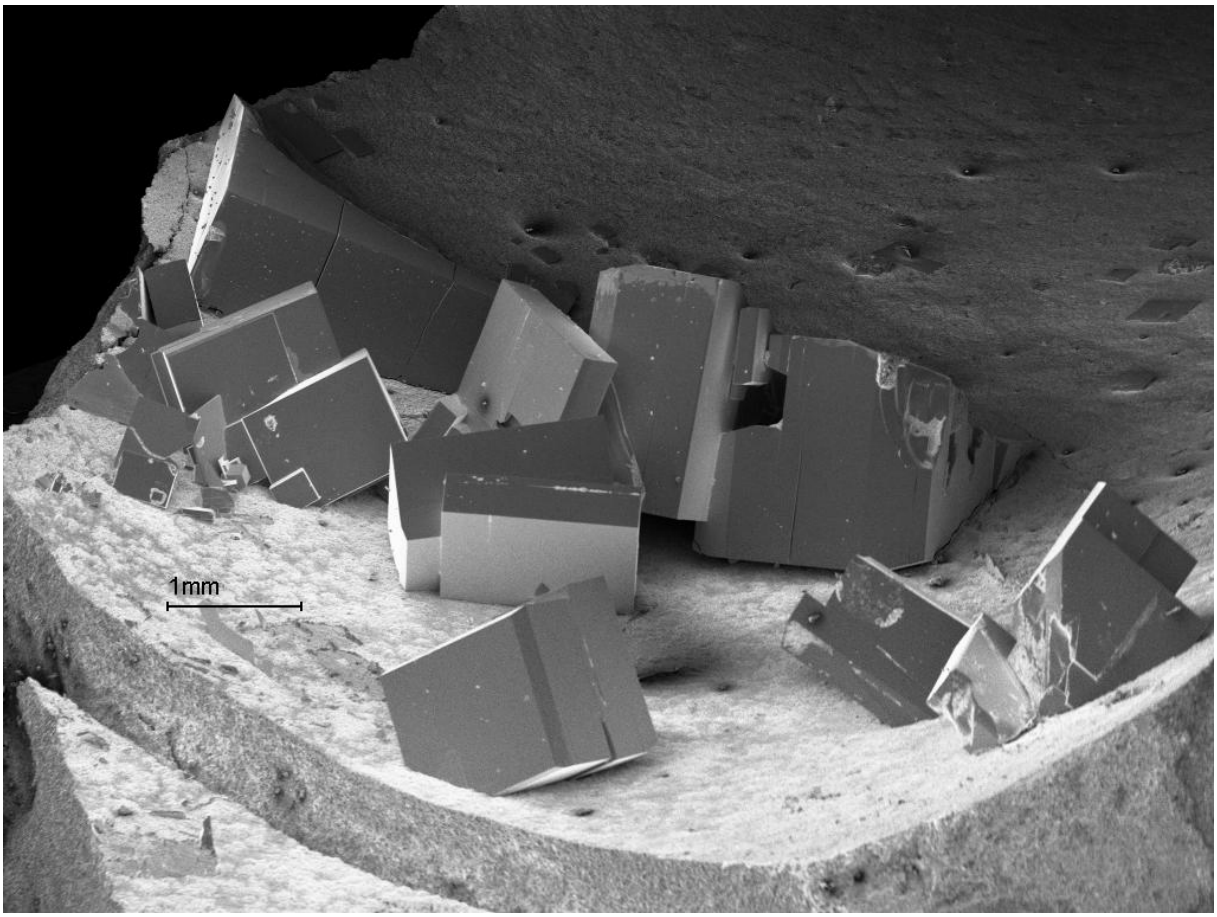

Thèse d'habilitation

présentée à la Faculté des Sciences de l'Université de Genève

par

Andreas Erb

Département de Physique de la Matière Condensée

Université de Genève

Avril 1999

In memory of
my mother

Inge Erb

(1930-1999)

Introduction

The discovery of high Tc superconductivity in the CuO related perovskite system BaLaCuO by Bednorz and Müller led to enormous efforts in many laboratories, both to find new compounds with even higher transition temperatures as well as to apply these new compounds in commercial products.

Early successes in the first direction revealed the finding of high temperature superconductivity in the YBaCuO and BiSrCaCuO system followed by the finding of high temperature superconductivity in the TlSrCaCuO and the HgBaCaCuO system, with the superconductor Hg-1223 having the highest transition temperature of 134 K to date. Table 1 gives an overview of the most important High-T_c-superconductors. The compound $YBa_2Cu_3O_{7-\delta}$, which is generally named YBCO or 123 was the first one found with a transition temperature above the boiling point of liquid nitrogen and is probably one of the most investigated compounds that do exist. The reason for this is that unlike the compounds with even higher transition temperatures it is relatively easy to synthesise and that the structure is still relatively easy to understand. Also in contrast with the other compounds it has a well defined metal stoichiometry of 123 and no or negligible substitution of the 3 different metals, which makes it the ideal subject for fundamental research. The even more suitable compound for these investigations would be the high pressure compound $YBa_2Cu_4O_8$ of the same family which also has a fixed oxygen stoichiometry, however, the preparation of such samples is only possible under high oxygen pressure.

Even though a lot of work has been already done on the 123 compound there are still or again new features in the physics of the 123 compound which were found with the availability of a new generation of high purity single crystals. As well the possible application of the 123 compound as a superconducting "wire", which came into reach with the development of the IBAD and RABBIT techniques justifies further research and major efforts since the superconducting properties and especially the robustness of the superconductivity in a magnetic field of the $YBa_2Cu_3O_{7-\delta}$ - compound are far superior to those compounds with even higher transition temperature.

It is the goal of this work to summarise the actual knowledge of this compound and to clarify some of the controversially discussed properties.

HTS-family	Stochiometry	Term	Most important representatives	T_c
123-HTS	$RBa_2Cu_3O_{7-\delta}$ R=Y, Nd, Gd, Eu, Sm, Yb, . . .	R-123, RBCO	Y-123, YBCO Nd-123, NBCO Gd-123	92 K 96 K 94 K
Bi-HTS	$Bi_mSr_2Ca_{n-1}Cu_nO_{2n+m+2}$ m=1, 2; n=1, 2, 3 . . .	Bi-m2(n-1)n, BSCCO	Bi-1212 Bi-2201 Bi-2212 Bi-2223	102 K 22 K ~ 90 K 110 K
Tl-HTS	$Tl_mBa_2Ca_{n-1}Cu_nO_{2n+m+2}$ m=1, 2; n=1, 2, 3 . . .	Tl-m2(n-1)n, TBCCO	Tl-1201 Tl-1212 Tl-1223 Tl-1234 Tl-2201 Tl-2212 Tl-2223	50 K 82 K 110 K 120 K 90 K 110 K 125 K
Hg-HTS	$Hg_mBa_2Ca_{n-1}Cu_nO_{2n+m+2}$ m=1, 2; n=1, 2, 3 . . .	Hg-m2(n-1)n	Hg-1201 Hg-1212 Hg-1223 Hg-2223 Hg-2234	97 K 128 K 134 K (164 K at 30 GPa) 45 K 114 K
Cu-HTS	$Cu_mBa_2Ca_{n-1}Cu_nO_{2n+m+2}$ m=1, 2; n=1, 2, 3 . . .	Cu-m2(n-1)n	Cu-1223 Cu-1234 Cu-2223 Cu-2234 Cu-2245	60 K 120 K 67 K 113 K < 110K
BiO-SC	$Ba_{1-x}A_xBiO_3$ A=K, Rb, Pb	BABO	BKBO BRbBO	31 K ~ 25 K

Tab. 1 Terminology and T_c values of the most important HTS

2. The Structure of the $YBa_2Cu_3O_{7-\delta}$ - compound

The basic structure of the 123 compounds consists of 3 superposed modified perovskite blocks in which the 2 copper oxide layers are imbedded. (Fig. 2.1).

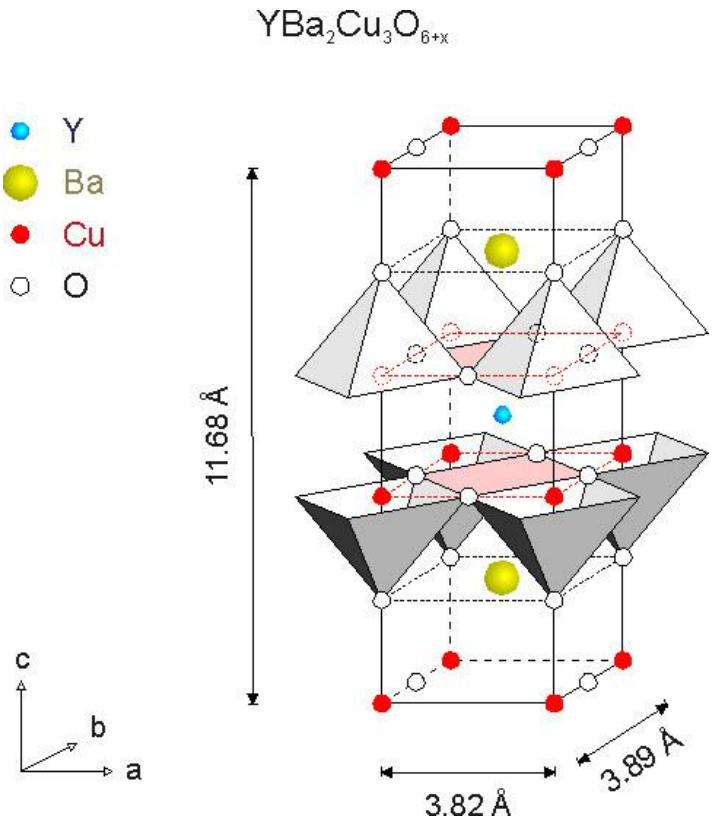

Fig.2.1 Structure of the $YBa_2Cu_3O_{7-\delta}$ - compound

Unlike these CuO- planes the basal plane only contains oxygen atoms along the b – direction of the unit cell; on the so-called O1 site ,forming CuO-chains, while in the a - direction the O5 site is unoccupied. In its fully oxygenated form $YBa_2Cu_3O_7$, as it is shown in Fig 2.1 belongs to the orthorhombic space group Pmmm with the lattice constants a,b, and c of 0.382 nm , 0.389 and 1.168 nm respectively.

However, the occupancy of this O1 site or in other words the oxygen content of the compound depends on temperature and oxygen partial pressure. In Fig 2.2 the oxygen content is given for various temperatures and oxygen partial pressures according to the calibration of Lindemer et al. [Lindemer]. Y-123 changes its equilibrium oxygen content from $\delta = 1$ for the high temperature region to $\delta = 0$ for the low temperature state. Thus, as it can be seen in Fig. 2.1

with increasing number of oxygen vacancies on the so called oxygen chain site (O1) the orthorhombic and superconducting compound $YBa_2Cu_3O_{7.0}$ transforms to the tetragonal non-superconducting compound $YBa_2Cu_3O_{6.0}$, belonging to the tetragonal space group P4/mmm. These 2 states are in fact the only well defined states from a strictly crystallographic point of view. However, normally the samples under investigation have oxygen contents which differ from the ideal states with full or zero occupation of the oxygen chain site, mainly because the maximum transition temperature is found for a oxygen concentration of 6.92, but also because relatively sophisticated techniques are required to achieve and maintain this ideal states. Hence, most investigations on the 123 compound are in fact rather performed on an alloy consisting of a mixture of unit cells of the 2 states $YBa_2Cu_3O_{6.0}$ and $YBa_2Cu_3O_{7.0}$.

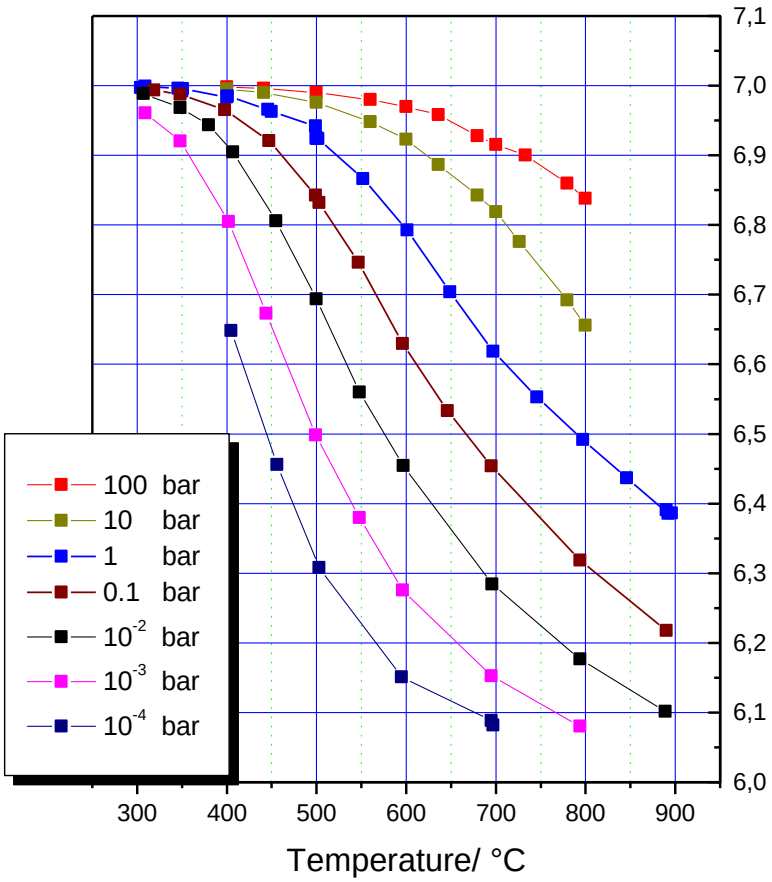

Fig. 2.2 Oxygen content of Y-123 compound as a function of the temperature and the oxygen partial pressure. After the calibration of Lindemer et al.[Lindemer]

The oxygen content determines the physical properties of the 123 compound as it can be seen in a tentative phase diagram (Fig. 2.3), representing the different physical properties of the

Y-123 compound. With oxygen contents below 6.4 the 123 compound is a non-superconductor with an antiferromagnetic ordering, reaching Neel-temperatures as high as 400 K for the state of $YBa_2Cu_3O_{6.0}$. From oxygen contents above 6.5 the Y-123 compounds exhibits superconductivity. The transition temperature depends on the oxygen content, reaching maximum transition temperatures as high as 93 K for the Y-123 and 96 K for the Nd-123 compound.

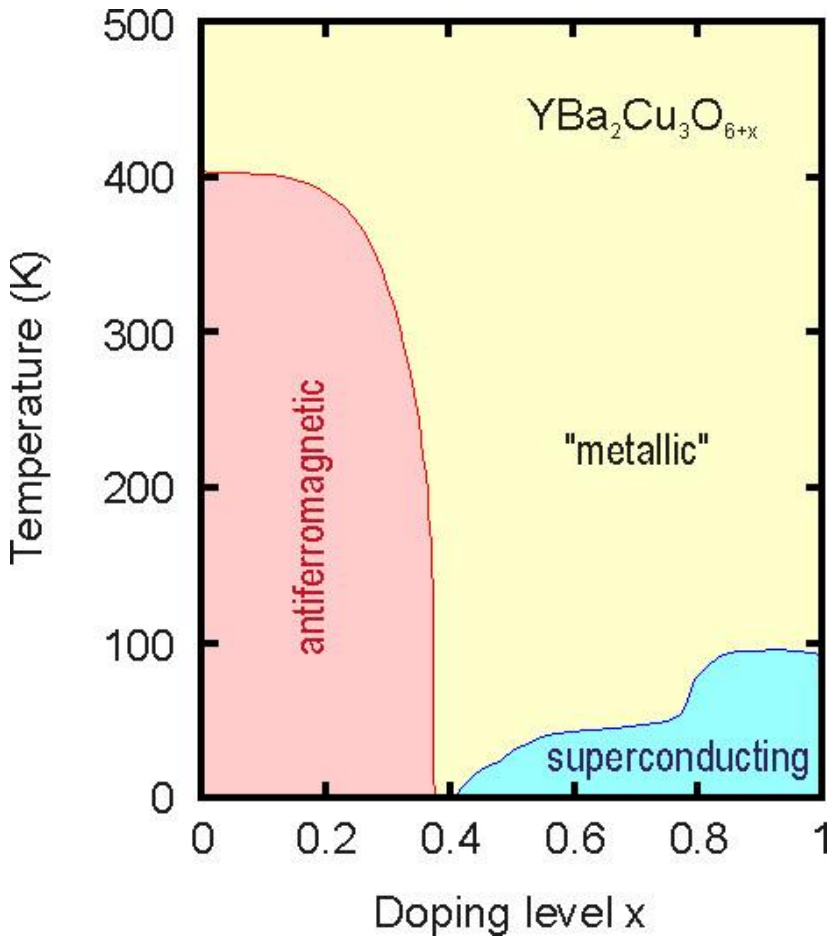

Fig. 2.3 Tentative phase diagram of the Y- 123 compound according to [Johnston]

The shape of T_c versus oxygen concentration has been explained by a model of charge transfer from the copper oxide chains to the planes according to Veal et al. [Veal]. By filling the copper chain sites the valence of the Cu(1) site, which is 2 co-ordinated in the $YBa_2Cu_3O_{6.0}$ state, changes from +1 to +2 for the 4 co-ordinated $YBa_2Cu_3O_{7.0}$ state. Depending on the co-ordination state of the 2 neighbouring Cu(1) sites, the 2 missing electrons to satisfy charge neutrality are delivered from the Cu(1) itself or, at higher oxygenation states, from the rest of

the structure. The resulting hole in the basal plane is partially transferred to the copper oxide plane, which generally is believed to host superconductivity. It has been noticed that oxygen ordering, especially the formation of long filled chain segments leading to a spatially inhomogeneous oxygen distribution, strongly influences the shape of T_c versus oxygen content. It can be already noted here that for quenched samples, where the oxygen vacancies are supposedly homogeneously distributed, the characteristic plateau at 60 K is generally not observed.

References

[Lindemer]

T. B. Lindemer, J .F. Hunley, J. E. Gates, Jr. A.L.Sutton, J. Brynestad, C. R. Hubbard and P. K. Gallagher, J. Am. Ceram. Soc., **72**, 1775 (1989)

[Johnston]

D.C. Johnston, S. Yang, A. P. Paulikas, D. W. Downey and B. W. Veal, Physica C 171 (1990) 205

[Veal]

B. W. Veal and A. P. Paulikas, Physica C 184 (1991) 321

3 Sample Preparation and Crystal Growth of the 123 Compounds

3.1 Principles of the solution growth of the 123 –compounds

Since the 123 – compounds are non congruently melting compounds, crystal growth of the these compounds can be only performed by high temperature solution growth. For this reason extensive investigations on the phase diagram were carried out and are still a subject of study. To perform crystal growth of the 123 compounds it is necessary to find a solvent in which the 123 compound can be dissolved and in which the solubility of the 123 compound is temperature dependent. Originally, it was not even clear if such a solvent exists and several more classical solvents like molten salts have been under investigation. It was, however, realised quite early that, due to the high chemical reactivity of the oxide compounds non-polluted crystals can be obtained only by a so–called self flux method, using a surplus of BaO and CuO as a starting composition. By investing the ternary phase diagram a suitable region to perform a solution growth of the 123 compounds has been found [Erb93, Erb94, ErbDiss and references therein]. Fig. 3.1 shows the simplified sketch of the composition diagram for the Y_2O_3 - BaO – CuO system.

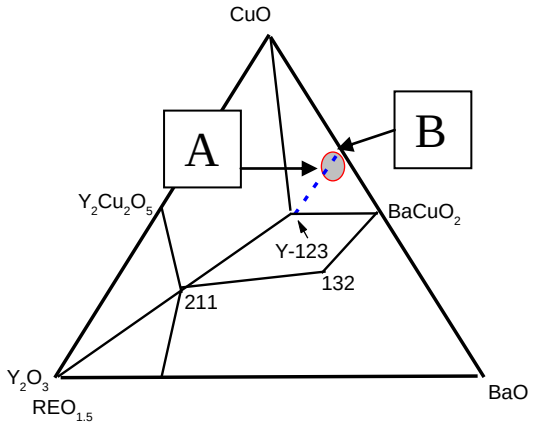

Fig. 3.1 Simplified sketch of the composition diagram for the Y_2O_3 - BaO – CuO system

In the pseudo-binary side system $BaCuO_2$ - CuO a eutectic composition has been found at molar CuO/BaO ratio of 7/3, in which about 10 weight percent Y-123 can be dissolved at a temperature of 1030 °C. Upon cooling this solution becomes over-saturated and Y-123 crystallises. Accordingly the composition of the remaining melt shifts away from the initial composition A in Fig. 3.1 into the direction of point B representing the ternary eutectic point, where all the remaining liquid solidifies. We have thus a temperature window for the crystallisation which has an upper limit given by the peritectic decomposition of the of the 123 compound (1030 °C for Y-123 in air ; somewhat different for the other RE-123 compounds) and has a lower limit due to the eutectic reaction at around 910 °C in air. Also sketched in the diagram is the approximate position of the primary crystallisation field for the 123 compounds (hatched area), in other words the composition region where the 123 compound is in thermodynamic equilibrium with the melt or, in still other words the 123 compound is the first phase to crystallise from a complete.

For the light rare earth elements like Pr, Nd, Sm and Eu the situation is more complicated. Unlike in the case of $YBa_2Cu_3O_{7-\delta}$, which has a well defined stoichiometry the light rare earth elements do form such solid solutions of the type $RE_{1+x}Ba_{2-x}Cu_3O_{7-\delta}$, due to the fact that the ionic sizes of the RE atoms increase when the atomic number decreases and become more comparable to the size of the Ba atom. Fig. 3.2 shows a schematic phase diagram explaining this situation . While for the Y and the heavier RE atoms like Er, Tm or Yb the 123 compound is a fixed point in this phase diagram the lighter RE –123 form solid solutions of the form $RE_{1+x}Ba_{2-x}Cu_3O_{7-\delta}$ so that the light rare earth 123 compounds are now represented by a line in the diagram. The value of x in this compounds can be varied either by lowering the oxygen content of the atmosphere during the synthesis [Nakamura] or by changing the ratio of BaO/CuO in the flux in a way that the 1:2:3 ratio for the compound can be retained [Yao]. Both methods are somewhat equivalent since lowering the oxygen content leads to a partial reduction of CuO to Cu_2O, thus changing the BaO/CuO ratio. Lowering the oxygen partial pressure, however, has the disadvantage that one changes not only the x value of the resulting compound but also the present phases in the diagram. While the phase diagram is in the meantime relatively well known for ambient oxygen partial pressure, little is known about the

phase relationships for oxygen partial pressures as low 0.001 bar, which have been reported [Zhou, Oka, Zou] to be necessary during synthesis of stoichiometric light rare earth –123 crystals (LRE-123). It is clear that in low oxygen partial pressures CuO at least partially transforms into CuO_2, that $BaCu_2O_2$ is present for such pressures rather than $BaCuO_2$ and that other new phases like, in the case of Pr-123, $PrBaO_3$ form. Nevertheless, the reduction of the oxygen partial pressure leads to a reduction of the x value in the RE –123, as it is sketched by the red lines in Fig. 3.2.

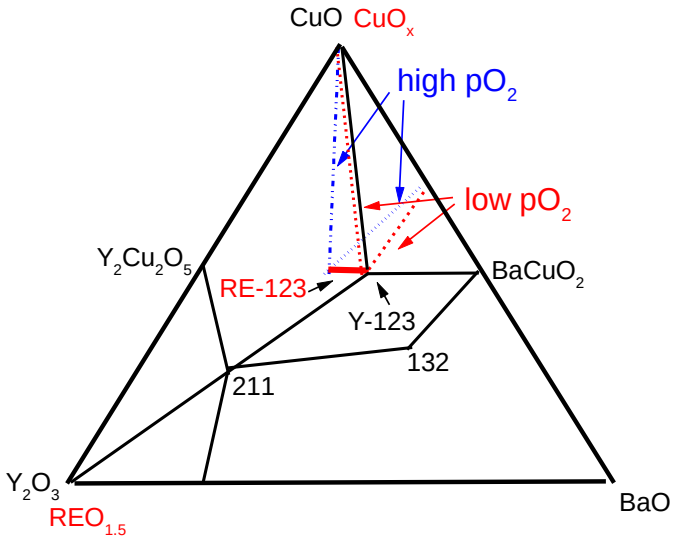

Fig. 3.2 Schematic composition diagram for the Light rare earth 123 compounds

The usual procedure for the solution growth of 123 compounds, besides the somewhat altered temperature and concentration regime can be described as follows :

The eutectic composition of the $BaCuO_2$ – CuO system is used as a solvent for the 123 compound. According to the phase diagram appropriate amounts of the 123 compound are mixed with the flux and then melted at a temperature about 5 °C below the peritectic decomposition of the 123 phase. After reaching a complete melt the temperature is lowered at a rate between 0.5 –2 K/h. Upon this cooling the solution becomes over- saturated and spontaneous crystallisation occurs. The slow rate of crystallisation of the 123 compound is

due to the very low solubility of 123 in the eutectic $BaCuO_2$ – CuO mixture and the relatively slow diffusion of the solute to the growing interface of the crystal. To increase the transport of the solute to the growing crystal the application of a temperature gradient is helpful, since it improves the transport of the solute to the growing interface of the crystal by enhanced convection. On the other hand, since the crystal growth of the 123 compounds is a solution growth the application of a temperature gradient over the crucible avoids constitutional supercooling [e.g. Gilman], which would result in flux inclusions and hence poorer crystal quality. To do so an air cooled alumina rod was brought in contact with one of the crucible walls, as it is shown in Fig. 3.3.

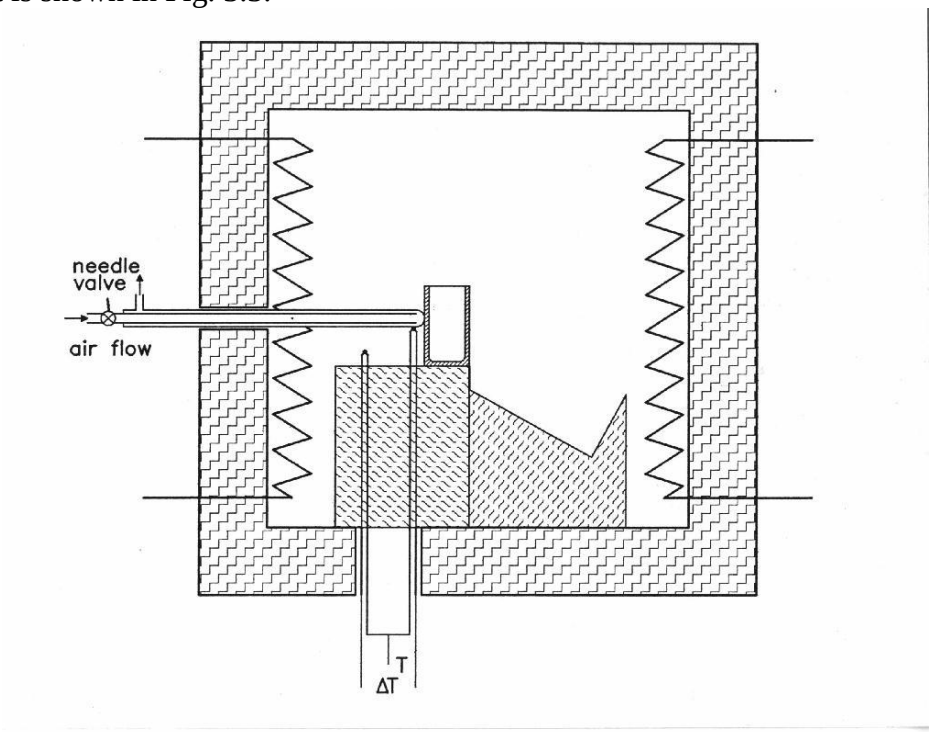

Fig. 3.3 Schematic drawing of the furnace used for crystal growth of the 123 - compounds

With this set-up a gradient of 5-10 K was applied over the crucible width of 22 mm as soon as the temperature was lowered to initiate the crystal growth. The temperature and the temperature gradient was measured with two thermocouples and could simply be adjusted by different airflow with the help of a needle valve.

For the growth of Y-123 single crystals the procedure is as follows: After melting and application of the gradient the batch was cooled down at a rate of 10 °C/h to 1005 °C, in order to reach the necessary supercooling to initiate growth and at rates between

0.3 and 0.7 °C/h to 950 °C during the crystal growth. At 950 °C the remaining flux was decanted inside the furnace, after which the furnace was cooled in about 1 hour to room temperature. Note, that for the other rare earth compounds the given temperatures are somewhat different.

For detailed temperature programs and starting concentrations see [Erb93,Erb94, ErbDiss] and the references therein.

3.2 Crucibles – the main problem !

The melts of the high temperature superconductors are chemically extremely reactive and it has been realised relatively early that no really inert crucible material existed among the commercially available refractory materials or the also commonly used noble metals.

This non-existence of an inert crucible to handle the highly reactive oxide melts was the main problem in the growth of single crystals of the oxide superconductors, preventing first the reproducible growth of crystals of several millimetres without impurities, and secondly preventing the exact determination of the phase diagram of these systems, which would be an essential tool for the use of more developed crystal growth techniques. This was the reason for searching less reactive or inert crucibles [Schneemeyer, Scheel, Dembinski, Tatarchenko, Gagnon, Berkowski, Barilo]. All conventional crucible materials, namely Al_2O_3, SnO_2, MgO, Au, Pt, ThO_2, Y_2O_3, but also the ZrO_2 crucibles, stabilised with CaO or Y_2O_3, react with the commonly used mixture of $BaCuO_2$ - CuO [Erb93], which is used as solvent for the crystal growth experiments. Table 1 gives some values for the contamination of the melt and the crystals for different crucible materials.

Crucible	**Crystals**	**impurities in the melt**	**impurities in the crystals**
Al_2O_3	*YBCO* *PBCO*	*up to 5 weight % Al* *up to 5 weight % Al*	*up to 5 at. % Al* *up to 5 at. % Al*
Gold	*YBCO*	*?*	*up to 1.5 at % Au*
SnO_2	*YBCO*	*up to 8 weight % Sn + traces of Si*	*2-4 at. % Si*
MgO	*YBCO*	*?*	*1 atomic % Mg*
FZY	*YBCO* *PBCO*	*Zr not detectable in the vol.* *Y disolved from crucible*	*Mg, Zn, Al, Fe, Mn, Ti,* *between 0.07 and 0.14 at. %* *+ up to 3 at % Y*

Tabl. 3.1 Typical impurity values of melt and single crystals for different crucible materials. Values taken from Ref. [Erb97, Erbdiss and references therein]

This corrosion takes place in all crucibles and has two effects:

1) Firstly the corrosion leads to a shift of the original composition of the melt. This shift in the composition can be strong enough to leave the appropriate primary crystallisation field of the desired phase. The shift of composition leads to a time limitation for crystallisation: this means that, the size of the single crystals is limited for a given growth rate. This shift depends on the material of the crucible, and even for the same crucible material it depends on its quality, which differs between crucibles obtained from different manufacturers. Since the shift in composition of the melt is normally not controlled and is anyway difficult to control, the crystal growth of the oxide superconductors was still in a state of trial and error and the

growth process had to be optimised with respect to the crucible used in the experiment. The Fig . 3.4 shows a typical result of crystal growth using Y-stabilised ZrO_2 crucibles.

Fig. 3.4 Broken ZrO_2 crucible after crystal growth experiment. Some crystals are visible (arrow), partly embedded in the flux, which have to be "mined" out mechanically

Even though there have been some remarkable success [Erb94, Wolf, Takei, Asoka, Liang] in single crystal growth by using these crucibles, the results suffer, however, from the lack of the exact knowledge of the phase diagram of the corresponding system, which of course can not be determined exactly without an inert crucible material. A comparison of the phase diagrams published for the system $BaCuO_2$ - CuO up to now [Erb93, Erb94, ErbDiss, Oka, Kawabata, Maeda, Zhang, Osamura, Aselage, Abbattista, Licci] leads to contradicting conclusions. The reason for this is that they were determined under different conditions, for example using different crucible materials or various atmospheres.

2) Secondly the corrosion of the crucible has a strong influence on the physical properties of the obtained crystals. As it can be seen in Table 1, the elements of the crucible can normally be detected in the crystals, some of them changing the physical properties of the single crystals over a wide range. Up to the development of a truly non reactive container material, the ″best″ crystals of $YBa_2Cu_3O_{7-\delta}$ have normally been obtained in ZrO_2 - crucibles (Y_2O_3 stabilised). The induced impurities in this case are Zr and also Y but also other metals (

typically Al, Ti, Si, Mg, Zn) deliberately added in commercially available crucibles of FZY-oxide by the manufacturer as sintering aids. These additives are normally not mentioned by the supplier, because in most cases these additions are part of the production secret of the ceramic industry. However, when working with such corrosive melts like in the case of crystal growth of the 123 compounds, these additives may also be incorporated in the grown crystal, altering the physical properties. Thus, nearly all measurements are performed on samples containing an unknown amount of impurities.

Since the Y in FZY-crucibles is already part of the desired compound it has no effect on the crystal quality of $YBa_2Cu_3O_{7-\delta}$. However, it plays a role when other 123 - compounds are grown, for example $ErBa_2Cu_3O_{7-\delta}$, $GdBa_2Cu_3O_{7-\delta}$, or $PrBa_2Cu_3O_{7-\delta}$. The crystals obtained in such growth experiments always contain some Y and should therefore be referred to as $RE_{1-x}Y_x Ba_2Cu_3O_{7-\delta}$ (RE = Er, Gd, Pr).

The impurity Zr firstly does not fit the lattice of $YBa_2Cu_3O_{7-\delta}$ and is therefore not incorporated in the crystals in a detectable amount. In addition Zr forms the solid compound $BaZrO_3$, which is not longer reactive with the flux. However this process changes the composition of the melt, leading to the problems mentioned above.

Even the use of Y_2O_3-crucibles for the growth of $YBa_2Cu_3O_{7-\delta}$ does not solve the problem of shifting in composition, beside the difficulties which arise from sintering additives Here especially Ti). Such crucibles, which are very expensive and additionally not tight [Karpinski, Tagami] to the used flux, have been used in liquid phase epitaxy (LPE) [Klemenz, Dubs] and Top Seeded Solution Growth (TSSG) [Yamada] of the 123 compounds. In such growth experiments the melt is permanently saturated with Y, while the composition of the residual melt changes due to the crystallisation of 123. Such growth experiments should therefore not be referred to as being controlled, but optimised crystal growth experiments - since the shift in the composition of the remaining flux is simply not controlled.

Since many experiments are performed on poorly or not characterised samples this circumstance leads to the fact that some results of physical measurements reported in literature for the same material - but measured on crystals of different source - contradict each other. A good example for this is the compound $PrBa_2Cu_3O_{7-\delta}$, the behaviour of which is reported in literature in a contradicting way. Some authors claim that $PrBa_2Cu_3O_{7-\delta}$ remains

tetragonal after oxygenation [Moran,LiangJ], while most of the others observe the well known twinning as it is typical for all the 123 compounds. For a long time $PrBa_2Cu_3O_{7-\delta}$, has been believed to be an intrinsic non-superconductor but recently several reports of superconductivity in this compound have been found in literature. The answer lies within the different kind of impurities and in different disorder mechanisms in these crystals, which will be discussed in a later chapter.

3.3 . A new approach – development of a adapted crucible material

The development of an inert crucible material followed the detailed studies of the corrosion reactions during crystal growth in ZrO_2 (Y-stabilised) [Erbdiss]. As mentioned already above $YBa_2Cu_3O_{7-\delta}$ crystals of the best quality were obtained from ZrO_2 crucibles, which have to be stabilised with 5-15 % Y_2O_3 in order to suppress the crystallographic phase transition of ZrO_2. These crucibles are also corroded by the highly reactive melts used as solvents, but in contrast to most of the other crucible materials like Al_2O_3 or Gold the container material is not dissolved in the melt but rather forms a solid corrosion product as it can be illustrated in Fig. 3.5. This corrosion product is $BaZrO_3$, which is solid in the temperature region around 1000 °C where the crystallisation of the 123 crystals takes place. $BaZrO_3$ forms near the crucible walls in a solid layer the thickness of which is increasing with time, overgrowing already grown $YBa_2Cu_3O_{7-\delta}$ - crystals which are therefore lost. Depending of the quality of the ZrO_2 ceramics, this layer of $BaZrO_3$ can reach up to several millimetres in thickness. It normally has a sharp interface to the uncontaminated melt. The sharp interface between $BaZrO_3$ and uncontaminated melt of course means that $BaZrO_3$ has only a very small solubility in the liquid and that $BaZrO_3$ is solid in the temperature region of 1000 °C. A solid compound with very small solubility, however, is the ideal crucible material. That this compound, but also the isomorphic compounds $BaHfO_3$, $SrZrO_3$, $BaSnO_3$, mixtures thereof and many others, could be promising crucible materials was already suggested in some reports [e.g. Taylor, Zhang2], but no attempts making crucibles of this compounds have been reported at the time.

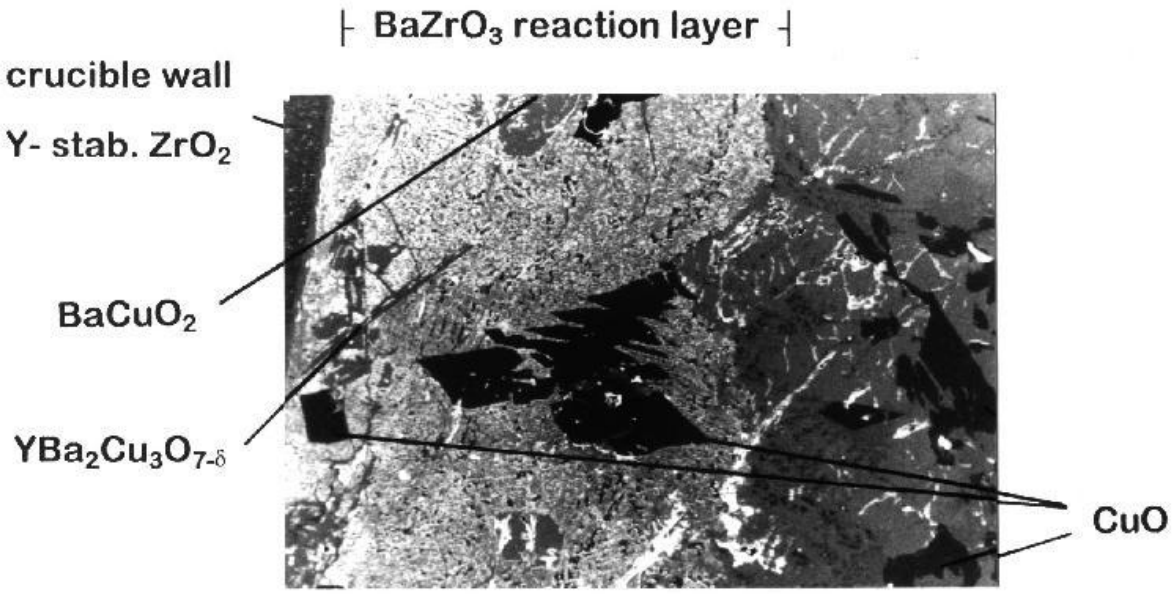

Fig 3.5 SEM – picture of the crucible corrosion in ZrO_2 – (Y stab.) with sharp interface in between the $BaZrO_3$ corrosion layer and the uncontaminated melt (right) [ErbDiss]

.

3.3.1 The compound $BaZrO_3$

$BaZrO_3$ has a cubic perovskite structure with a lattice constant of 0.419 nm and a high density of 6.242 g/cm^3. The powder of $BaZrO_3$ can be produced relatively easily by solid state reaction of well mixed $BaCO_3$ and ZrO_2 in air at a temperature of 1200 °C as one can see from Fig. 3.6. This Figure shows the heating of a mixture of $BaCO_3$ and ZrO_2 in DTA. There are 2 thermal peaks which can be detected upon heating. The first one at around 780 °C is due to a crystallographic phase transition of the $BaCO_3$ compound. The second one around 900 °C originates from the chemical reaction of $BaCO_3 + ZrO_2 \rightarrow BaZrO_3 + CO_2 \nearrow$. The peak at 780 °C has a strong thermal signature can actually be used to check the phase purity of the resulting $BaZrO_3$. For the use of a ceramic compound as a crucible material it is essential that the compound shows no crystallographic phase transitions in the temperature region of interest. This is in fact the case for $BaZrO_3$ as it can be seen from Fig. 3.7.

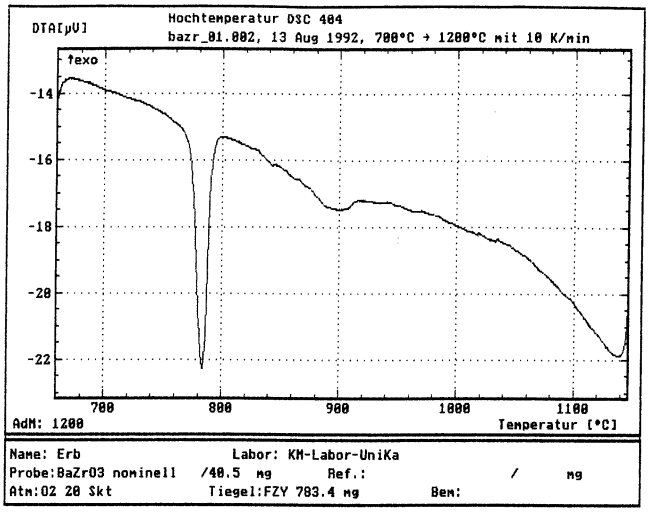

Fig.3.6 Differential thermal analysis of a mixture of $BaCO_3$ and ZrO_2. The peak at 780 °C is due to a crystallographic phase transition of $BaCO_3$, The one at 900 °C is due to formation of $BaZrO_3$

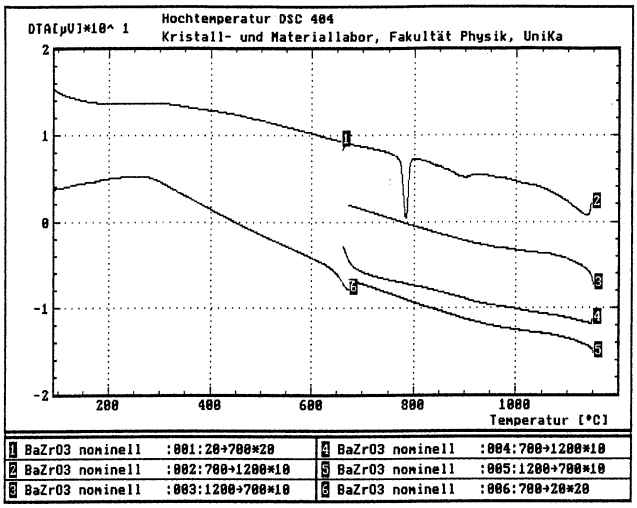

Fig.3.7 Differential thermal analysis of a mixture of $BaCO_3$ and ZrO_2. The peak at 780 °C is due to a crystallographic phase transition of $BaCO_3$, the one at 900 °C is due to formation of $BaZrO_3$. Once the $BaZrO_3$ compound is formed no crystallographic phase transitions occur upon further thermal cycling

Since $BaZrO_3$ is a binary ceramics it is extremely important to obtain the exact stoichometry for the compound because any deviation from the stoichometric composition will lead to precipitation of the off-stoichometric surplus at the grain boundaries of the ceramics. When

then used with the highly corrosive melts of th high T_c superconductors then corrosion can take place along such precipitations on grain boundaries. Furthermore a precipitation of ZrO_2 would lead to breaking of the ceramic piece upon thermal cycling, firstly because of the crystallographic phase transition of the ZrO_2 and secondly because of the higher thermal expansion coefficient of ZrO_2 when compared to that of $BaZrO_3$.

To obtain single phase powder of $BaZrO_3$ the mixtures of $BaCO_3$ and ZrO_2 where prepared by 3 repeated firings at 1250, 1300 and 1300 °C respectively. Intermediate ball milling using a ZrO_2 ball mill was applied to homogenise the powder. Phase purity was checked by X-ray powder diffraction and was found to be better than the detection limit for this method after the second calcination step. An even better control of phase purity is offered by the measurement of the weight loss, due to the loss of CO_2 during reaction. The theoretical weight loss is usually obtained after the third reaction.

The grain size is a very important parameter during sintering of the ceramics: it was found that it is necessary to obtain powders with an average grain size of about 0.5 μm with no grains above 1 μm. The final ball milling was performed for at least 24 hours in a ZrO_2 ball mill. The grain size was checked with the help of a laser granulometer (HR 850 Cilas) To obtain grains fine enough we had to add an organic milling aid (3-5 weight % stearic acid) during the final ball milling, which has to be burned off prior to the form shaping process. An alternative method, which avoids the organic milling aids is wet milling in alcohol, which is not only quicker but also avoids the firing at 900 °C to remove the milling aid. In that case only the alcohol needs to be evaporated.

After removal of the milling aid or alcohol the resulting lumps were sieved to obtain a free flowing powder consisting of agglomerates (< 0.5 mm) of the single grains, which have grain sizes around 0.5 μm.

The form shaping process was done by Cold Isostatic Pressing (CIP) of the fully reacted powders at a pressure of about 3-4 kbar. After cold isostatic pressing one obtains the so-called green forms of the crucibles (white crucibles in Fig. 3.8)

Fig. 3.8 $BaZrO_3$ -crucibles: "Green" forms before sintering (white crucibles) and sintered crucibles (dark green)

Since $BaZrO_3$ has a very high melting point of about 2600°C the sintering process has to be performed at very high temperatures of around 1700 °C in air. To further increase the sinter activity the initial grain size of the powder plays an important role. In general the sintering process should not last too long (in the order of 4-6 hours) to allow a good connectivity of the single grains without extended grain growth, which would be detrimental to the thermal shock stability of the ceramic piece. An optimisation of the 3 basic parameters, namely initial grain size, sintering temperature and sintering time led to the following procedure.

With an initial grain size of around 0.35 μm the sintering process can be carried out in air at 1730 °C for 4 h. After this sintering process the ceramic pieces have densities of up to 99 % of the theoretical value. The final ceramic piece has an average grain size of around 2-5 μm, providing excellent thermal shock resistance and good connection in between the single grains. Fig 3.9 shows a crucible wall after a growth experiment of $YBa_2Cu_3O_x$ were single grains can be observed along with a $YBa_2Cu_3O_x$ single crystal grown in that experiment.

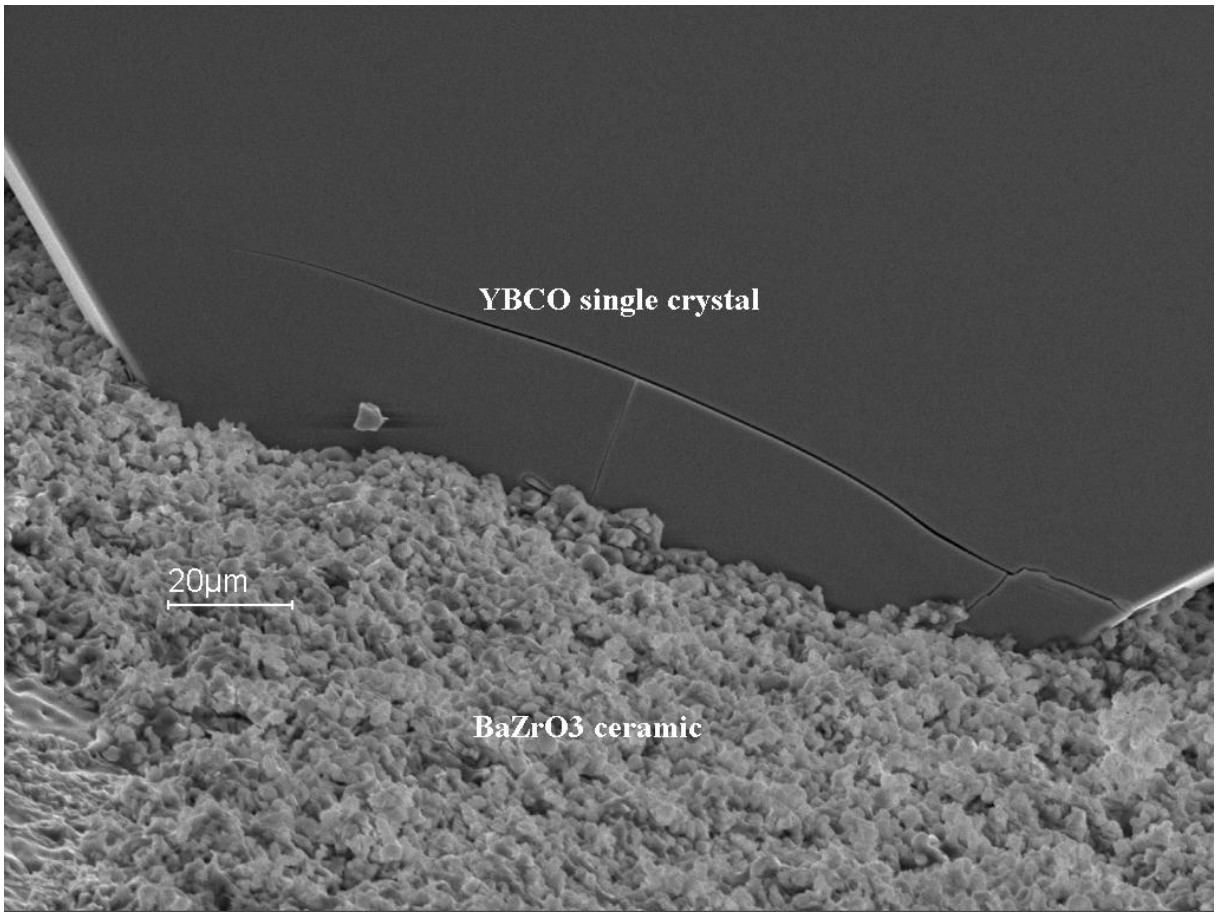

Fig 3.9 $BaZrO_3$ crucible wall after a growth experiment of $YBa_2Cu_3O_x$. Single ceramic grains can be observed along with a $YBa_2Cu_3O_x$ single crystal grown in that experiment.

3.4 Crystal Growth of $YBa_2Cu_3O_{7-\delta}$ and $HREBa_2Cu_3O_{7-\delta}$ in $BaZrO_3$ crucibles (HRE = Heavy Rare Earth like Er, Dy)

The crystal growth process was done in the widely used way, using as a flux the eutectic composition, of the $BaCuO_2$ - CuO phase diagram [Erb93] (see Fig. 3.1).

The concentration of the prereacted $YBa_2Cu_3O_{7-\delta}$ and $HREBa_2Cu_3O_{7-\delta}$ to the prereacted flux was 10 weight % for both $YBa_2Cu_3O_{7-\delta}$ and $HREBa_2Cu_3O_{7-\delta}$. Flux and $HREBa_2Cu_3O_{7-\delta}$ powders were well mixed and pressed into the crucibles with a volume 7.5 cm^3 (Smallest crucible size). The total weight of the batch prior to melting was about 18 g. The crucible was covered with a lid of $BaZrO_3$, placed in a a chamber furnace (Nabertherm,Lilienthal-Bremen, Germany) and held at 1030°C for 10-20 hours in air. Complete melting was checked by direct observation of the melt.

The furnace we used can be heated on 5 sides and the wiring has been done in a way that temperature gradients can be applied, to produce a temperature field suitable for the solution growth.

After melting the batch was cooled down at a rate of 10 °C/h to 1005 °C and at a rate of 0.5 °C/h to 950 °C. At 950 °C the remaining flux was decanted inside the furnace. After decanting the furnace was cooled in about 1 hour to room temperature. In marked contrast to the melts obtained during decanting when ZrO_2 crucibles are used, the melts in $BaZrO_3$ crucibles show much lower viscosity. This lower viscosity may lead to a faster transport to the growing interface and therefore to higher growth rates in this new crucibles.

In contrast with the ZrO_2 crucibles (Fig.3.4) there is neither a reaction layer, nor remaining flux on the walls of the crucible after decanting as it can be seen in Fig. 3.10. Another big difference is that the separation of crystals and flux is almost complete. The crystals were only slightly attached to the crucible walls and could thus be extracted very easily.

With an ingot of 1.8 g a total mass of 1g single crystalline $YBa_2Cu_3O_{7-\delta}$ can be obtained. This corresponds to an unusually high ratio of output : ingot in the growth of $YBa_2Cu_3O_{7-\delta}$. Since the separation of flux and crystals happened at a temperature about 40 °C above the eutectic one [Erb93], the remaining 0.8 g $YBa_2Cu_3O_{7-\delta}$ was still dissolved in the flux.

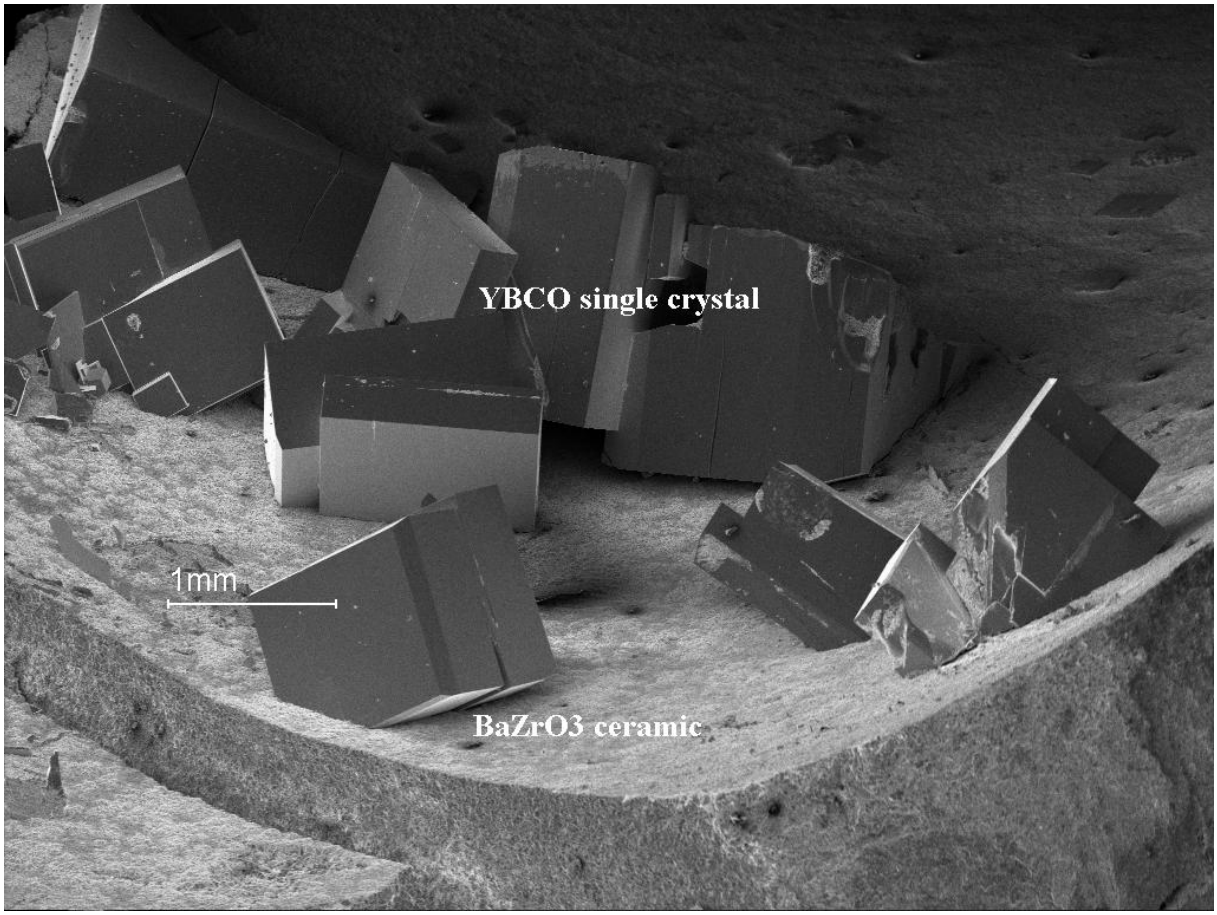

Fig. 3.10 Piece of a broken $BaZrO_3$ crucible with some $YBa_2Cu_3O_{7-\delta}$ single crystals slightly attached to the crucible wall, proving excellent flux separation and non-reactivity of the crucible with the flux.

As seen in Fig. 3.10 the crystals obtained in such a growth experiment have (a,b,c) dimensions of up to 2 x 2 x 1 mm^3, which is a good value for the applied cooling rate of 0.7 K/h in this experiment, especially for the c direction. The reason for this relatively large crystals may be the lower viscosity of the melt, when compared to that obtained in ZrO_2 crucibles, which was already mentioned above. Fig. 3.10 proves not only the excellent surface morphology and flux separation, but also the lack of reactivity of the melt with the container material. Perhaps most remarkable when comparing the crystals grown in $BaZrO_3$ with those obtained from ZrO_2 crucibles is the state of the surface. As already seen in Fig. 3.9 the surfaces of the crystals are extremely clean and show no traces of remaining flux attached to

them. This again is due to the low viscosity of the melt allowing better flux separation during decanting.

3.5 Crystal Growth of and $LREBa_2Cu_3O_{7-\delta}$ in $BaZrO_3$ crucibles (LRE = Light Rare Earth like Eu, Sm, Nd, Pr)

As mentioned in a earlier chapter the light rare earth 123 compounds do not exhibit a well defined stoichiometry of 1:2.3 in all cases but form solid solutions of the type $RE_{1+x}Ba_{2-x}Cu_3O_{7-\delta}$ due to the fact that the ionic size of the RE atoms increases when the atomic number decreases and becomes more comparable to the Ba atom. It has been reported that the value of x in this compounds can be varied either by lowering the oxygen content of the atmosphere during the synthesis [Nakamura] or by changing the ratio of BaO/CuO in the flux in a way that the 123 ratio for the compound can be retained [Yao]. As mentioned before, both methods are somewhat equivalent since lowering the oxygen content leads to a partial reduction of CuO to Cu_2O, so that both methods result in a nominal increase of the BaO/CuO ratio. This, however, has the disadvantage that one changes also the phase diagram and especially the primary crystallisation fields. Thus, parasitic phases can be formed, e.g. $BaCuO_2$ and for strongly reduced oxygen partial pressures other new phases like, in the case of Pr-123, $PrBaO_3$. A departure from the primary crystallisation field of the $LREBa_2Cu_3O_{7-\delta}$ can sometimes lead to well crystallised phases like the $BaCuO_2$ single crystal shown in Fig. 3.11, which was obtained as a side product during the crystallisation of Nd-123 using a BaO rich solvent. Some of these additional compounds which crystallise in the same temperature window lead to nucleation of the desired 123- compounds or they produce intergrowth with these compounds making the crystal growth less effective compared with the heavier rare earth 123-compounds or $YBa_2Cu_3O_{7-\delta}$. In general crystals of the light rare earth compounds tend to grow in a more 3-dimensional manner, while the Y- 123 crystals normally form platelets with aspect ratios of 10:1 for the a,b:c directions.

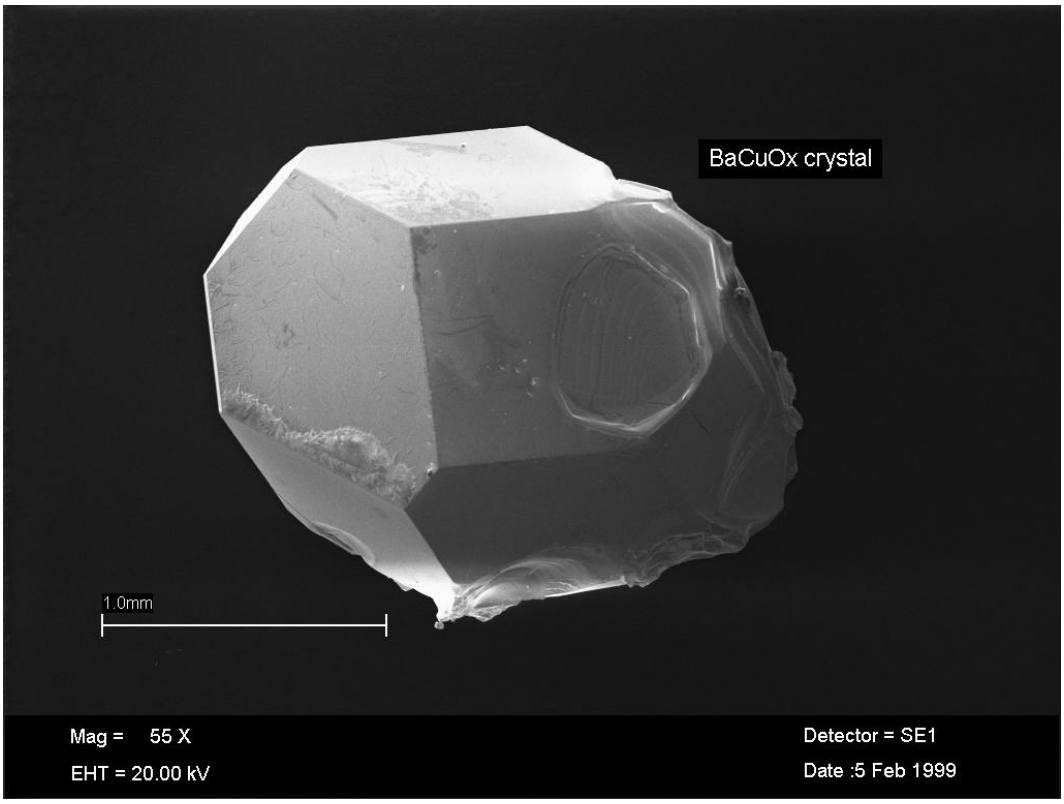

Fig. 3.11 Single crystal of $BaCuO_2$ which was obtained as a side product during the crystallisation of Nd-123 using a BaO rich solvent

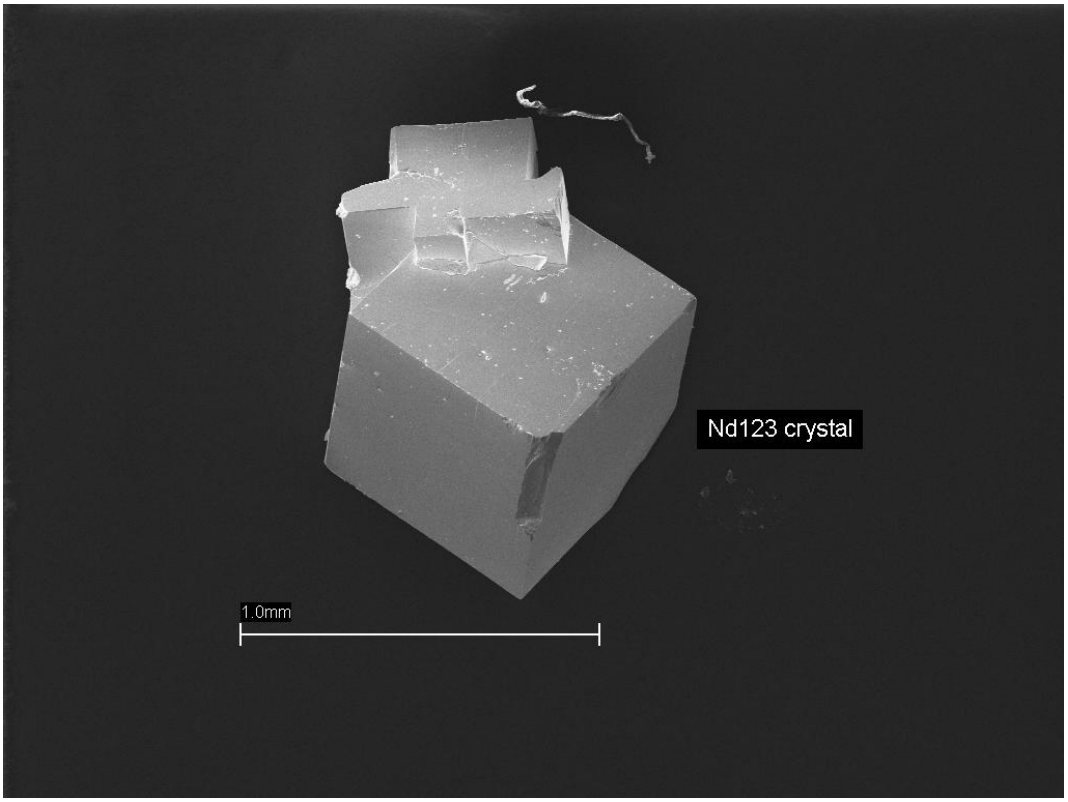

Fig. 3.12 Inter-growth of 2 single crystal of $NdBa_2Cu_3O_{7-\delta}$

3.6 Sample characterisation and results in experiments on $REBa_2Cu_3O_{7-\delta}$ single crystals

Chemical analysis of the samples was done with the help of an EDX (Tracor Northern Micro-Z II) mounted into a scanning electron microscope (Stereoscan 360 , Cambridge Instruments) and showed no detectable Zr contamination of the crystals. Wet chemical analysis (ICP-MS, Mikroanalytisches Labor Pascher, Remagen-Bandorf, Germany) was done and showed Zr impurities between 0.0005 (detection limit) and 0.001 at %, which is in fact consistent with the purity of the starting materials (5N). Further impurities are Sr and La both with values of about 0.0005 - 0.001 at % . Impurities of other elements where found to be below their detection limits. This means that the purity of the single crystals has been increased by 1 –2 orders of magnitude with respect to the formerly cleanest crystals obtained from Y – stabilised ZrO_2 crucibles (see also Tab. 3.1)

Since the crystals were cooled to room temperature in about one hour after growth, they had to be annealed in oxygen in order to reach the desired oxygen content and hence exibit the superconducting transition.

All heat treatments were performed in pure oxygen (purity 99.998 %) at temperatures between 400 and 700 °C and oxygen partial pressures between 1 and 100 bar. The standard annealing was carried out in pure flowing oxygen for 1-2 weeks at the different annealing temperatures between 450 and 600 °C, followed by quenching to room temperature.

The superconducting transition temperature T_c of the $REBa_2Cu_3O_{7-\delta}$ crystals was measured inductively and was found to depend on the annealing temperature during the oxygenation and thus from the oxygen content according to the calibration of Lindemer et al. [Lindemer]. In addition, a strong difference was found between the crystals of $YBa_2Cu_3O_{7-\delta}$ and the light rare earth 123 compounds like Eu –123 and Nd-123 as it can be seen in Fig 3.13. The bell shaped curve for the dependence of T_c versus δ was already reported by Claus et al. [Claus] on single crystals of $YBa_2Cu_3O_{7-\delta}$ grown in Y-stabilised ZrO_2. Compared to those crystals used by Claus et al. [Claus] the annealing temperature to obtain the highest T_c was shifted to somewhat higher temperatures and the absolute value of the T_c maximum was about 1 K higher for crystals from $BaZrO_3$ crucibles. This fact can be explained with the lower purity of

the crystals used by Claus et al. [Claus]. The reasons for this lower purity are firstly the starting materials (99 %) and secondly the fact that the crucibles (Y-stabilised ZrO_2, Friatec Mannheim, FRG) used for these experiments [Erb94] contain a considerable amount (≈3 weight %) of Al, which was introduced for sintering purposes. Due to the corrosion of the crucibles a small amount (0.1 at. %) of this Al also contaminated those crystals.

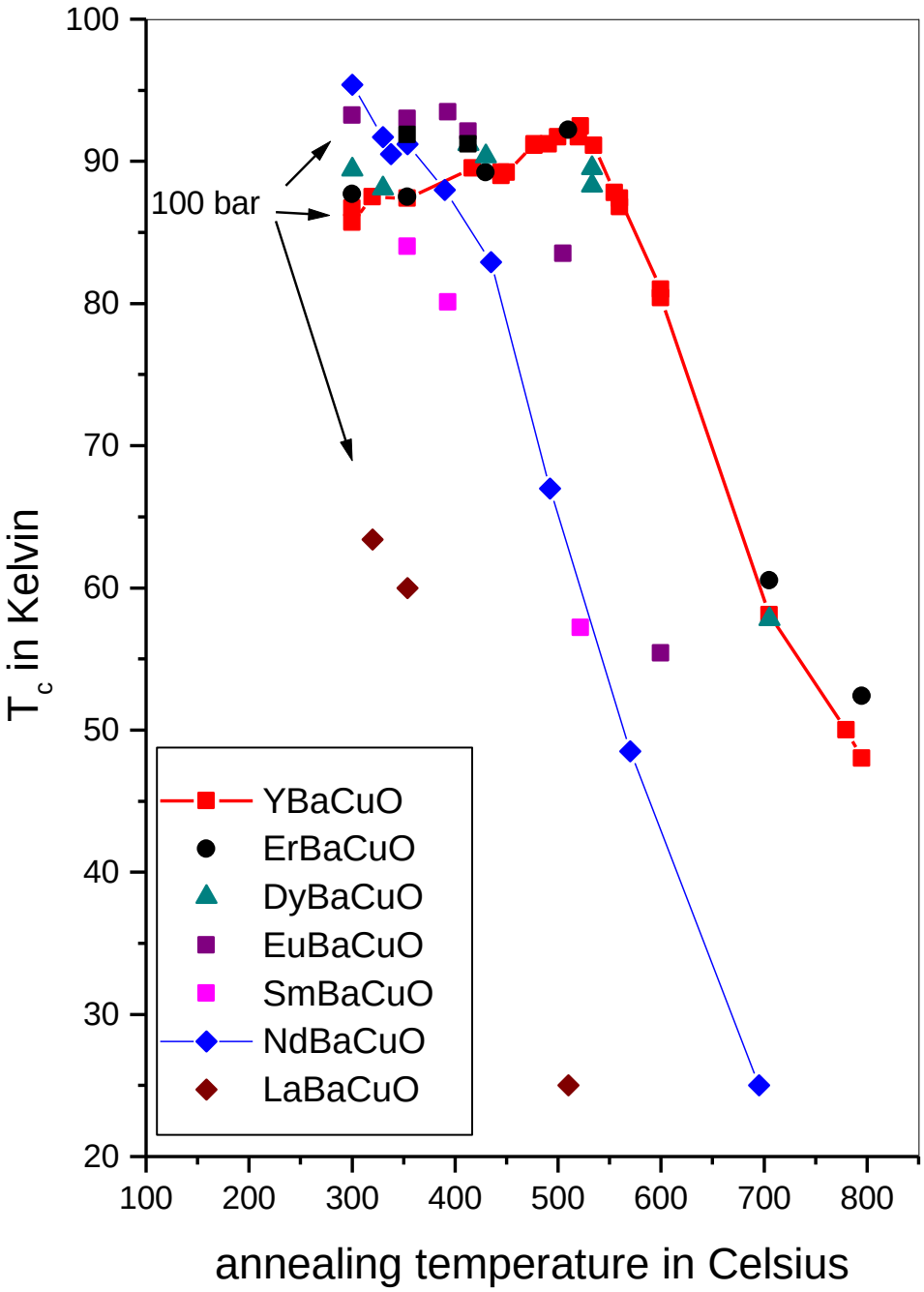

Fig.3.13 T_c versus oxygenation temperature for the different RE –123-compounds

The superconducting transitions of the crystals are normally very sharp as it can be seen from Fig. 3.14 showing transitions for a 40 mg $YBa_2Cu_3O_{7-\delta}$ single crystal in different oxygenation states (overdoped O_7 (red) and optimally doped $O_{6.9}$ (blue)). The superconducting transitions are not merely due to good oxygen homogeneity on the crystal surface. This was mainly probed in a surface sensitive measurement like the shielding measurement in Fig. 3.14, but has been verified many times by specific heat measurements, which probe bulk properties.

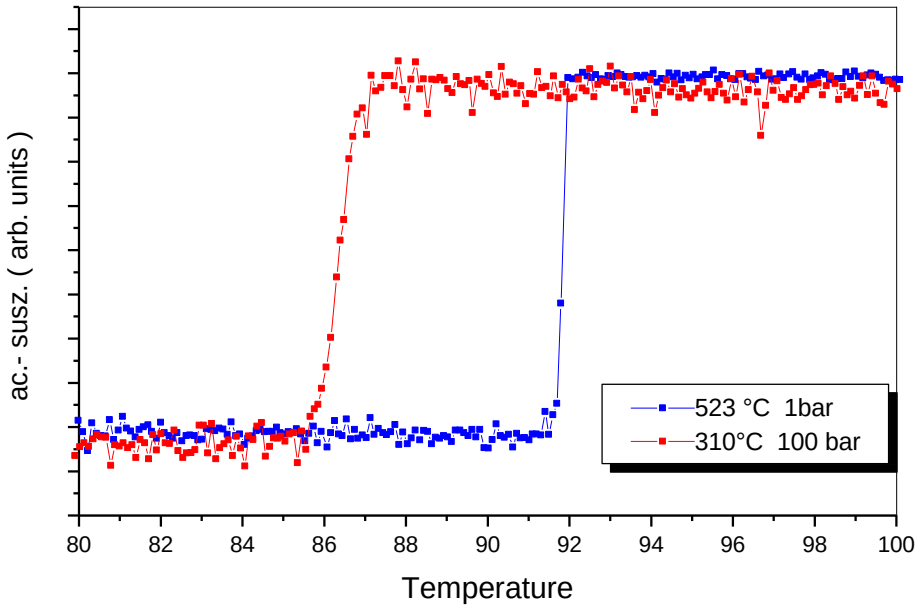

Fig. 3.14 Superconducting transitions for a 40 mg $YBa_2Cu_3O_{7-\delta}$ single crystal in different oxygenation states (overdoped O_7 (red) and optimally doped $O_{6.9}$ (blue)

With some of the $YBa_2Cu_3O_{7-\delta}$ single crystals we performed another series of oxygenation experiments in order to diminish the time required for oxygenation as well as for some questions concerning the so-called fishtail anomaly (chapter 5 & 6) . With a oxygenation time of 18 h at a temperature of 700 °C and a oxygen pressure of 100 bar it is possible to oxygenate the crystals to a state close to the maximum of T_c. The inductively measured T_c has value of 92.4 K with a transition width of only about 40 mK.

An important difference to earlier grown single crystals of the 123 family, related to the excellent surfaces, is the observation of the flux line lattice on these single crystals without any surface conditioning or cleaving [Maggio–Aprile]. The possibility to perform Scanning Tunneling Spectroscopy (STS) and to probe the superconducting gap directly on the surfaces proves not only that the crystals are superconducting up to the uppermost layer and that no isolating or so called "dead layer" is covering the samples but in addition allowed to draw a map of the tunnelling data in respect to their spatial variation (Fig. 3.15).

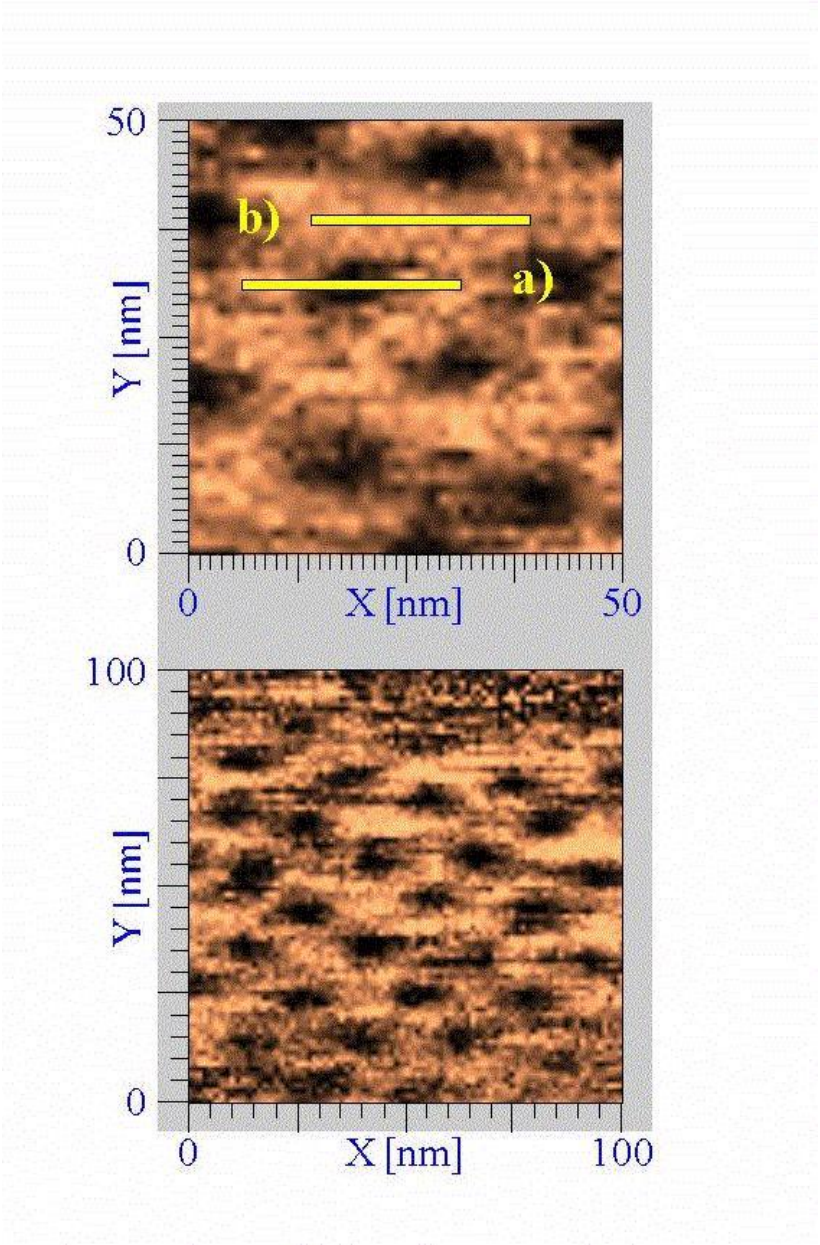

Fig. 3.15 Spectroscopic images of the vortex lattice on a 001 YBCO surface. The dark spots represent the vortex cores.

This remarkable result has been reproduced in the meantime by Lang et al. [Lang] at the University of Basel, Switzerland with the same type of crystals, while no other groups have so far succeeded to perform STS on other single crystals of $YBa_2Cu_3O_{7-\delta}$. The same working group also achieved atomic resolution on these crystals. Fig. 3.16 shows such a picture where the metallic sub-lattice has been imaged. On some of the crystal surfaces the oxygen sub-lattice has also been imaged, as a weak contrast in one direction (CuO –chains), which is missing in the perpendicular direction, indicating the basal plane being the terminating layer of the crystal. However, this is not the case for all surfaces, which is consistent with the fact that also 0.4 nm steps have been observed on the crystal surfaces, when doing topography on such specimens.

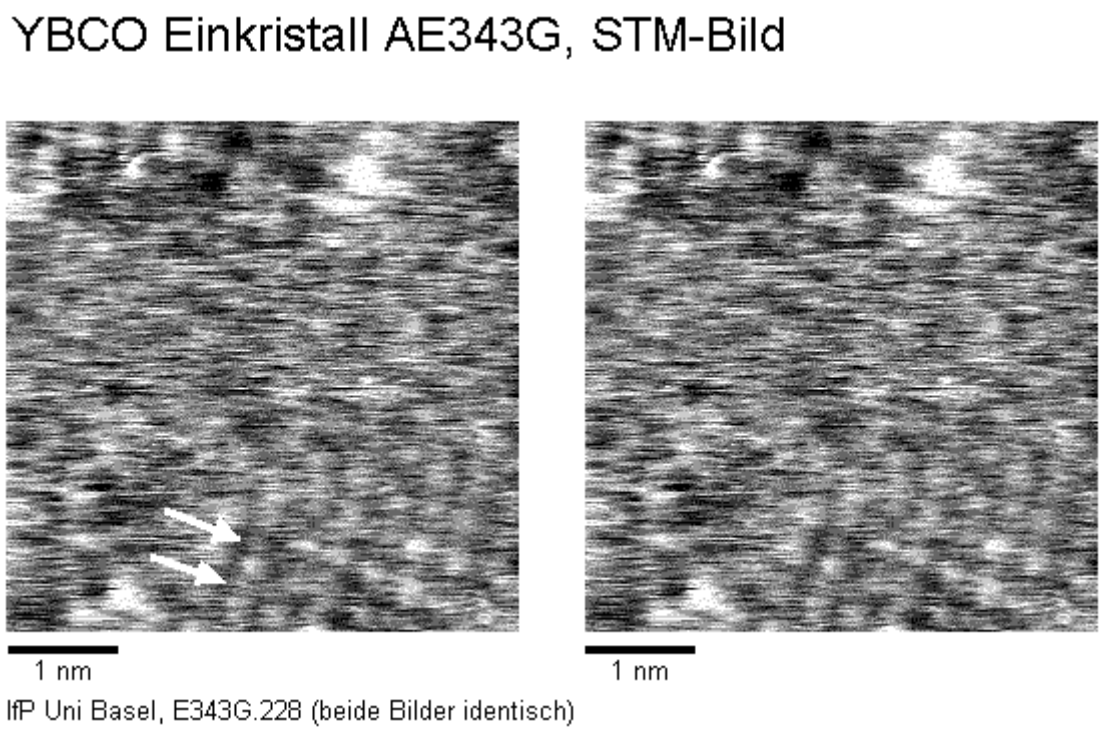

Fig. 3.16 STM picture showing atomic resolution on a 001 YBCO surface. The weak contrast (arrows) in one direction is missing in the perpendicular direction, which indicates that the basal plane is the terminating layer of this crystal surface.

References:

[ErbDiss]

A. Erb, Dissertation , Universistät Karlsruhe, FRG, (1994)

[Erb94]

A. Erb, T. Traulsen and G. Müller-Vogt, J. Cryst. Growth 137 (1994) 487

[Erb93]

A. Erb, T. Biernath and G. Müller-Vogt, J. Cryst. Growth 132 (1993) 389

[Nakamura]

M. Nakamura, M. Kambara, T. Umeda, Y. Shiohara, Physica C 266 (1996) 178

[Yao]

X. Yao, M. Kambara, T. Umeda, Y. Shiohara, Physica C 296 (1998) 69

[Zhou]

Z. Zhou, K. Oka, T. Ito, Y. Nishihara, Jap. J. of Applied Physics 36 (1997) L18

[Oka]

K. Oka, Z. Zou, J. Ye, Physica C 300 (1998) 200

[Zou]

Z. Zou, J. Ye, K. Oka, Y. Nishihara, Phys. Rev. Lett. 80 (1998) 1047

[Gilman]

e.g.: J. J. Gilman (Editor), The Art and Science of Growing Crystals, Page 293 ff., John Wiley and Sons, Inc., New York, London; B. R. Pamplin, Crystal Growth, Pergamon Press Ltd. (1975)

[Schneemeyer]

L. F. Schneemeyer, J. V. Waszczak, T. Siegrist, R. B. van Dover, L. Batlogg, R. J. Cava and D. W. Murphy, Nature 328 (1989) 601

[Scheel]

H.J.Scheel, W. Sadowski and L. Schellenberg, Supercond. Sci. Technol. 2 (1989) 17

[Dembinski]

K. Dembinski, M. Gervais, P. Odier, J. P. Odier, J. P. Coutures, Journ. of the Less Comm. Met. 164 & 165 (1990) 177-186

[Tatarchenko]

V. A. Tatarchenko, G.A. Emelchenko, N. V. Abrosimov, V. A. Borodin, L. Y. Vinnikow, O. V. Zharikov, A. A. Zhokhov, P. A. Kononovich, V. M. Masalov, I. M. Romanenko, V. V. Ryazanov, L. I. Chernyshova, International Journal of Modern Physics B 3 (2) (1989) 289

[Gagnon]

R. Gagnon, M. Oussena and M. Aubin, J. Crystal Growth 121 (1992) 559

[Berkowski]

M. Berkowski, P. Bowen, T. Liechti, H. J. Scheel, J. Am. Ceram. Soc. 75(4) (1992)1005

[Barilo]

S. N. Barilo, A. P. Ges, S. A. Guretskii, D. I. Zhigunov, A. V. Zubets, A. A. Igantenko, A. N. Igumentsev, i.D. Lomako, A.M. Luginets, V. N. Yakimovich, L. A. Kurochkin, L. V. Markova and O. I. Krot, J. Crystal Growth 119 (1992) 403

[Erb97]

A. Erb et al Physica C 282-284 (1997) 89

[Wolf]

Th. Wolf, W. Goldacker, B. Obst, G. Roth and R. Flükiger, J.Cryst. Growth 96 (1989) 1010

[Takei]

H. Takei, H. Asaoka, Y. Iye and H. Takeya, Japn. J. Appl. Phys. 30 L1102

[Asoka]

H. Asoka, H. Takei and Y. Iye, Physica C 190 (1991) 64

[Liang]

R. Liang, P. Dosanjh, D.A. Bonn, D.J. Baar, J.F. Carolan and W.N. Hardy, Physica C 195 (1992) 51.

[Oka]

K. Oka, K. Nakane, M. Ito, M. Saito and H. Unoki, Japn. J. Appl. Phys. 27 (1988) L1065

[Kawabata]

S. Kawabata, H. Hoshizaki, N. Kawahara, H. Enami, T. Shinohara and T. Imura, Japn. J. Appl. Phys. 29 (1990) L1490

[Maeda]

M. Maeda, M. Kadoi and T. Ikeda, Japn. J. Appl. Phys. 28

(1989) 1417

[Zhang]

W. Zhang, K. Osamura and S. Ochiai, J. Am Ceram. Soc. 73 (1990) 1958

[Osamura]

K. Osamura and W. Zhang, Z. Metallkde. 82 (1991) 408

[Aselage]

T. Aselage and K. Keefer, J. Mater. Res 3 (1988) 1279

[Abbattista]

F. Abbattista, M. Vallino and D. Mazza, Mater. Chem. Phys. 21 (1989) 521

[Licci]

F.Licci, P. Tissot and H.J.Scheel, J. Less-Common Met. 150 (1989) 201

[Karpinski]

J. Karpinski, ETH Zürich, Switzerland, private communication

[Tagami]

M. Tagami, M. Sumida, Ch. Krauns, Y. Yamada, T. Umeda, Y. Shiohara, Physica C 250 (1995) 240

[Klemenz]

C. Klemenz, H. J. Scheel, J. Crys. Growth 129 (1993) 421

[Dubs]

C. Dubs, K. Fischer, P. Görnert, J. Crys. Growth 123 (1992) 611

[Yamada]

Y. Yamada, Y. Shiohara, Physica C 217 (1993) 182

[Moran]

E. Moran, U. Amador, M. Barahona, M. A. Alario-Franco, A. Vegas, J. Rodriguez-Carvajal, Solid State Comm. 67 No. 4 (1988) 369

[LiangJ]

J. Liang, X. Chen, X. Wang, W. Chen, Z. Chen, Z. Qiao, Y. Zhang, S. Xie, Y. Ni,
Solid State Comm. 76 No. 7 (1990) 903

[Taylor]

K. N. R. Taylor in Studies of HighTemperature Superconductors Vol. 6, ed. A. Narlikar, Nova Science Publishers, New York (1990)

[Zhang2]

J. L. Zhang, J. E. Evetts, J. of Mat. Science 29 (1994) 778

[Lindemer]

T. B. Lindemer, J .F. Hunley, J. E. Gates, Jr. A.L.Sutton, J. Brynestad, C. R. Hubbard and P. K. Gallagher, J. Am. Ceram. Soc., **72**, 1775 (1989)

[Claus]

H. Claus, M. Braun, A. Erb, K. Röhberg, B. Runtsch, H. Wühl, G. Bräuchle, P. Schweiß, G. Müller-Vogt, H. v. Löhneysen, Physica C 198 (1992), 42

[Maggio-Aprile]

I. Maggio-Aprile, Ch. Renner, A. Erb, E. Walker, ∅. Fischer, Phys. Rev. Lett. 75 No. 14 (1995) 2754

[Lang]

H. P. Lang, A. Erb, P. Jess, U. Hubler, H.-J. Güntherrodt, J. Low Temp. Phys. 105 (1996) 1373

4. Oxygen diffusion coefficients in the 123 –compounds

4.1 Introduction

Oxygenation of bulk samples of 123 superconductors is a major problem, both for the preparation of samples for fundamental research as well as for samples with optimised transition temperature and pinning properties for applications. In most cases the oxygenation is done more or less according to empirical experience rather than being based on the knowledge of the actual mechanism. The reason is that there were little and contradicting informations about the diffusion coefficients of oxygen in the YBCO and the rare earth 123 – compounds.

The knowledge of the diffusion coefficient, however, is important to assure complete and homogenous oxygenation of samples used in fundamental research, but also due to the fact that for the different rare earth compounds the annealing temperature leading to the maximum T_c is lowered by about 20, 100 and 200 K for the Dy, Eu and Nd systems, respectively, if compared with Y-123 as we have seen in the former paragraph.

Comparing the papers about oxygen diffusion in $YBa_2Cu_3O_{7-\delta}$ leads to the statement that the values given for the diffusion coefficients D(T) vary over about 5 orders of magnitude. This is especially the case when measurements are performed on ceramic samples, where an estimation of the effective diffusion length has to be made.

Even for the more reasonable values given for diffusion in single crystals the diffusion coefficients vary over at least 3 orders of magnitude [Erb96a]. This of course could be due to different crystal quality, because every imperfection e.g. impurities or dislocations in the $YBa_2Cu_3O_{7-\delta}$ crystal may favour the diffusion.

However, what may be even more severe is that the diffusion coefficients reported for in- and out-diffusion of oxygen seemed to be different even for one individual single crystal. This, of

course, is not reasonable for a thermally activated process like diffusion and implies the necessity to study the diffusion process of oxygen in the 123-superconductors in more detail.

4.2 Resistivity measurements during the oxygenation of 123 crystals

All the resistivity measurements were done in pure (99.995 %) O_2 atmosphere in a quartz tube placed inside a homebuilt tube furnace of about 1 m length with a temperature gradient of less than 1 K /cm in the region of the sample holder. The temperature of the sample was measured using a Pt/PtRh10% thermocouple, placed directly beside the sample.

For the resistivity measurements real four point geometry has been chosen so that the contact resistivities can be neglected. For experimental details on these measurements see [Erb96a, Kläser].

To determine oxygen diffusion coefficients from resistivity curves the crystals were held at a given temperature until they reached an equilibrium resistivity value. Then the annealing temperature was changed rapidly ($\approx$ 100 K/h) to a new annealing temperature above or below the recent one (Fig. 4.1). There the samples were held until a new equilibrium state of the oxygen content was achieved. This was done for several annealing temperatures in the temperature range between 400 and 555 °C. To prove that no irreversible reactions occurred the crystals were brought to a temperature of 425 °C and were given time to equilibrate at that particular temperature after they had been treated at other temperatures. Even after several month of annealing at different temperatures the crystals reached the same value for the electrical resistivity at 425 °C, proving that this value corresponds indeed to equilibrium. As a further test for the homogeneity of the oxygen content of the crystals several measurements of T_C on such equilibrated samples have been performed. In all cases they showed sharp ($\Delta T_C \leq 1K$) transition curves, thus proving homogeneity.

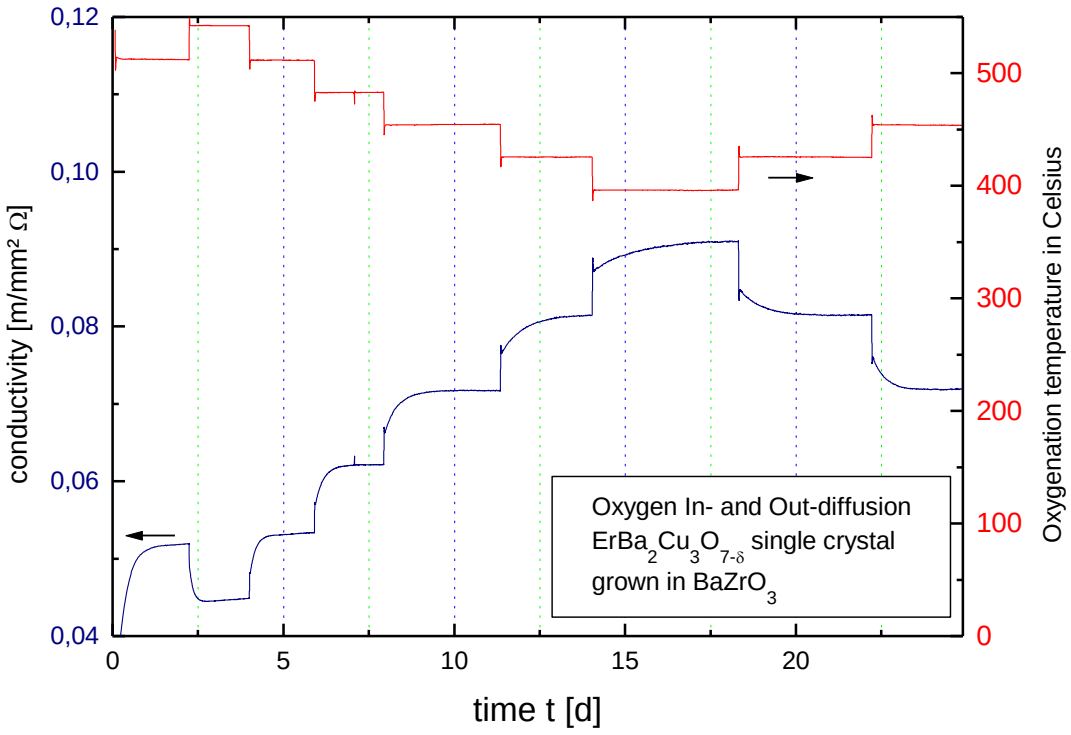

Fig 4.1 Temperature program and conductivity dependence as a function of annealing time and temperature.

4.3 Theory

From the long term dependency of the resistivity after the temperature change (Fig. 4.1) the diffusion coefficient D(T) can be determined. Since oxygen diffusion in the c-direction of the crystals has been reported to be much slower [Rothman,Tsukui] than in the a and b direction and because of the chosen sample geometry (long strip) the problem can be treated as a one-dimensional diffusion within the a - b plane of YBCO.

According to Crank [Crank] and Jost [Jost] such a 1 dimensional diffusion process can be described with the following equation,

$$c(x,t) = c_0 \cdot \frac{4}{\pi} \sum_{\nu=0}^{\infty} \frac{1}{2\nu+1} \sin\left[\frac{2\nu+1}{b}\pi x\right] e^{-\left(\frac{2\nu+1}{b}\pi\right)^2 Dt} \qquad (1)$$

where c(x,t) is the concentration as a function of the local coordinate and time, c_0 the starting concentration, b the width of the sample and D the diffusion constant. Since the local dependence is not measurable with this method, equitation (1) has to be integrated over the width of the sample. By doing this and by calculating only relative changes in concentration equation (1) can be rewritten in the following form

$$\frac{c(t) - c_e}{c_0 - c_e} = \frac{8}{\pi^2} \sum_{\nu=0}^{\infty} \frac{1}{(2\nu+1)^2} \cdot e^{-\left(\frac{2\nu+1}{b}\pi\right)^2 Dt} \qquad (2)$$

where c(t) is the concentration as a function of time, c_0 the starting concentration, c_e the saturation concentration, b the width of the sample and D the diffusion constant. With the approximation $\nu = 0$ this can be rewritten in the form

$$\frac{c(t) - c_e}{c_a - c_e} = \frac{8}{\pi^2} \cdot e^{-\frac{t}{\tau}} \qquad \tau = \frac{b^2}{\pi^2 D} \qquad (3)$$

where τ is the relaxation time.

As the concentrations are not directly measurable the conductivities were used in this formula instead of the concentrations. This linear approximation, which is commonly used, may be not

valid for higher oxygen deficiencies, but may be used in a temperature region, where only small changes in the oxygen content occur.

The relaxation time τ has been determined from the slope of the expression

$$\ln\left[\frac{\pi^2}{8}\cdot\frac{\sigma(t)-\sigma_e}{\sigma_a-\sigma_e}\right] \qquad (4)$$

plotted vs. time.

4.4 Results for $YBa_2Cu_3O_{7-\delta}$ and for the $ReBa_2Cu_3O_{7-\delta}$ single crystals

4.4.1 Oxygen in- and out-diffusion

The time constants and therefore the diffusion coefficients which have been reported in literature have different values for the in- and out-diffusion in $YBa_2Cu_3O_{7-\delta}$. In some papers [LaGraff1, LaGraff2] slower in-diffusion than out-diffusion has been reported for measurements on single crystals. In other papers [Tu], even of the same authors [LaGraff3], faster in- than out-diffusion has been reported. Since diffusion is a thermally controlled process, there is no reason for a difference for the two diffusion processes if no surface controlled processes occur. Surface controlled processes, on the other hand would indicate the existence of a barrier which hinders the measurement of the intrinsic oxygen diffusion coefficient, making the results of this reports questionable.

In contrast to these results we have shown by in-situ resistivity measurements that values for oxygen in- and out-diffusion in $YBa_2Cu_3O_{7-\delta}$ [Erb96a] are exactly the same.

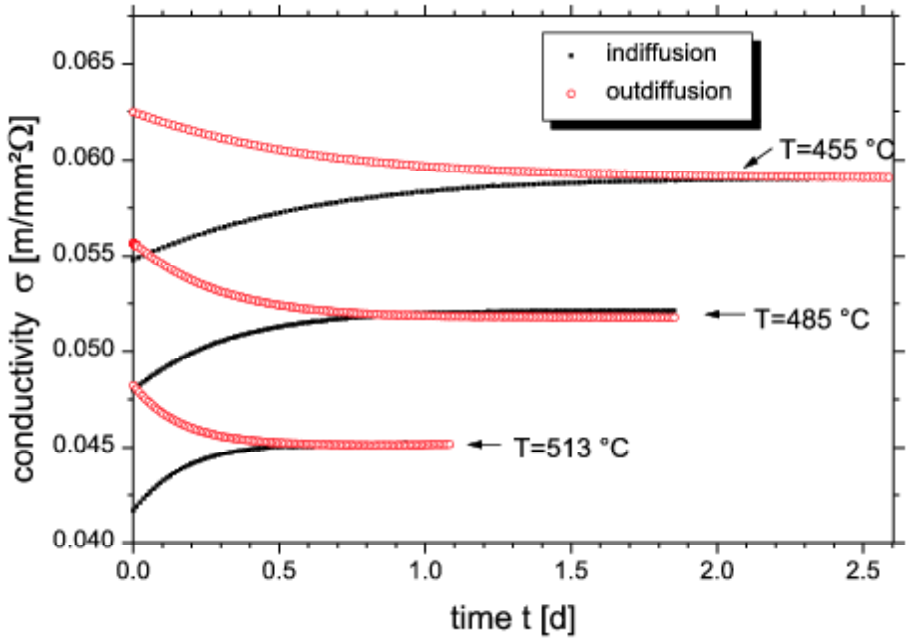

Fig 4.2 Oxygen in- and out –diffusion at different temperatures [Kläser]

As it is shown in Fig. 4.2 the time needed to reach an equilibrium resistance value at a given temperature is the same, no matter whether this equilibrium resistance value is approached from temperatures above or below. This means that the coefficients for in- and out-diffusion in $YBa_2Cu_3O_{7-\delta}$ depend only on the temperature and are not surface controlled.

4.4.2 Temperature Dependence of D(T)

In the literature data about oxygen diffusion in single crystals of $YBa_2Cu_3O_{7-\delta}$, the temperature dependence of D(T) does not always follow an Arrhenius law, which should be valid for a thermally controlled processes like diffusion. In our investigations, however, we have shown that the determined values of D(T) can very well be fitted by an Arrhenius law [Erb96a], making these results reliable.

Fig. 4.3 shows the dependence of the diffusion constant D(T) from temperature for different single crystals of Er- and Dy-123, both with different rare earth central atoms and with different impurity content due to crucible corrosion.

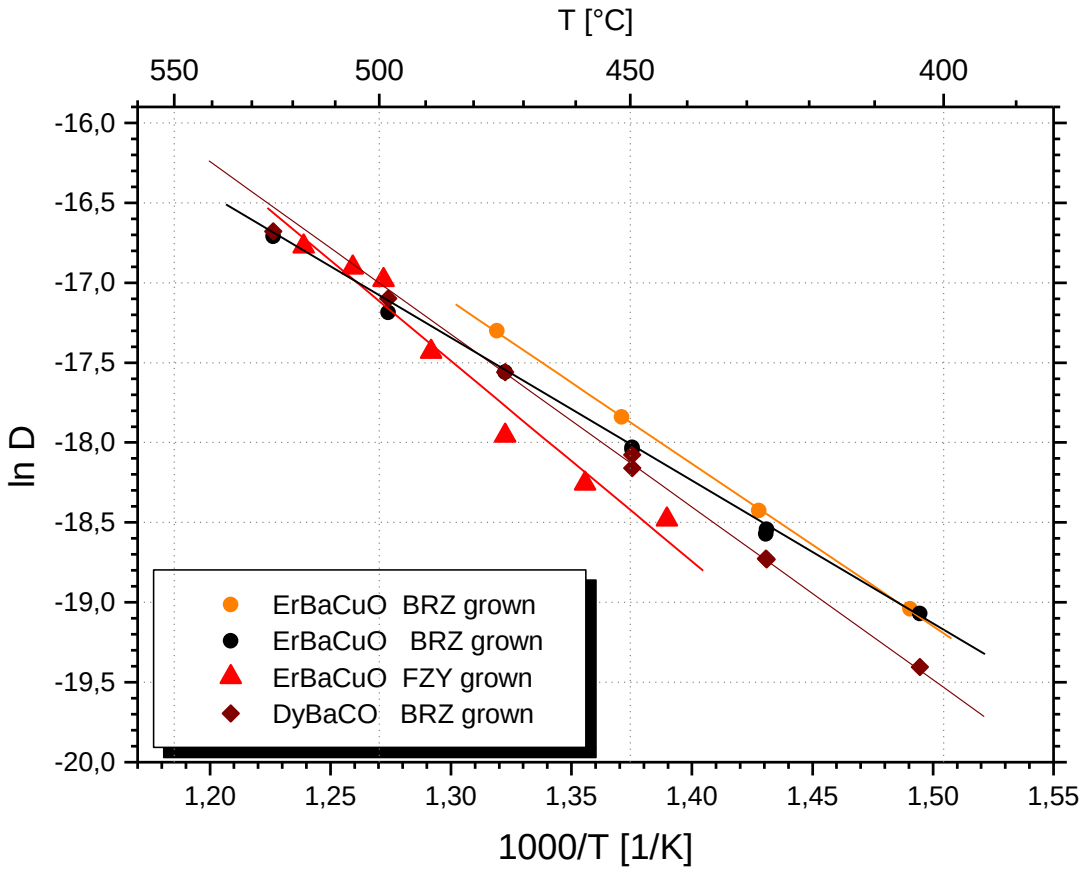

Fig 4.3 ln D (T) versus inverse temperature for different rare earth 123 single crystals with different impurity content

From the slope of the straight line in the ln D(t) vs. 1/T plot the activation energy ΔE for the oxygen diffusion can be determined according to the formula,

$$D(T) = D_0 \cdot e^{-\frac{\Delta E}{kT}} \qquad (5)$$

For all the crystals under study [Erb, Kläser] the values for the activation energy was found being ΔE = 1 eV with an scatter of about 10 % in agreement to earlier estimations [Claus, Conder].

The absolute values for the diffusion coefficient found for all the samples under study has an accuracy of about ± 50 % and no dependence of the diffusion coefficient can be found neither in respect to residual impurity concentrations nor and this is even more important with respect to the central rare earth atom.

4..5 Implications

The finding that the diffusion coefficient is independent of the central rare earth atom has several implications, even though it is not too surprising if one takes into account that the path for oxygen diffusion is the Cu-chain site, which is relatively far away from the central atom and thus should be little influenced by size differences of the latter.

The independence of the diffusion coefficients stands in contrast with a report of Tallon et al. [Tallon] who reported greatly enhanced diffusion coefficients for Gd-, Nd- and La- 123 compounds, but those values were deduced from rather indirect measurements of the mechanical damping of ultrasounds in ceramic samples.

For application purposes this independence of the diffusion coefficient from the rare earth central atom means that there exists an major obstacle for a technical application of Nd, Sm and Eu compounds, since the final oxygenation has to be performed at much lower temperature to obtain T_c values above 90 K (e.g. at about 300 °C for the Nd- and Sm-compounds instead of 520 °C for the Y-123 system). At those low temperatures however the diffusion coefficients are reduced by 2 orders of magnitude and thus the diffusion or oxygenation time needs to be increased by these 2 orders of magnitude.

Using the Einstein formula for diffusion processes $d_{eff} = \sqrt{6 \cdot D(T) \cdot t}$, with d_{eff} being the effective diffusion length and the extrapolated diffusion constant for Nd-123 at 300 °C being $3x10^{-10}$ cm^2/s one can calculate for an cube of 1 cm, being a realistic sample size for application purposes of melt-textured samples of Nd-123, on an oxygenation time of

5.5×10^8 sec or 17.6 years instead of 65 days as one would finds for an optimally doped Y-123 sample of the same size.

Of course the melt-textured samples are not ideal single crystals and the oxygenation is favoured in this case by the fact that there are many open channels like micro-cracks and dislocations for oxygenation of these samples. As a consequence, the existing melt-textured samples actually oxygenate much faster than single crystals. However, these open channels for oxygenation are undesired in terms of high critical currents and thus the ideal melt-textured sample will resemble something very close to a single crystal so that the estimation made above should be valid. The main interest in those light rare earth elements arises from the somewhat higher T_c and the better pinning properties, which will be discussed in chapter 6, but it is already clear that the low final oxygenation temperatures will be an obstacle for the use of pure light rare earth compounds.

References:

[Erb96a]

A.Erb, B. Greb and G. Müller-Vogt Physica C 259 (1996), 83

[Kläser]

Marion Kläser, Joachim Kaiser, Fredy Stock, German Müller-Vogt and Andreas Erb, Physica C 306 (1998) 188

[Crank]

J. Crank, The mathematics of diffusion, Oxford University Press, (1956)

[Jost]

W. Jost, Diffusion, Steinkopf Verlag, Darmstadt, FRG, (1957)

[Rothman]

S. J. Rothman, J. L. Routbort, U. Welp and J. E. Baker, Phys. Rev. B 44, (1991) 2326

[Tsukui]

S. Tsukui, T. Yamamoto, M. Adachi, Y. Shono, K. Kawabata, N. Fukuoka, S. Nakanishi, A. Yanase, Y. Yoshioka, Jap. Journ. of Appl. Phys. 30, Nr.6A (1991), 973

[LaGraff1]

J. R. LaGraff, D. A. Payne, Phys. Rev B 47 No.6, (1993) 3380-3390

[LaGraff2]

J. R. LaGraff, D. A. Payne, Physica C 212 (1993) 470-477

[Tu]

K. N. Tu, N.C. Yeh, S. I. Park, C. C. Tsuei, Phys. Rev. B 39 No.1, (1989) 304

[LaGraff3]

J. R. LaGraff, D. A. Payne, Physica C 212 (1993) 478

[Claus]

H. Claus, S. Yang, H.K. Viswanathan, G.W. Crabtree, J.W. Downey, B.Veal, Physica C 213, (1993) 185-189

[Conder]

K. Conder, Ch. Krüger, E. Kaldis, D. Zech, H. Keller, Physica C 225 (1994) 13

[Tallon]

J. L. Tallon and B.-E. Mellander, Science Vol 258 (1992) 781

5. Fishtail anomaly in the 123 Compounds

5.1 Introduction

Soon after the discovery of the 90 K superconductor $YBa_2Cu_3O_{7-\delta}$ an anomaly in the curves of the irreversible magnetisation, often revered to as "fishtail effect" has been reported [Däumling]. This anomaly consists of an increase in the magnetisation upon increasing magnetic field which is equivalent to an increase of the critical current j_c high above Hc_1. An typical example is given in Fig 5.1. While for all other high temperature superconductors a technical use at liquid nitrogen temperatures seems to be limited due to their poor critical current density in magnetic fields, this fishtail anomaly of the 123 superconductors implies a probable technical use of these superconductors even at high fields.

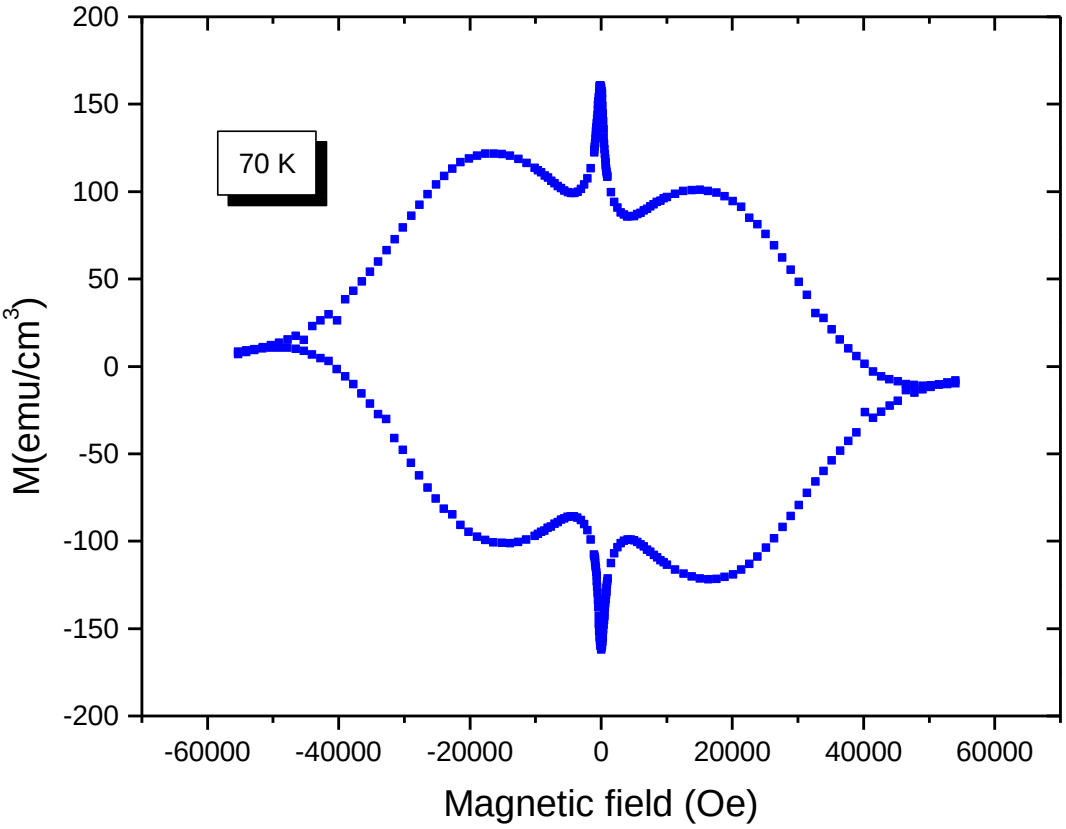

Fig. 5.1 Typical example of a so-called fishtail anomaly in a single crystal of $YBa_2Cu_3O_{7-\delta}$

To illustrate this circumstance one can compare the critical currents of the more 2 dimensional superconductor Bi-2223 with the 123 –compound. Even though the T_c of the Bi-2223 compound is somewhat higher than that of the 123 family the critical currents at 77 K, the temperature where an application is proposed, range in between 20-50 KA/cm^2 in self field and drop substantially in magnetic field to values of about 3 kA/cm^2 in magnetic fields of 2 T. [Grasso]

In contrast to this the more 3 dimensional structure of the 123 family supports higher critical currents not only under self field conditions but also in higher magnetic fields. Values of j_c for mono-crystalline or melt-textured samples at 77 K range typically between 10 – 80 kA/cm^2 in selffield and 20-200 kA/cm^2 at 2 T [Hergt]. For biaxially aligned coated tapes of the 123 superconductors even higher values (2 MA/cm^2, 77 T, 0T and 100 kA/cm^2, 5T) have been reported [Lubkin].

One of the reasons of this relatively robust superconductivity lies within the above mentioned anomaly in the magnetisation curves of the 123 family. Since its importance for technical applications of the 123 –compounds was soon recognised this effect and its explanation has been the subject of study and controversial discussion now for nearly a decade.

The publications about the origin of this anomaly can be divided into 2 groups: The first group uses physics and tries to explain the anomaly as being due to crossovers of different pinning regimes as for instance the crossover from single vortex pinning to collective pinning [e.g. Klein] or, more recently the crossover from plastic to elastic flow of the vortices [Abulafia]. All of these more theoretical approaches have in common that they consider the anomaly as being intrinsic to the 123-compounds rather than being a result of the microstructure. The reason for this treatment of the problem was that the anomaly was virtually present in all the samples, even though the absolute values for the anomaly were highly sample dependant (see for instance [Hergt]).

The second group of papers pays more attention to the variation of the absolute values of the anomaly and uses material science namely inhomogeinities of either the oxygen sublattice or the metal- sub lattice in order to explain this effect. This approach is actually also used by a the majority of groups that try to commercialise the 123 compounds for applications and a

commonly used technique to increase the effect is to deliberately provoke such inhomogeinities by doping with various metals.

5.2 The fishtail effect as a result of field induced pinning

As mentioned above one of the approaches to understand the fishtail anomaly is that local inhomogeinities turn normal on increasing magnetic field, thus turning into pinning centers and thereby increasing the critical current.

This interpretation is not based on a quantitative physical model but rather concluded on analogy on the case of low-T_c materials containing superconducting precipitates which turn normal on increasing magnetic field producing more pinning and thus an increase in the critical current [Livingston]. In some alloys with very regular spatial distribution such precipitations lead actually to a very sharp increase of the critical current at a distinct field, the so-called matching field ; where the distance between vortices match the distance between the precipitations producing most effective pinning at exactly this value of magnetic field. This matching field normally shows no temperature dependence in contrast with the situation of the fishtail effect where in most cases the maximum in the magnetisation curves is found at increasing magnetic field values with decreasing temperature. I will address this point later on.

To understand why in the most samples of $YBa_2Cu_3O_{7-\delta}$ the fishtail anomaly is found it is referred to chapter 3, where it was shown that most of the crystals under investigation contain a considerable and often unknown or undetermined amount of metallic impurities and that those could lead to uncontrolled precipitates producing the anomaly. The already mentioned strong sample dependence of the anomaly is one hint in this direction. The development of the new sample generation of $BaZrO_3$ grown crystals gave the opportunity to overcome the uncertainties due to the metallic impurities and to start a series of investigations on the origin of this anomaly with respect to the specific microstructure of firstly the oxygen sub-lattice

which turned out to be the only origin responsible for the fishtail anomaly in pure $YBa_2Cu_3O_{7-\delta}$ and secondly the metal sub-lattice which plays an additional role for the anomaly in the light rare earth compounds like $NdBa_2Cu_3O_{7-\delta}$, $SmBa_2Cu_3O_{7-\delta}$ and $EuBa_2Cu_3O_{7-\delta}$.

5.2.1 The fishtail effect in $YBa_2Cu_3O_{7-\delta}$ - micro segregation of oxygen vacancies

This chapter summarises a series of publications over the last few years [Erb96, Erb97, Genoud, Erb97a, Erb99] which shed light in the microstructural origin of the fishtail effect in single crystalline $YBa_2Cu_3O_{7-\delta}$.

The standard annealing to obtain high transition temperatures well above 90 K in $YBa_2Cu_3O_{7-\delta}$ single crystals consists of a treatment under 1 bar of oxygen at around 500 °C for 100 - 200 hours, followed by quenching to room temperature. The oxygenation of YBCO under such conditions, however, is only performed in this way due to the simplicity of the procedure. According the phase diagram of Lindemer et. al [Lindemer] which gives the equilibrium oxygen concentrations as a function of oxygen partial pressure and temperature, the same oxygen content can be obtained as well by annealing at higher temperatures in higher pressure oxygen atmospheres. Fig.5.2

The advantage of annealing at higher temperatures and higher oxygen partial pressures lies not only in the shorter annealing times due to higher oxygen diffusion coefficients (see chapter 4) but also in the presumable more homogenous oxygenation since at temperatures as high as 700 °C the oxygen deficient regions are more likely to be randomly distributed, while at lower temperatures a clustering effect of oxygen deficient unit cells may occur due to the smaller entropy term in the free energy [Vargas, Semenovskaya and references therein].

To test the idea of a clustering effect being responsible for the anomaly in the magnetisation curves $BaZrO_3$ grown $YBa_2Cu_3O_{7-\delta}$ crystals were annealed at 700 °C in 100 bar of O_2 for periods of 12 - 40 h, followed by rapid quenching (5 seconds to 1 min) to room temperature, so that the high temperature oxygen state can be maintained. For the case of optimally doped

YBCO pairs of oxygen partial pressures and temperatures were chosen which lead to the same equilibrium oxygen content in the crystal according to Fig 5.2.

The crystals used for the oxygenation experiments showed the usual twinning within the a-b plane and no attempts were made to detwinn the crystals. The influence of twin boundaries on pinning will be discussed later.

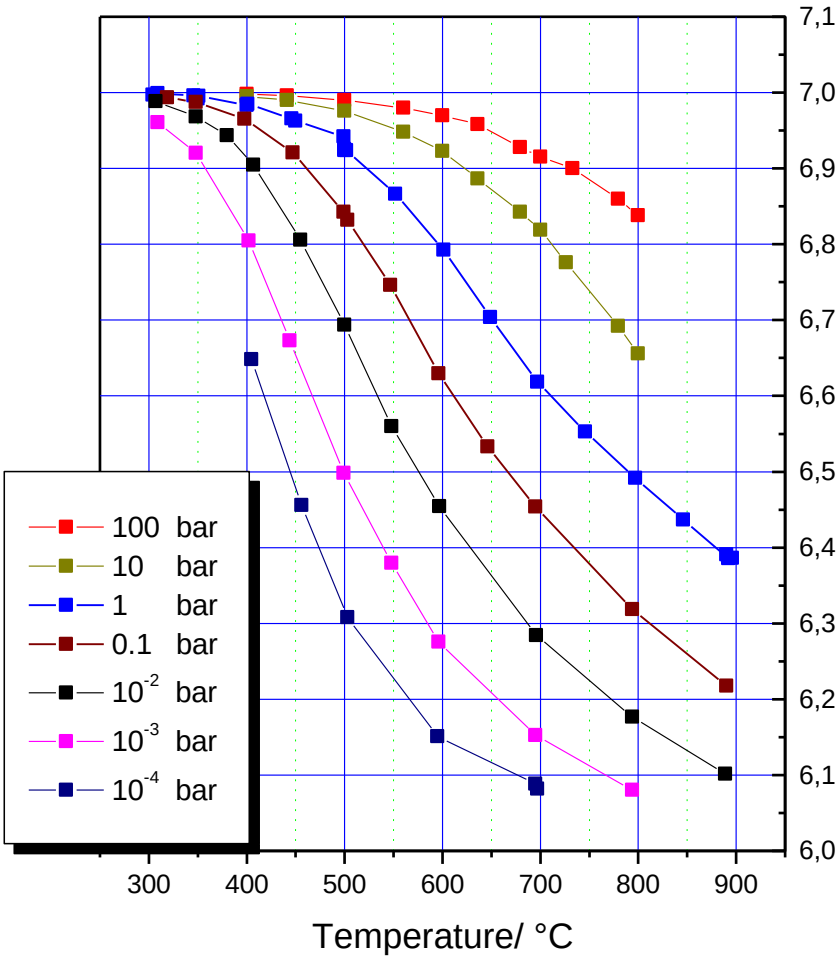

Fig. 5.2 Oxygen content in $YBa_2Cu_3O_{7-\delta}$ as a function of temperature and oxygen partial pressure, according to the calibration of Lindemer et al. [Lindemer]

The magnetisation measurements were performed in a SQUID Magnetometer (Quantum Design) with the field parallel to the c-axis of the crystal. The result of an oxygenation treatment at 700 °C for 40 h can be seen in Fig. 5.3, where M(H) is shown for a temperature

of 70 K. Clearly no fishtail behaviour is present after this oxygenation treatment. Reannealing the same crystal similar to the standard oxygenation (520 °C, 160 h under 1 bar oxygen), leads to the reappearance of the fishtail anomaly (also shown in Fig 5.3). According to Lindemer et al. the overall oxygen content of the samples has the same value of 6.91 for the 2 different treatments (520 °C / 1 bar , 700 °C / 100 bar). Therefore only a locally altered oxygen distribution or oxygen ordering must be responsible for this effect. It should be noted here that the T_c remains virtually unchanged after such a treatment as it is shown in the inset of Fig. 5.3.

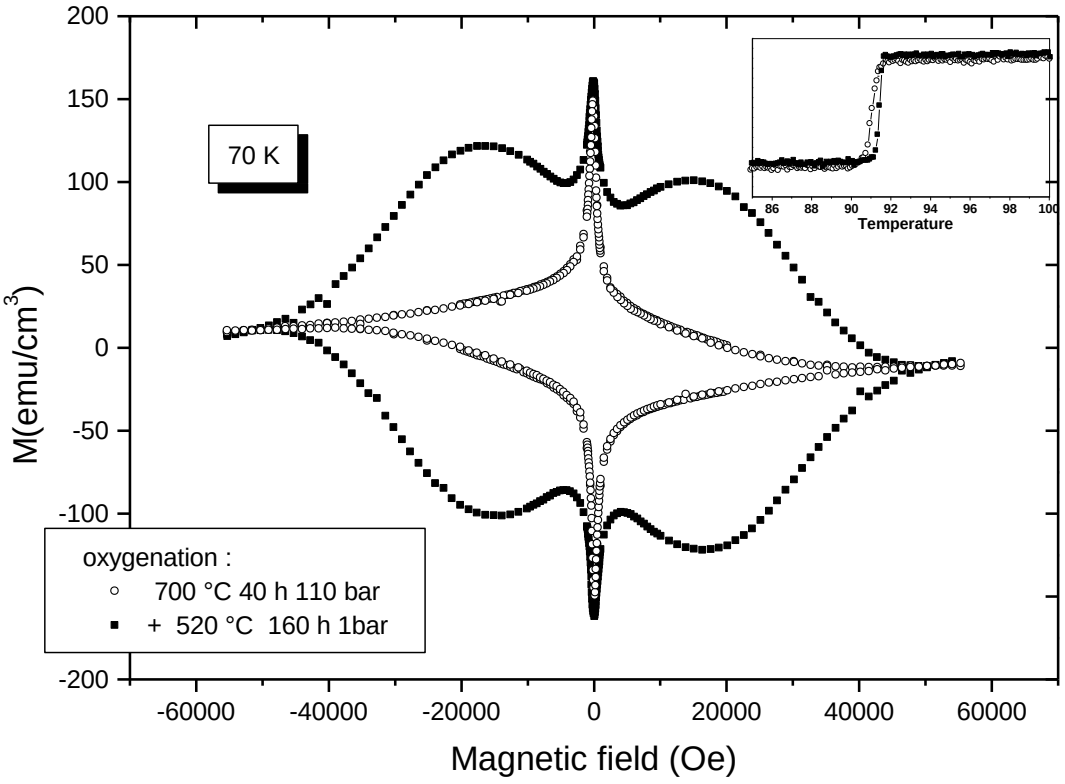

Fig 5.3 Magnetisation of $YBa_2Cu_3O_{6.91}$ after different annealing regimes.
The inset shows the inductively measured transition curves.

Since the oxygen deficiency expressed by δ= 0.09 is the same for both treatments, it can be concluded that the local distribution of the oxygen vacancies must be correlated to this effect. Taking into account that the oxygen sites in the copper oxide planes do not contribute to the oxygen deficiency this circumstance simply means that for the well- known optimal doping at

an oxygen content of about 6.91, the single crystals contain 9 % of oxygen deficient unit cells $YBa_2Cu_3O_{6.0}$. Allowing half filled cells of $YBa_2Cu_3O_{6.5}$ this value doubles to 18 % and if one assumes a single oxygen deficiency in one of the 4 possible oxygen chain sites there are about 36 % oxygen deficient cells of $YBa_2Cu_3O_{6.75}$ in a single crystal. Fig 5.4 illustrates the amount of oxygen vacancies for a oxygen doping of $YBa_2Cu_3O_{6.94}$. Shown are the basal planes of 100 unit cells of $YBa_2Cu_3O_{6-\delta}$ with the 6 vacancies distributed in different microstructural arrangements how they can be expected for different temperatures.

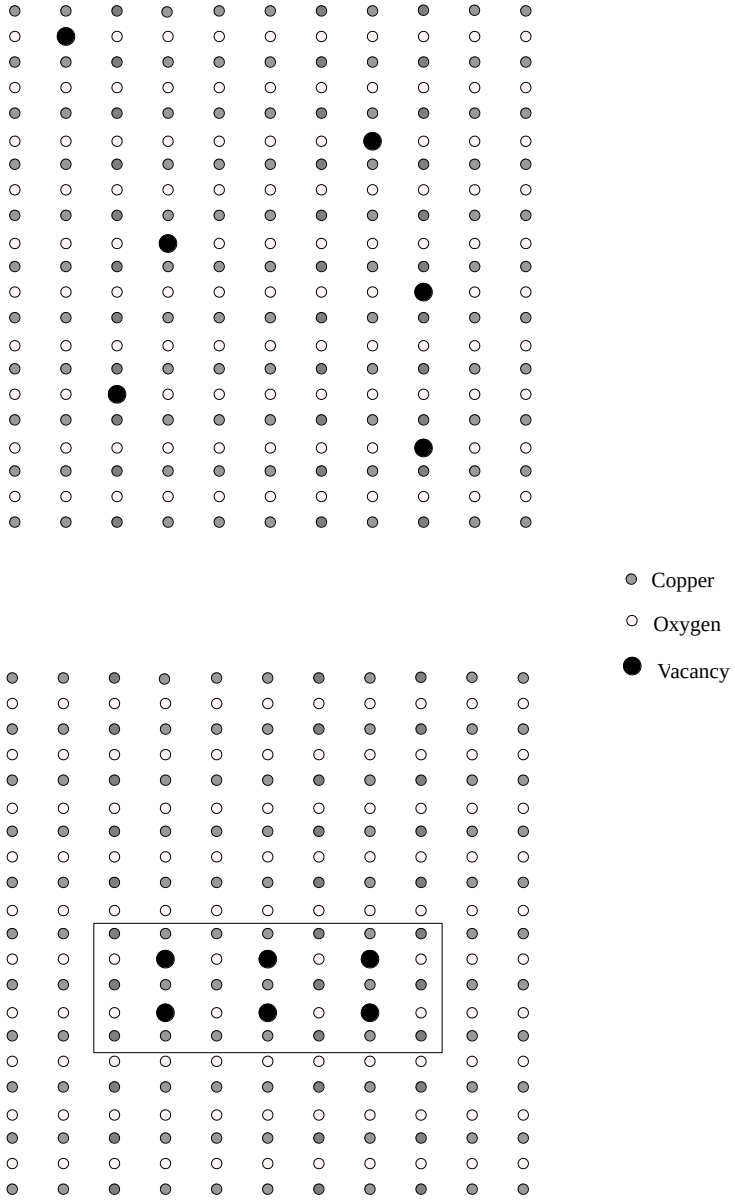

Fig 5.4 Different arrangements of the oxygen vacancies in the basal plane of $YBa_2Cu_3O_{6.94}$; the upper one corresponding to higher temperatures than the lower one

At temperatures as high as 700 °C the oxygen deficient regions are more likely to be randomly distributed, while at lower temperature a clustering effect of the oxygen vacancies may occur due to the smaller entropy term in the free energy [Vargas, Erb96 and references therein]. Such clusters which are present after the standard oxygenation at 520 °C in 1 bar of oxygen have a different T_c as well as a different $B_{c2}(T)$ than the matrix and may turn normal on increasing magnetic field providing additional pinning. On the other hand single vacancies are unlikely to pin the vortices at the elevated temperatures of around 70 K due to thermal activation and the fact that the pinning potential of a single vacancy is very small.

Note that the overall oxygen content is unchanged by the different annealing procedures and that also the different treatments have no influence on the state of twinning. Thus, it has been concluded [Erb96] that only the locally altered distribution of the oxygen vacancies, e.g a cluster formation is on the origin of the fishtail effect and that this effect can be interpreted as being a matching effect like in the case of classical superconductors. As mentioned earlier, the fishtail effect normally has a temperature dependence and it is this temperature dependence which is mostly used when arguing against an interpretation against the matching field scenario. However, the temperature dependence of the fishtail anomaly follows quite naturally when we assume that the cluster size is not uniform but has a gaussian distribution as sketched in Fig.5.5.

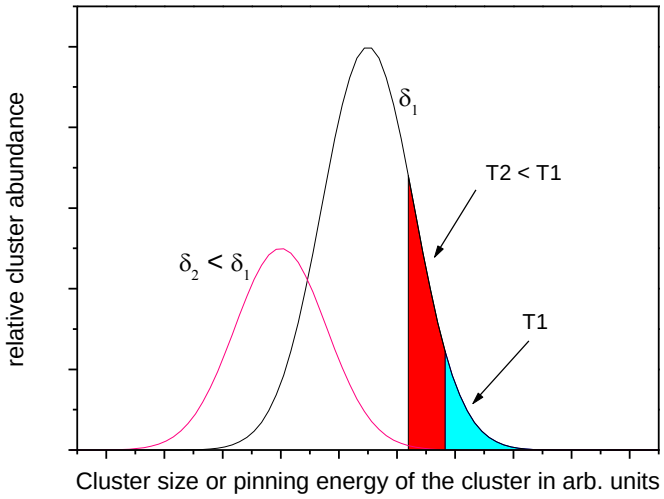

Fig. 5.5 Gaussian distribution of the cluster size for 2 different δ values. Effective pinning centers indicated by the coloured area for 2 different temperatures

At the temperature T1 only the cluster sizes indicated by the blue area are effective for pinning ,the pinning energy being > $k*T_1$. At the lower temperature T_2 also the clusters having a size and /or pinning energy as indicated by the red area contribute to pinning, the density of pinning centers is raised and the corresponding matching field is shifted to higher fields. Thus the temperature dependence of the fishtail anomaly is no argument against the interpretation of the fishtail anomaly being a peak effect, produced by oxygen vacancy clusters.

5.3 Testing the oxygen vacancy cluster model

5.3.1 The case of $YBa_2Cu_3O_7$

The first and most obvious test of the cluster model of course is to measure the magnetisation of fully oxygenated samples. To obtain such samples I refer again to the calibration of Lindemer et al. (Fig. 5.2) , where we can see that such samples can be produced by low temperature annealing at high oxygen partial pressures, e.g. 300 °C 100 bar oxygen partial pressure. No fishtail behaviour is observed (Fig. 5.6) in this case since the amount of oxygen vacancies is practically zero and it is not possible for those oxygen vacancies to form clusters of oxygen deficient unit cells, which can act as effective pinning centres on increasing magnetic field. Further support for this explanation of the fishtail anomaly as being due to clusters of oxygen deficient regions arises from the absence of this anomaly in $BaZrO_3$ grown single crystals of the naturally untwinned and stoichiometric high pressure compound $YBa_2Cu_4O_8$, where no vacancies are present [Genoud].

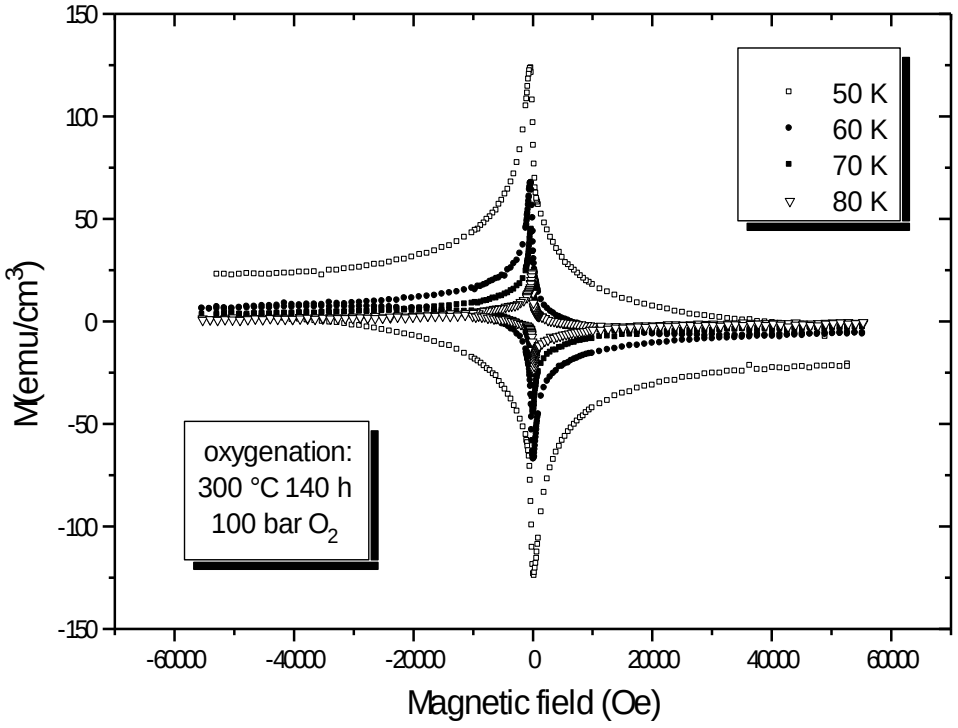

Fig 5.6. Magnetisation of a $YBa_2Cu_3O_7$ single crystal

5.3.2 Time evolution of the fishtail anomaly

To study the reorganisation of the oxygen vacancies upon re-annealing under standard oxygenation conditions a detailed study of the re-establishment of the anomaly has been performed [Erb99].

First the anomaly has been suppressed by an oxygenation treatment at 700 °C for 12.5 h at 100 bar as it can be seen in Fig. 5.7, where again M(H) is shown for a temperature of 70 K.

No fishtail behaviour is present after this oxygenation treatment. Re-annealing the same crystal similar to the standard oxygenation (510 °C, under 1 bar oxygen), leads to the reappearance of the fishtail anomaly already after a short re-annealing time of only half an hour. If the crystal is further annealed at this temperature the maximum in the reversible magnetisation, which has been re-established at a value of around 3.3 Tesla shifts to lower field values of about 1.5 T for an annealing time of 160 hours, however the height of the maximum increases indicating a increase in the critical current. Again, according to Lindemer the overall oxygen content of the sample has the same value of 6.92 for the 3 treatments.

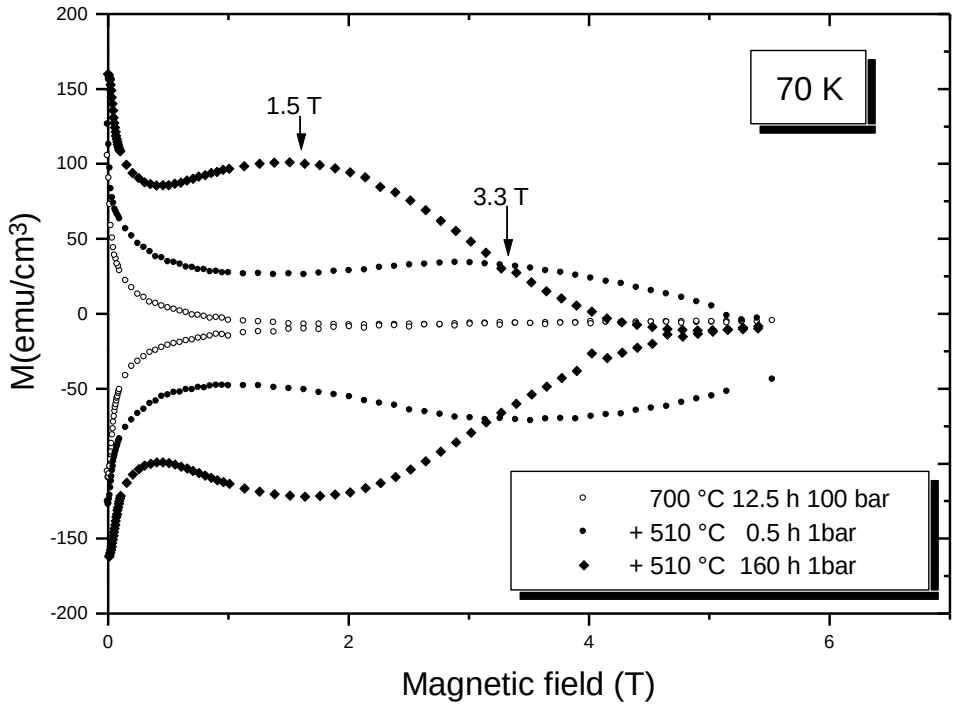

Fig. 5.7 Magnetisation of $YBa_2Cu_3O_{6.92}$ after different annealing regimes. The fishtail anomaly is re-established already after short annealing times and moves to lower field values for longer anneals.

This time evolution of the anomaly is a direct confirmation of the earlier interpretation of clusters of oxygen vacancies being responsible for the fishtail effect. At temperatures as high as 700 °C the oxygen deficient regions are more likely to be randomly distributed, while at lower temperatures a clustering effect of oxygen deficient unit cells tend to cluster due to the smaller contribution of the entropy term to the free energy. Thus, by re-annealing the crystals the clusters will form, however their size and mean distance depends on the re-annealing time, forming small clusters with small distances between them for short times anneals, which grow to larger size with larger distances between them for longer anneals. Since pinning of vortices is most effective if the distance between vortices corresponds to the mean distance of the pinning centers, e.g. the oxygen vacancy clusters we find for the short re-annealing times a maximum at higher fields (3.3 Tesla). This maximum is shifted to lower fields for longer annealing times, when clusters grow making their average distance larger. That the amplitude of the maximum increases with increasing re-annealing time is a further indication that the

clusters grow – small clusters will only produce a shallow pinning potential while the bigger clusters after long time anneals produce deeper pinning potentials increasing the maximum critical current.

A simple calculation defining the maximum of the anomaly as a matching field enables us to calculate the average spacing in between the oxygen vacancy clusters. Doing this we find a spacing of about 25 nm for a matching field of 3.3 T or 37 nm for the maximum at 1.5 T respectively. Assuming that all vacancies present within the space between the clusters would contribute to its formation one calculates for the present concentration of $YBa_2Cu_3O_{6.92}$ that the around 350 vacancies are in a clustered state after the short term annealing, thus we find a upper limit for the size of cluster being about 18 x18 unit cells. For longer annealing these clusters would then contain some 750 vacancies, setting the upper limit for cluster sizes to 27 x 27 unit cells.

That such a short range reorganisation of the vacancies is indeed possible can be seen by calculating the effective diffusion length, using the diffusion coefficients measured on identical samples [Erb96a, Kläser]. With the self diffusion coefficient, defined as the chemical diffusion coefficient divided by the thermodynamic factor, the chemical diffusion coefficient at 510 °C being 8×10^{-8} cm^2/s and the thermodynamic factor having a value of about 10 [Conder,Faupel] an estimation of the effective diffusion length for the short re-annealing of half an hour using the Einstein formula $d_{eff} = \sqrt{6D_{self}(T)t}$ yields an possible migration of vacancies of about 90 μm - far more than needed.

5.3.3 Positron annihilation studies

The small size of the clusters of interest strongly limits the tools to probe or image such local variations. On the other hand, even methods which have in principle the spatial resolution like TEM must be disregarded, because the sample preparation for TEM measurements most probably destroys the oxygen ordering, because of its high mobility. Positron annihilation spectroscopy (PAS), however, is a site-sensitive method, the annihilation characteristics being dependent of the neighbourhood of the positron at the annihilation time [Dupasquier]. In YBCO, the positron density is large only between the CuO chains, therefore PAS is well suited to investigate oxygen disorder in the chains.

For that reason $N(p_x,p_y)$ the 2-dimensional measurements of the angular correlation of the

annihilation radiation has been measured. The temperature of the twinned YBCO single crystals was 450 K to favour the thermally activated migration of the positron trapped by shallow structural defects like oxygen single vacancies [von Stetten]. Shown in Fig. 5.8 are, from bottom to top, the momentum-dependent annihilation lines $N(p_x,0)$ for a single crystal after full oxygenation ($YBa_2Cu_3O_{7.0}$), optimal doping (high pressure high temperature) and optimal doping (1 bar treatment). The curves are normalised to equal area.

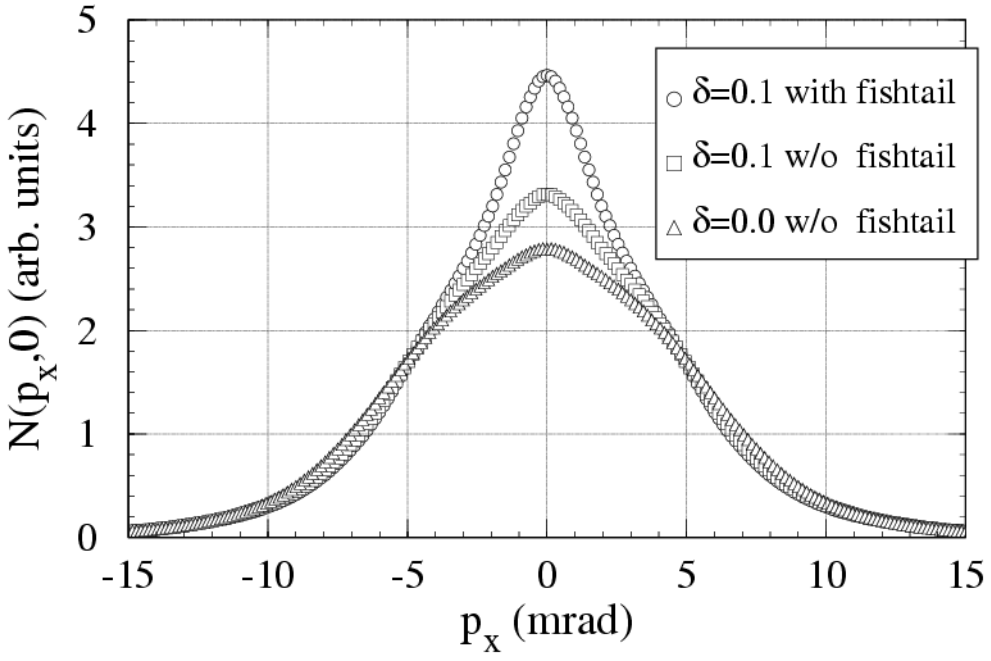

Fig. 5.8 Momentum-dependent annihilation lines $N(p_x,0)$ for a single crystal after (from bottom to top) full oxygenation ($YBa_2Cu_3O_{7.0}$), optimal doping (high pressure high temperature) and optimal doping (1 bar treatment). The curves are normalised to equal area

In metals, it is well known that the peak height of normalised $N(p_x,0)$ curves corresponds to the degree of localisation of the positron [Siegel], and is positively correlated with the positron lifetime. The same relations holds in cuprates [von Stetten]. We observe the most delocalized positrons in the case of fully oxygenated YBCO. This can be expected since, as no clusters of vacancies nor single vacancies are present, the positrons annihilate in delocalized Bloch states. In the case of optimally doped YBCO, were we expect oxygen vacancy clusters being present and where the fishtail anomaly is seen, the annihilation line is the most peaked. This is easily understandable as, when the oxygen vacancies are in large clusters [Peter], a positron trapped in a vacancy has a higher chance to find another vacancy in the

neighbourhood during its thermally activated migration and therefore annihilate in a trapped state. The curve for the optimally doped sample without fishtail anomaly lies between the two other ones, indicating a partial trapping which is attributed to vacancy clusters not large enough to act as pinning centers. For optimally doped samples the peak of the fishtail sample is about 35 % higher than that with the same overall oxygen concentration were the fishtail effect is suppressed. This correlates well with a previous measurement [Manuel] where an increase of this peak was observed when the oxygen content was changed from about 7 to < 6.2 in a crystal. This points out that in the optimally doped state with fishtail the positrons sample a local $YBa_2Cu_3O_6$ structure. This can only be achieved if the oxygen vacancies form clusters

The clear correlation we observe between the positron localisation and the presence of the fishtail strongly supports the hypothesis that the anomaly of the magnetisation is a peak effect induced by the clustering of the oxygen vacancies. One can estimate the maximum size of the cluster from positron diffusion length (about 90 nm in a metallic material), finding that the size of the cluster should be 500 – 1000 vacancies , which is in agreement with the estimation made above using matching fields.

5.3.4 NMR - studies

As a further probe to illuminate the arrangement of the oxygen vacancies Cu NMR was used. It is an appropriate method since the resonance frequency of Cu1 (chain copper) depends strongly on the co-ordination by nearest-neighbour oxygen ions. The magnetic shift and electric field gradient tensors are well-known for Cu2 (plane copper) [Pennington], $(Cu1)_4$ (copper in a filled chain, i.e. co-ordinated by four oxygen ions) [Pennington] and $(Cu1)_2$ (copper in an empty chain, i.e. co-ordinated by two apex oxygen only) [Mali].

NMR in $YBa_2Cu_3O_7$ yielded four Cu peaks (Fig.5.9a): Two of them are very narrow and correspond to the central lines ($-1/2 \leftrightarrow +1/2$ transitions) of plane Cu2 and chain $(Cu1)_4$ and the broader double peak at 102.15 MHz consists of the two satellite lines ($\pm 3/2 \leftrightarrow \pm 1/2$ transitions) of $(Cu1)_4$. The intensity of a line is given by the integral over the line and is proportional to the number of the corresponding nuclear spins. As expected from the crystal structure, the intensity of the Cu(2) central line turned out, within the error, to be twice the intensity of the $(Cu1)_4$ central line. The absence of other Cu lines indicates that the chains are perfectly filled and thus confirms the extremely low defect concentration of the fully

oxygenated crystal. In addition, a tiny signal of sodium showed up at 101.3 MHz, probably stemming from sweat in the crumpled piece of cotton wool fixing the crystal.

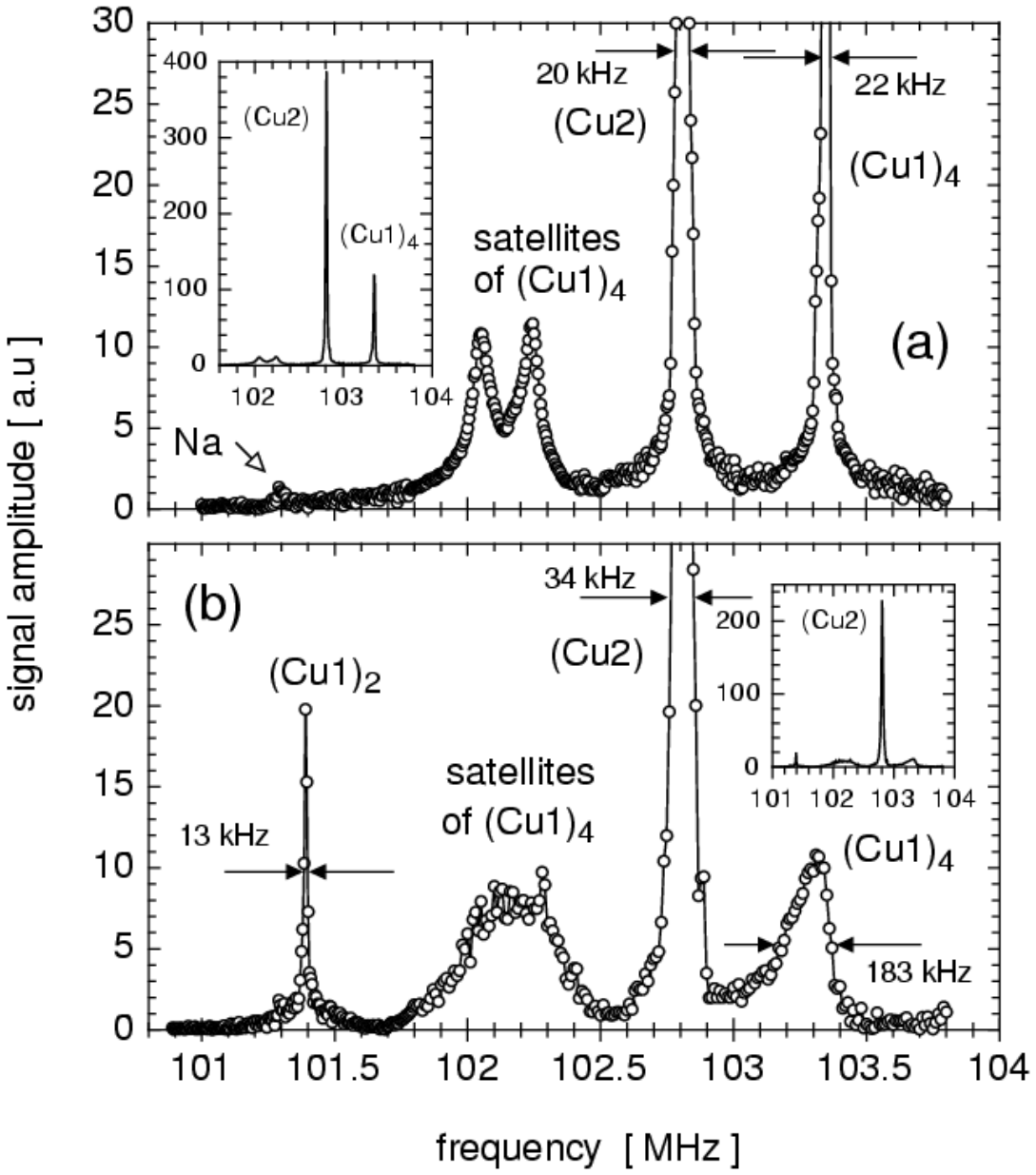

Fig. 5.9 ^{63}Cu central (and satellite) lines of different sites are shown (a) for $YBa_2Cu_3O_7$ and (b) for $YBa_2Cu_3O_{6.9}$ at room temperature. The external magnetic field (8.995 Tesla) was oriented along the c-axis of the single crystal. The indicated linewidths are defined as the FWHM. The insets show the full size of the lines.

Fig. 5.10 shows the magnetisation curves of the same crystal at the 2 oxygenation states under investigation.

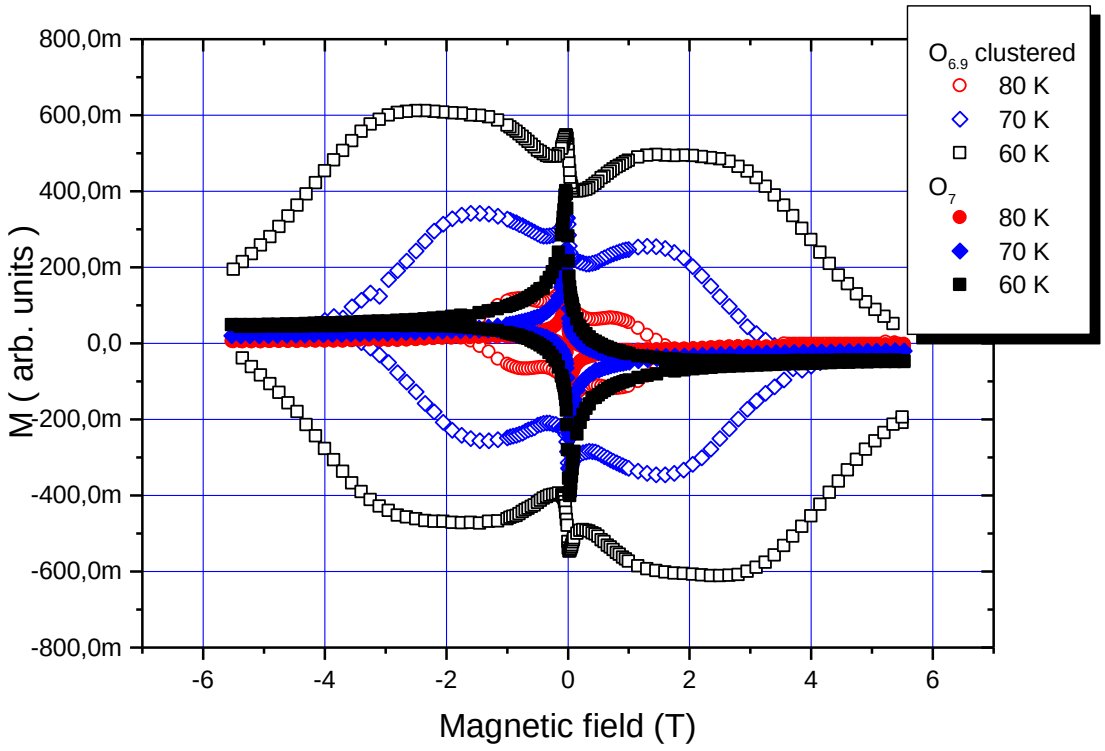

Fig. 5.10 Magnetisation curves at 60,70 and 80 K of $YBa_2Cu_3O_x$ - single crystal AE276G after full oxygenation to a O_7 (empty symbols) and $O_{6.90}$ (full symbols)

In $YBa_2Cu_3O_{6.9}$, annealed at 510 K, the lines discussed above become much broader (Fig.5.9b). Furthermore, a new signal appears at 101.4 MHz that corresponds to chain $(Cu1)_2$. By comparing the intensities of Cu2 and $(Cu1)_2$ lines corrected for their spin-spin-relaxation times and frequencies, one can conclude that along the chain 6(1)% of Cu sites have on both sides an oxygen vacancy as a neighbour(see also Fig. 5.4). Furthermore the very narrow $(Cu1)_2$ line (FWHM = 13 kHz) reveals a high degree of local order at this sites, indicating that $(Cu1)_2$ must be sitting in rather large empty chain clusters. Formation of such large clusters would also explain why a $(Cu1)_3$ (chain copper site that has only one oxygen vacancy as a neighbour) signal is absent. $(Cu1)_3$ sites appear at the interface between filled and empty chain segments and their relative abundance diminishes with increasing length of the empty segments. The corresponding NMR experiments with $YBa_2Cu_3O_{6.9}$ and suppressed fishtail are in progress.

5.4 Influence of metallic impurities

To further investigate the influence of other impurities and to clarify the question why the presented observations have not been made earlier, a test on a single crystal grown in a Yttrium stabilised ZrO_2 crucible (FZY) - the crucible material most commonly used for growing 123 single crystals - has been performed. Starting materials were of 99.5 % purity, which is also common for the crystal growth of this compounds. A crystal grown in such an FZY crucible was oxygenated together with a single crystal grown in $BaZrO_3$ under high pressure / high temperature conditions (700 °C, 20 h under 100 bar of oxygen) and the magnetisation curves were again measured at 70 K.

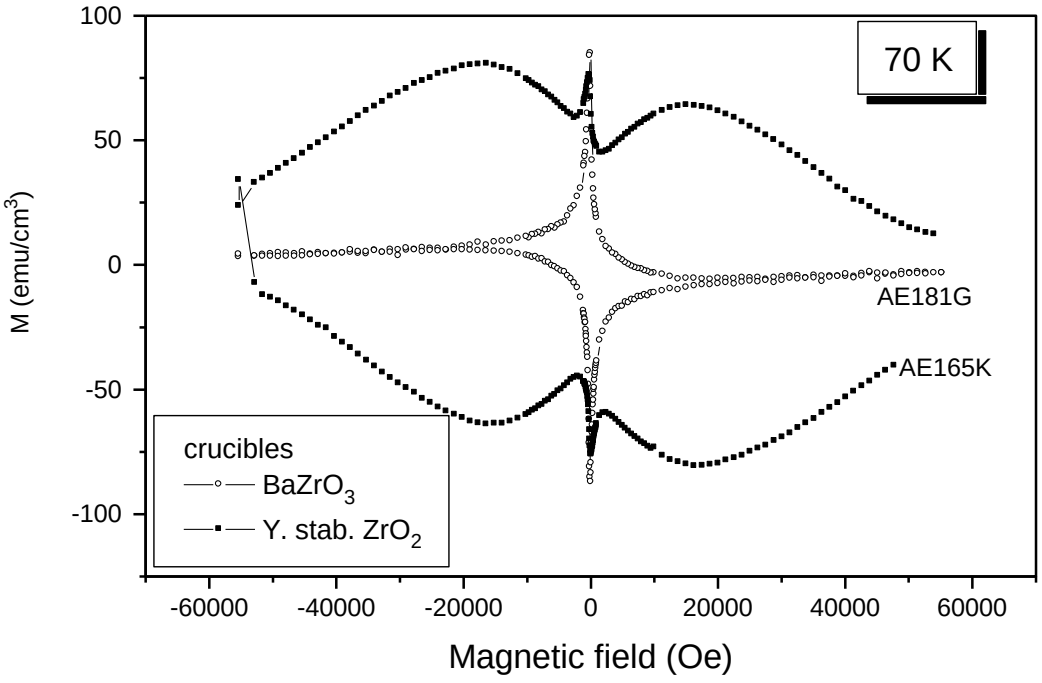

Fig. 5.11 . Magnetisation of $YBa_2Cu_3O_{6.91}$ with different impurity level after high pressure high temperature annealing (700 °C, 20 hours, 100 bar)

As shown in Fig 5.11, the crystal grown in a FZY crucible still exhibits the normal fishtail behaviour while the crystal grown in a $BaZrO_3$ crucible does not show this anomaly. Since crystals grown in a FZY crucible exhibit a purity of at best 99.9 %, one must conclude that a sufficient amount of impurities contained in these crystals, prevents the suppression of the

fishtail effect. This can be either be due to the blocking of a free mobility of oxygen by a 3^+ ion on a Cu –chain site like in the case of aluminium or by formation of precipitations of impurity rich phases like in the case of doping with gold or platinum [Storey]. It follows that the fishtail effect and the correlated strong pinning in less pure samples has two different sources, i.e. the local oxygen distribution and the presence of metallic impurities. Both effects can be superposed and influence each other.

5.5 Conclusions

As presented in this chapter 3 different and complementary measurements give evidence that the formation of oxygen vacancy clusters is the origin of the fishtail anomaly in $YBa_2Cu_3O_{7-\delta.}$ Note that the single vacancies or point defects can not be responsible for this anomaly, since it can also be suppressed in the optimally doped state where vacancies are present. It is thus necessary that a formation mechanism leading to larger, but still microstructural inhomogeneities must be responsible for this effect. In the case of $YBa_2Cu_3O_{7.0}$ the anomaly is always absent unless the crystals contain metallic impurities.

For application purposes the understanding of the formation mechanism offers the possibility to tailor the samples according to the required properties influencing the maximum value of the critical current and the irreversibility field.

References:

[Däumling]

M. Däumling, J. M. Seuntjens, D. C. Larbalestier, Nature 346 (1990) 332

[Hergt]

R. Hergt , R. Hiergeist, A. Köhler, M. Zeisberger, A. Erb, Physica C 235-240, (1994) 2751

[Lubkin]

G. B. Lubkin , Physics Today (March1996) 48

[Grasso]

Giovanni Grasso , Thesis No 2962 (1998) University of Geneva Switzerland

[Abulafia]

Y. Abulafia, A. Shaulov, Y. Wolfus, R. Prozorov, L. Burlachkov, Y. Yeshurun, D. Majer, E. Zeldov, H. Wühl, V.B. Geshkenbein, V.M. Vinokur

Phys. Rev. Lett. 77 (1996) 1596

[Klein]

L. Klein, E. R. Yacoby, Y. Yeshurun, A. Erb, G. Müller-Vogt, V. Breit, H. Wühl

Phys. Rev. B 49 (1994) R4403

[Livingston]

J. D. Livingston, Appl. Phys. Lett. 8 (1966) 319

[Erb96]

Erb, J.-Y. Genoud, F. Marti, M. Däumling, E. Walker and R. Flükiger, J. of Low Temp. Phys. 105, (1996) 1023

[Erb97]

A. Erb, J. –Y. Genoud, M. Dhalle, E. Walker, R. Flükiger, Physica C 282-287 (1997) 2145

[Genoud]

J.-Y- Genoud, A. Erb, B. Revaz and A. Junod Physica C 282-287 (1997) 457

[Erb97a]

Andreas Erb, Jean-Yves Genoud, Marc Dhalle, Frank Marti, Eric Walker and René Flükiger Applied Superconductivity 158 (1997) 1109 ,Institute of Physics Publishing, Bristol and Philadelphia

[Erb99]

Andreas Erb, Alfred Manuel, Riccardo Pozzi, Mihael Mali, Marc Dhalle, Frank Marti, Jean - Yves Genoud , Bernard Revaz, Alain Junod, Dharmavaram Vasumathi, Shoji Ishibashi , Abhay Shukla , Eric Walker, Øystein Fischer, Detlef Brinkmann and René Flükiger Submitted to Solid State Comm. (March 1999) , cond-mat/9805222

[Lindemer]

T. B. Lindemer, J .F. Hunley, J. E. Gates, Jr. A.L.Sutton, J. Brynestad, C. R. Hubbard and P. K. Gallagher, J. Am. Ceram. Soc., 72, (1989) 1775

[Vargas]

J. L. Vargas and D. C. Larbalestier, Appl. Phys. Lett. 60, (1992) 1741

[Semenovskaya]

S. Semenovskaya and A.G. Kachaturyan Phys. Rev. B 46, (1992) 6511

[Erb96a]

A.Erb, B. Greb and G. Müller-Vogt, Physica C 259 (1996) 83 - 91

[Kläser]

M. Kläser, J. Kaiser, F. Stock and G. Müller-Vogt, A. Erb, Physica C 306 (1998) 188

[Conder]

K. Conder and Ch. Krüger, Physica C 269 (1996), 92-98

[Faupel]

F. Faupel et al. Z. Metallkd. 84 (1993) 8

[Dupasquier]

A. Dupasquier and A.P. Mills jr, ed., Positron Spectroscopy of Solids (OPS Press, Amsterdam, 1995)

[von Stetten]

E.C. von Stetten, S. Berko, X.S. Li, R.R. Lee, J. Brynestad, D. Singh, H. Krakauer, W.E. Pickett and R.E. Cohen, Phys. Rev. Lett., 60, 2198 (1988)

[Siegel]

R.W. Siegel, Experimental study of defect states in metals and alloys, in Lecture Notes in Physics 283, M. Yussouff, ed., (Springer, Berlin, 1987) p. 364.

[Peter]

M. Peter, A. Shukla, L. Hoffmann and A.A. Manuel, Nuova Acta Leopoldina NF 72, Nr. 294, p. 257 (1996); A. Shukla, PhD thesis Nr. 2744, University of Geneva, unpublished (1995)

[Manuel]

A.A. Manuel et al., to be published.

[Pennington]

H. Pennington, D. J. Durand, C. P. Slichter, J. P. Rice, E. D. Bukowski, and D. M. Ginsberg, Phys. Rev. B **39**, 2902 (1989)

[Mali]

M. Mali, I. Mangelschots, H. Zimmermann, and D. Brinkmann, Physica C 175, 581 (1991)

[Storey]

B. G. Storey et al. Physica C 246 (1995) 46

6. Fishtail anomaly in the RE - 123 Compounds - Magnetisation Measurements as a probe for disorder

6.1 Introduction

As we have seen in the former chapter, the fishtail anomaly and thus pinning in $YBa_2Cu_3O_{7-\delta}$ can be suppressed and re-established by appropriate annealing procedures with or without changing the overall oxygen content. As already mentioned in chapter 3 additional complications occur for other rare earth 123 - systems due to inhomogeneities in the metal sub-lattice. These additional complications have different sources both leading at the end to increased pinning, sometimes with well separated second maxima in the magnetisation curves, making these compounds very interesting for the technical use. Especially the light rare earth elements like Nd, Sm, and Eu as well as mixtures of those have gained great interest due their superior critical currents, their somewhat higher T_c as well as their higher irreversibility fields when compared with $YBa_2Cu_3O_{7-\delta}$. Several different explanations have been proposed to explain those superior properties- in this applied research field all based on microstructural inhomogeinities. One of the problems in these explanations is that very often they can not be verified or falsified because in most cases several parameters are changed at the same time, mainly due to problems in sample preparation. Having solved the problems with sample preparation and with the effect of oxygen vacancies on pinning and the fishtail effect it was consequent to expand the studies on the rare earth 123 compounds using magnetisation measurements as a tool to probe local disorder on scales comparable to the coherence length – a length scale not easily accessible by other means.

6.2 Substitution of Ba by RE : Disorder of the type $RE_{1+x}Ba_{2-x}Cu_3O_{7-\delta}$

Unlike in the case of $YBa_2Cu_3O_{7-\delta}$, which has well defined stoichiometry and no solid solutions of the type $RE_{1+x}Ba_{2-x}Cu_3O_{7-\delta}$ are formed, the light rare earth elements do form such solid solutions due to the fact that the ionic sizes of the RE atoms increase when the atomic number decreases and becomes more comparable to the Ba atom. Fig. 3.2 in chapter 3 shows a schematic phase diagram explaining this situation . While for the Y and the heavier RE atoms the 123 compound is a fixed point in this phase diagram the lighter RE – 123 form solid solutions of the form $RE_{1+x}Ba_{2-x}Cu_3O_{7-\delta}$ so that the light rare earth 123 compounds are now represented by a line in the diagram. The value of x in this compounds can be varied either by lowering the oxygen content of the atmosphere during the synthesis [Nakamura1] or by changing the ratio of BaO/CuO in the flux in a way that the 123 ratio for the compound can be retained [Yao]. Both methods are somewhat equivalent since lowering the oxygen content leads to a partial reduction of CuO to Cu_2O, thus changing the BaO/CuO ratio. This, however, has the disadvantage that one changes not only the x value of the resulting compound but also the present phases in the composition diagram. Nevertheless, the reduction of the oxygen partial pressure is reported to lead to a reduction of the x value in the RE –123, as it is sketched by the red lines in Fig 3.2. The surplus of Nd in the 123 – compound is then thought to produce Nd - rich precipitates in the samples, again turning the samples granular [Murakami] – this time as a consequence of disorder on the metal sub-lattice. Such Nd rich regions have been observed by TEM measurements [Egi] and by STM –measurements [Ting]. These regions were reported to be oval clusters of about 10-30 nm in diameter finely dispersed in the matrix of undisturbed Nd –123; a size very suitable to act as a pinning center. While this interpretation for Nd rich samples is most probably correct, it is difficult to understand why also stoichiometric Nd-123 should show structured magnetisation curves with more than one maxima in the magnetisation curve like shown in Fig 6.1. Beside the compared to Y-123 somewhat increased absolute critical currents the main difference of this sample, which had the nominal composition of 1:2:3 according to

EDX measurements, is that the maximum in the j_c curves is rather broad with a structure suggesting 2 maxima .

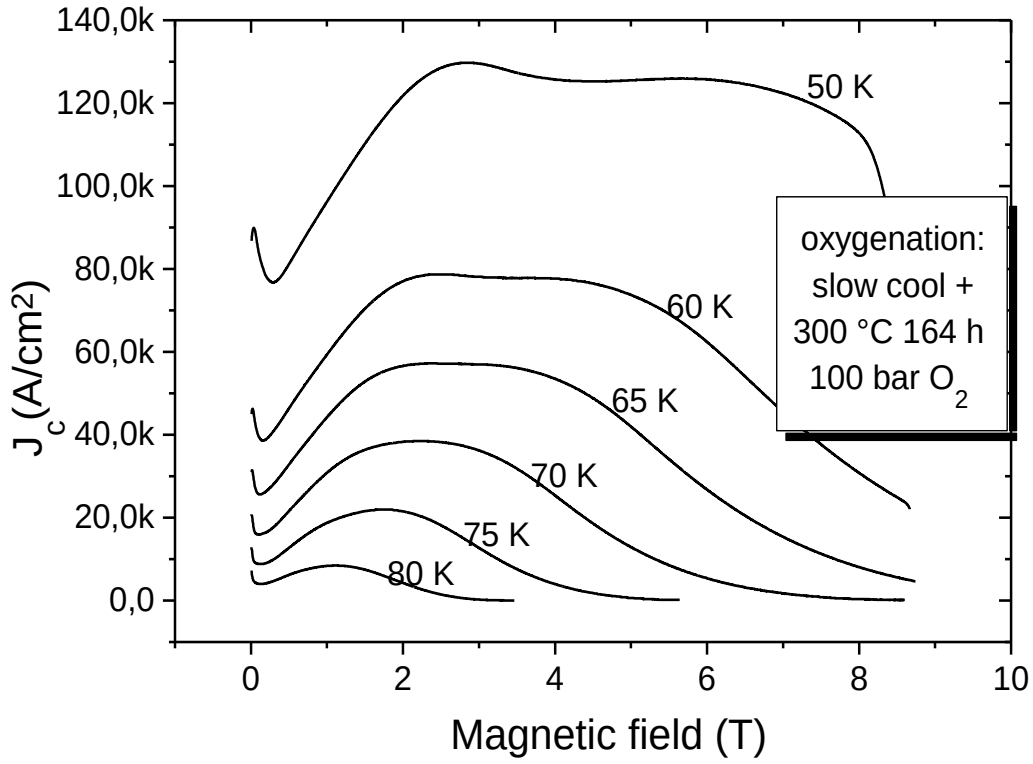

Fig. 6.1 Critical currents for a $NdBa_2Cu_3O_{7-\delta}$ single crystal (AE159G)

To understand this behaviour in stoichiometric or near stoichiometric compounds another mechanism than precipitation of the surplus of Nd in a undisturbed matrix of Nd-123 needs to be present.

6.3 Spinodal decomposition of the light rare earth $REBa_2Cu_3O_{7-\delta}$ compounds:

Disorder of the type $RE_{1-x}Ba_x(Ba_{1-x/2}RE_{x/2})_2Cu_3O_{7-\delta}$

This type of disorder has been proposed by Nakamura et al. [Nakamura2] as being present in the light rare earth 123 systems. The Nd 123-system may here serve as an model compound, which has the advantage that superconducting samples may be more easily obtained and that in this case measurements of the irreversible magnetisation can serve as a probe of the local

microstructure [Erb97a,Nakamura2]. Fig. 6.2 illustrates the nature of a spinodal decomposition.

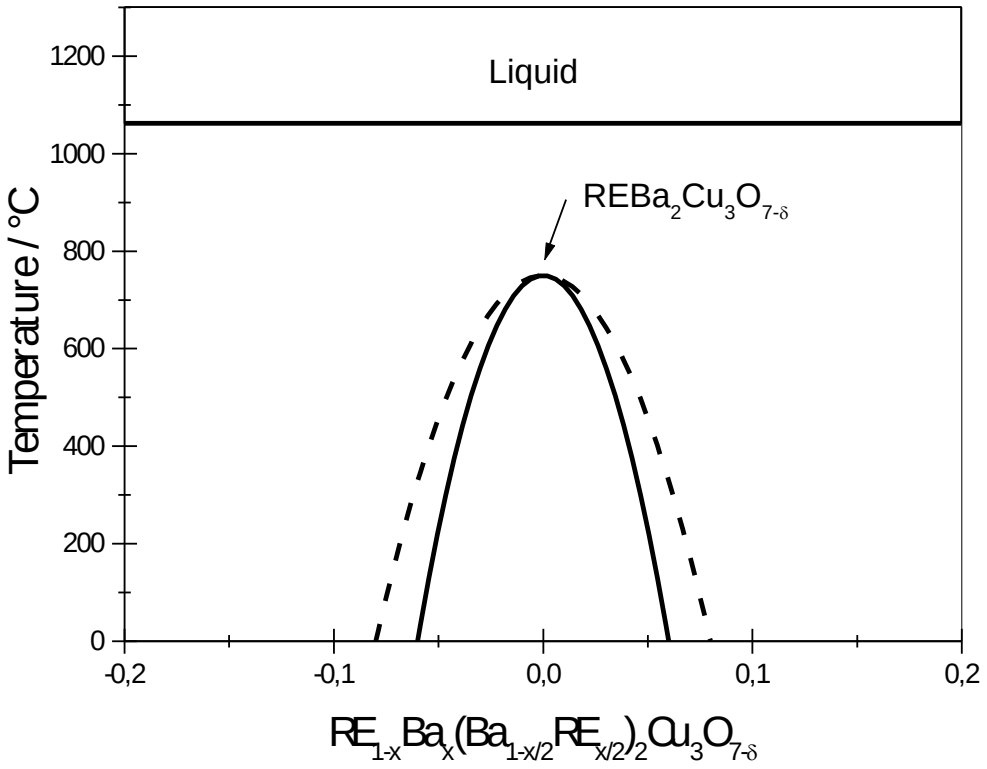

Fig 6.2 Spinodal decomposition of the Light rare earth 123-compounds

Light rare earth 123-compounds, like Nd and Sm , show an intrinsic tendency to produce a local variation in the metallic sublattice upon cooling. This local variation of the concentration on the Ba and RE site does not alter the overall 123 composition and can be described in terms of a spinodal decomposition of these compounds, where Ba partially occupies RE sites and vice versa. Since the overall stoichiometry is unchanged it impossible to be detect this microstructural inhomogeneity by integral EDX-measurements and does also not conflict with the neutron diffraction results obtained by Merz et al. [Merz,Schweiss] on $NdBa_2Cu_3O_{7-\delta}$ and $PrBa_2Cu_3O_{7-\delta}$ samples.

Such a spinodal decomposition produces a local off-stoichiometry of the type $RE_{1-x}Ba_x(Ba_{1-x/2}RE_{x/2})_2Cu_3O_{7-\delta}$ as sketched in Fig. 6.3. Here a spatial variation of the Nd / Ba ratio is hypothetically shown for a sample. Primary results for Nd-123 of the ISTEC group

[Shiohara] using and EDX mounted in transmission electron microscope seem to justify this drawing.

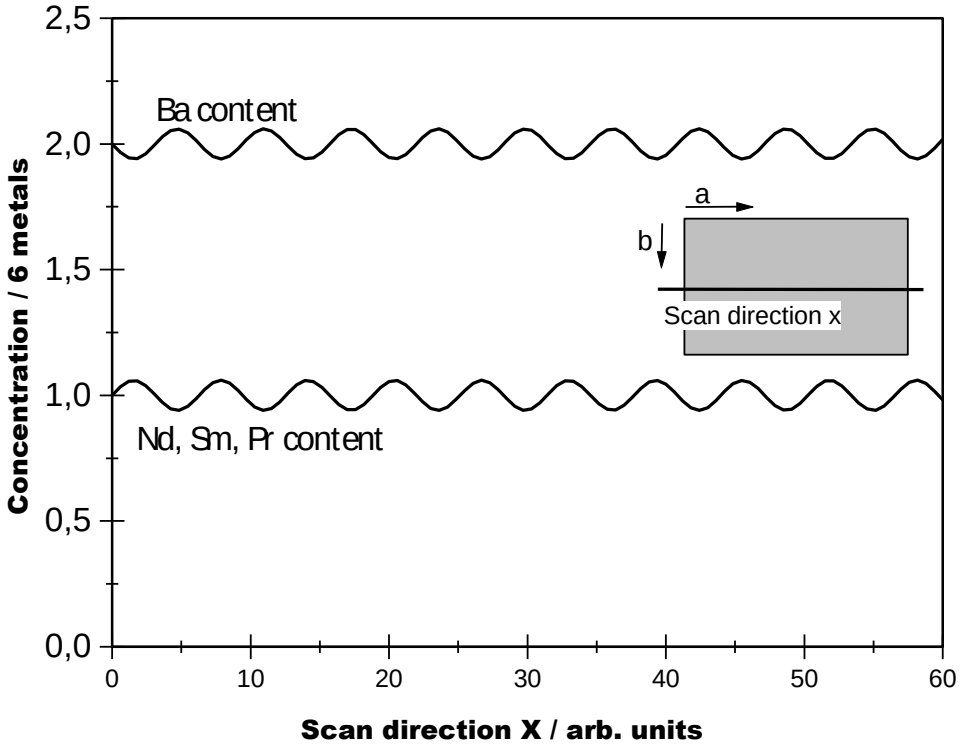

Fig 6.3 Spinodal decomposition of the Light rare earth 123-compounds

The local variation of the Nd to Ba content may again be responable for the increased pinning in this compounds.

As an test for this explanation and the presence of such an spatial variation a stoichiometric sample of Nd- 123 (the same sample shown in Fig, 6.1) was reannealed at a temperature above 700 °C and subsequently quenched to room temperature. This treatment has again been performed in 100 bar of oxygen to maintain an oxygen content close to 6.9 and to suppress the fishtail effect caused by oxygen vacancy clustering. As one would expect from Fig.6.2 the spinodal decomposition does not occur in that case because, due to quenching, it is kinetically hindered.

Fig. 6.4 shows the magnetisation curves after this treatment. Apparently there is no or only a minor anomaly left after this treatment. However, the high temperature annealing (700 °C

20 h 100 bar O_2) which is suitable to suppress both the oxygen clustering as well as the spinodal decomposition of the Nd 123 system lowers T_c to only about 50 K in the case of the Nd system.

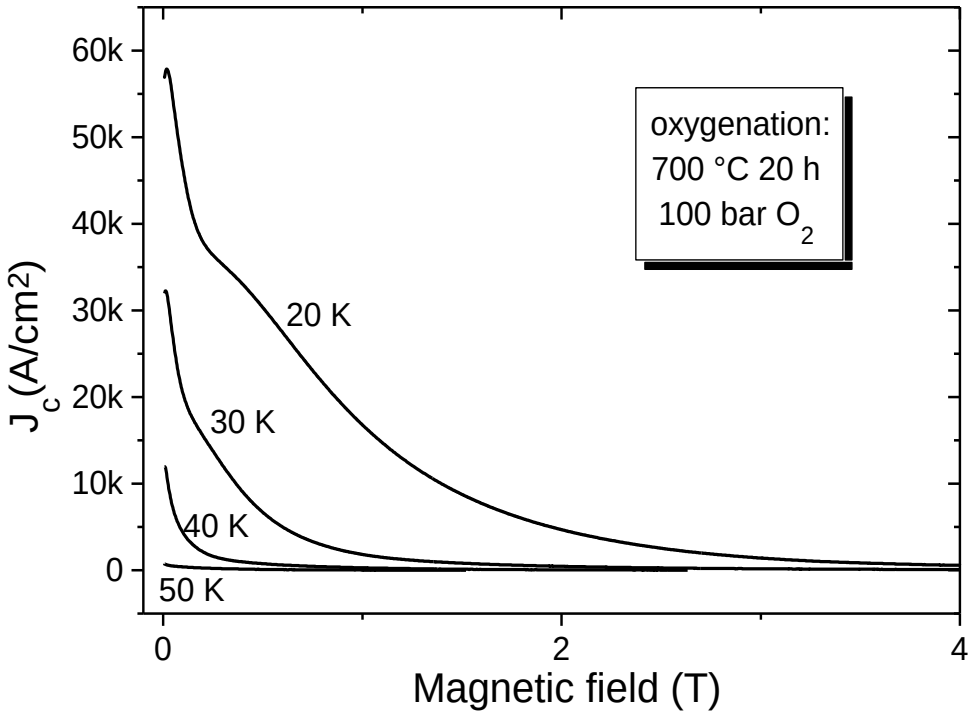

Fig. 6.4 Critical currents for a $NdBa_2Cu_3O_{7-\delta}$ single crystal (AE159G)

Hence, the oxygen content has to be raised by a further annealing treatment at low temperature to increase the transition temperature.

The result of such an annealing at 320 °C 100 bar, which rises the oxygen content and the T_c again back close to the original values is compared with the original state after the slow cooling and subsequent low temperature annealing of 300 °C, 100 bar (dashed lines) in Fig. 6.5. The remarkable differences not only in the absolute values of j_c but also in the irreversibility fields seems to be solely due to the slow cooling process during which the spinodal decomposition should occur. When this spinodal decomposition is suppressed by quenching through the temperature region where the metals are still sufficiently mobile, the Nd –123 compound looses its most effective pinning mechanism. Evidently the low oxygenation temperature does not allow the metal atoms to change site and to re-establish the state with a local inhomogeneity of the metallic sublattice, since the high J_c values at

higher fields are not re-established. This is explained by the fact that the site change of metallic ions requires a markedly higher activation energy than the diffusion of oxygen.

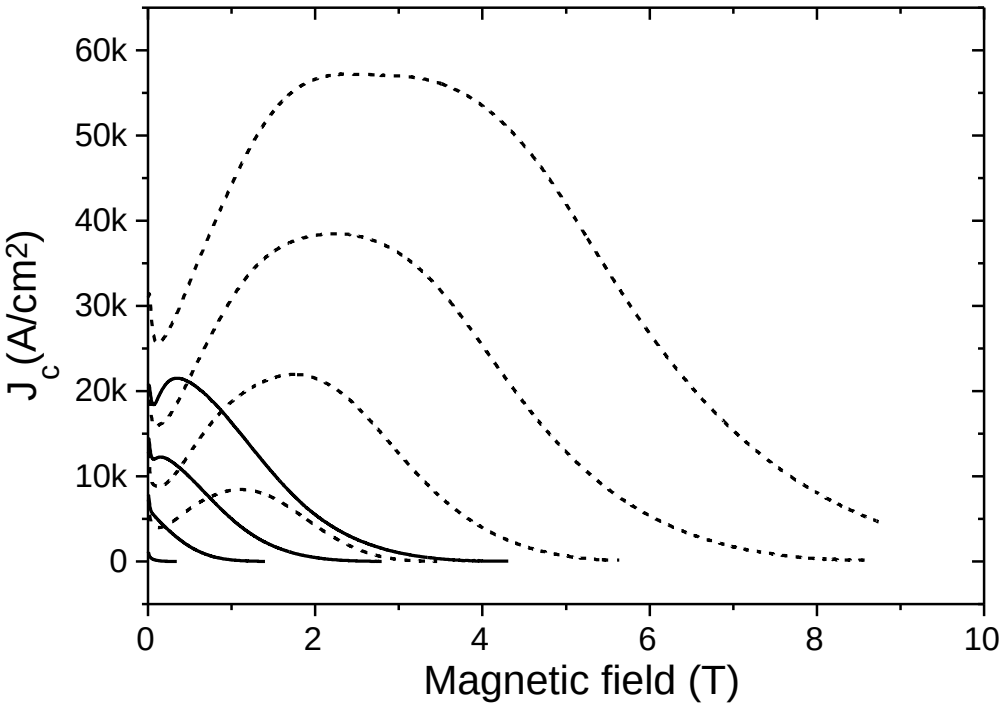

Fig.6. 5 Critical currents for a $NdBa_2Cu_3O_{7-\delta}$ single crystal (AE159G) after different annealing regimes. J_c at 65, 70, 75 and 80 K(see text)

This systematic study on the $NdBa_2Cu_3O_{7-\delta}$ system strongly supports the idea of an spinodal decomposition in the light rare earth compound. It can be followed from Fig. 6.5 that this disorder mechanism can be as effective or even more effective on pinning of the vortices than the oxygen clustering in systems like $YBa_2Cu_3O_{7-\delta}$ or $ErBa_2Cu_3O_{7-\delta}$, which do not show this type of disorder. Indeed for fully oxygenated $NdBa_2Cu_3O_{7-\delta}$ no influence of oxygen disorder on pinning can be expected since there are no vacancies, thus for the samples with the highest T_c one of the mechanisms producing pinning is absent and the observed pinning must thus be due to the spinodal decomposition.

For application purposes I believe that the $NdBa_2Cu_3O_{7-\delta}$ is overestimated, since serious problems in sample preparation (e.g. the formation of solid solutions with inhomogeneous T_c`s [Murakami]) as well as the very low final oxygenation temperatures (e.g. 300 °C, see also chapter 4) needed to raise T_c above 90 K overcompensate the benefit of a somewhat

increased T_c and the presence of a second disorder mechanism effective for pinning. In the following some proposals for other systems which do not have these disadvantages are presented.

6.4 $Nd_{0.41}Er_{0.59}Ba_2Cu_3O_{7-\delta}$ (RE1-RE2 123 compounds)

As mentioned above the major disadvantage of the $NdBa_2Cu_3O_{7-\delta}$ system for practical application lies in the very low annealing temperatures required for achieving the highest T_c values as one can see from Fig 6.6 , which shows the dependence of T_c for the different rare earths as a function of annealing temperature or oxygen content. As already mentioned in chapter 4 this would lead to an increase in required oxygenation time by a factor of 100 compared to Y-123 samples. Since one would like to keep the good pinning properties of the

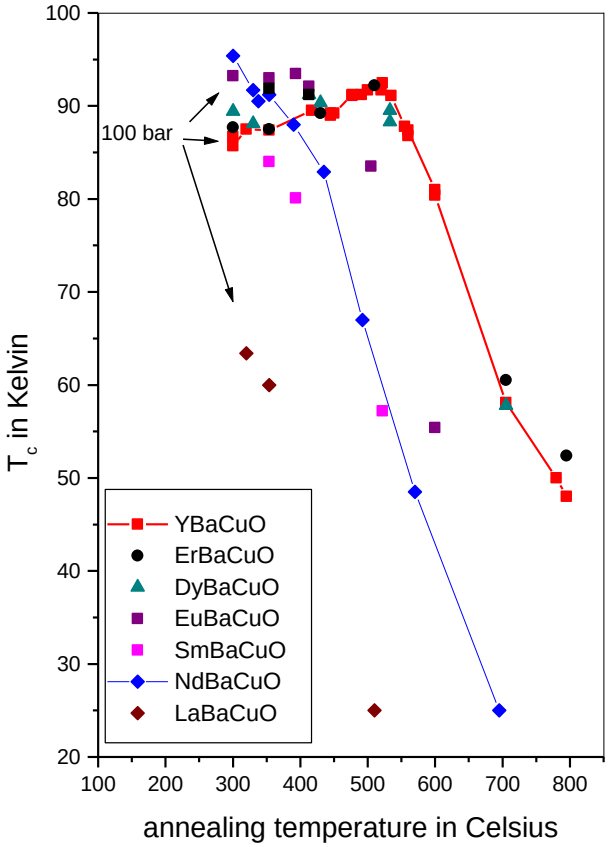

Fig. 6.6 T_c versus annealing temperature for different RE-123 compounds

Nd-123 system caused by the spinodal decomposition combined with the effects of oxygen clustering one approach is to increase the temperature were the maximum T_c is obtained

[Erb97a]. This can be done by addition of a heavier RE – element or Y. For instance the doping of the Nd system with Er leads to an pronounced increase of T_c for the same annealing temperature when compared to the pure Nd system as it can be already expected from Fig.6.6 For the strongly doped $Nd_{0.41}Er_{0.59}Ba_2Cu_3O_{7-\delta}$ single crystal we obtain a T_c of 89 K after oxygenation at 460 °C. This doping increases not only the final oxygenation temperature but also shifts the compound back into a region were optimal T_c is found when oxygen vacancies are present allowing both pinning mechanisms being present. The curves for the critical currents are shown in Fig. 6.7 for the same temperatures than those of the pure Nd-123 crystal presented in Fig.6.5.

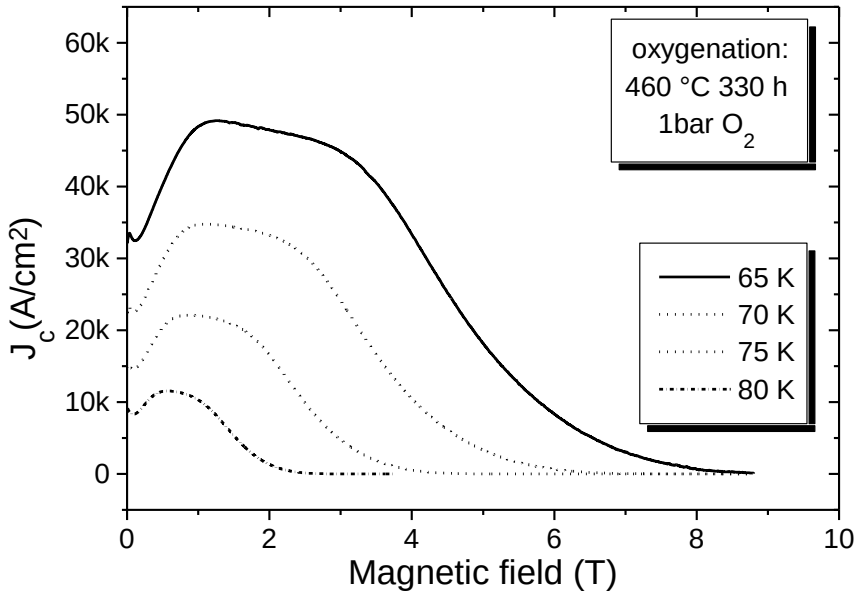

Fig. 6.7 : $Nd_{0.41}Er_{0.59}Ba_2Cu_3O_{7-\delta}$ single crystal, j_c- curves

While the J_c values and irreversibility fields are comparable to those for the pure $NdBa_2Cu_3O_{7-\delta}$ single crystal the diffusion coefficients are raised by more than an order of magnitude, hence avoiding the major disadvantage of the pure $NdBa_2Cu_3O_{7-\delta}$ system.

6.5 $EuBa_2Cu_3O_{7-\delta}$

A similar approach consists of choosing one of the rare earth elements which already show some solid solution and spinodal decomposition but where the $T_{c\ max}$ is not shifted to such

high oxygen concentrations or low annealing temperatures. The Eu –123 compound already shows a higher degree of disorder on the metal sub-lattice but does not require annealing temperatures as low as in the case of Nd-123. For single crystals of Eu-123 the maximum T_c of 93.7 K is found at an annealing temperature of 400 °C or at an oxygen content of 6.98. In Fig 6.8 the j_c curves are compared for such an Eu-123 crystal again in comparison with a Nd-123 single crystal for temperatures of 70, 75 and 80 K.

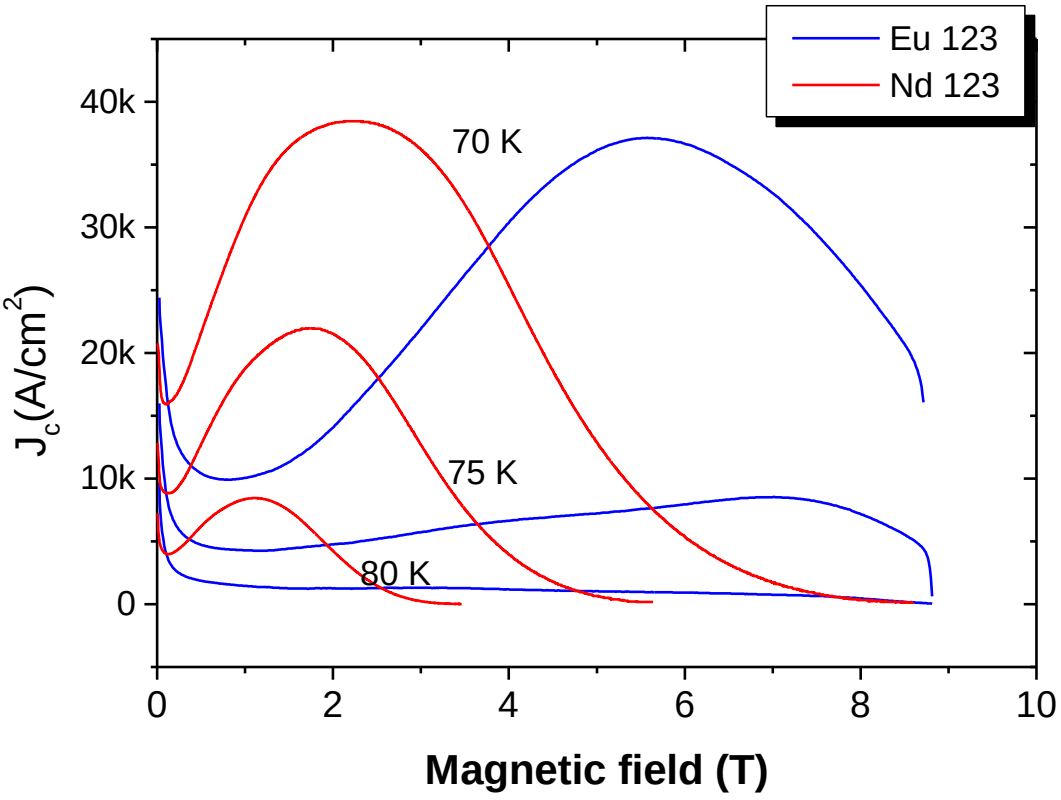

Fig. 6.8 j_c for and Eu-123 crystal (blue) in comparison with a Nd-123 single crystal (red) for temperatures of 70, 75 and 80 K.

At 70 K the maximum at the peak position has about the same value that that of Nd –123 but at even higher field which for itself is remarkable. However, as we can see from Fig. 6.9, the origin of the marked anomaly in this case is unlikely to be solely due to a spinodal decomposition or precipitation of Eu rich regions, but rather to very finely dispersed small oxygen vacancy clusters. This can be concluded since in the same crystal as used in Fig. 6.8, but oxygenated to a state close to O7 the critical currents are greatly suppressed and the curve at 70 K only shows a maximum at field values around 9 T with relatively low critical currents, which may be attributed to disorder on the metal sub-lattice. Whether the unusual

fine dispersion of the oxygen vacancies which lead to the high irreversibility fields and critical currents in Fig. 6.8 may be triggered or assisted by disorder in the metal sub-lattice is not completely clear.

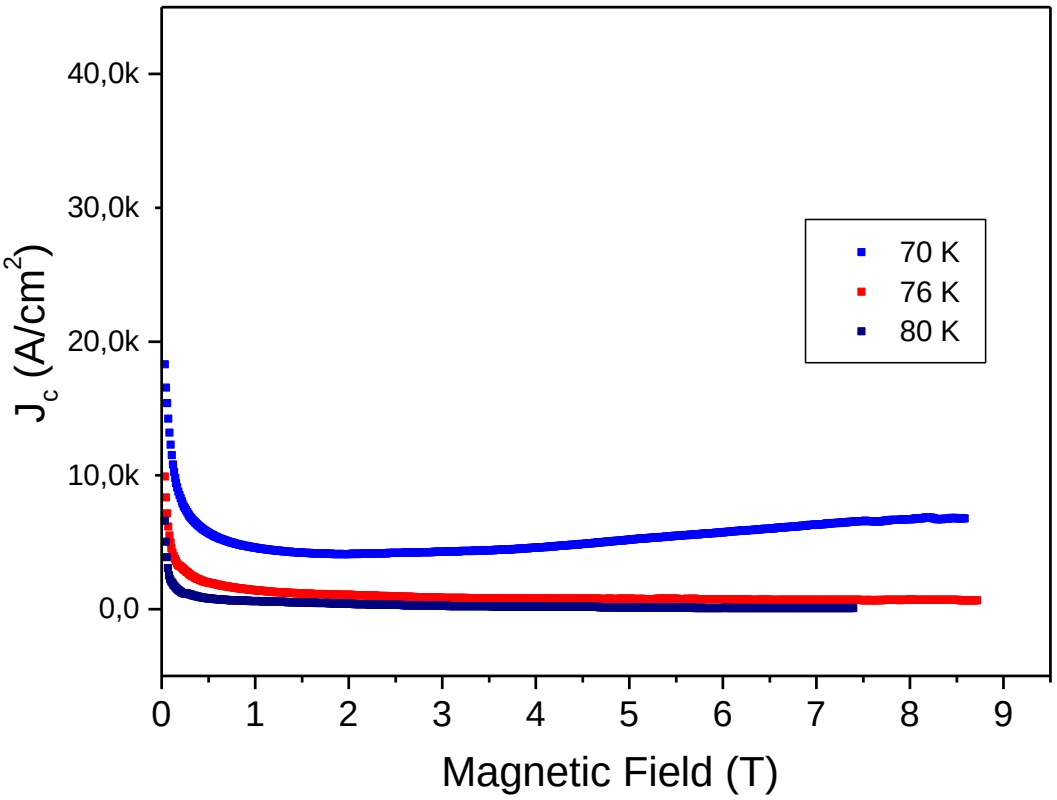

Fig. 6.9 j_c for the same Eu-123 crystal shown in Fig. 6.8 but oxygenated to a oxygen content close to O_7

References :

[Nakamura1]

M. Nakamura, M. Kambara, T. Umeda, Y. Shiohara, Physica C 266 (1996) 178

[Yao]

X. Yao, M. Kambara, T. Umeda, Y. Shiohara, Physica C 296 (1998) 69

[Murakami]

M. Murakami, N. Sakai, T. Higuchi, N. Chikumoto, D. I. Yoo, J. Low. Temp. Phys. 105 (1996) 1751

[Egi]

T. Egi, et al. , Appl. Phys. Lett. 67 (1995) 2406

[Ting]

W. Ting et al. unpublished

[Nakamura2]

M. Nakamura, Y. Yamada, T. Hirayama, Y, Ikuhara, Y. Shiohara, S. Tanaka, Physica C 259 (1996) 295

[Erb97a]

A. Erb, J-Y Genoud, M. Dhalle, F. Marti, E. Walker, R. Flückiger, Appl. Superconductivity 158 (1997) 1109 , Inst. Phys. Conf. Ser. IOP Publishing Ltd

[Merz]

M. Merz, N. Nücker, E. Pellegrin, P. Schweiss, S. Schuppler, M. Kielwein, M. Knupfer, M. S. Golden, J. Fink, C. T. Chen, V.Chatarian, Y. U. Idzerda, A.Erb, Phys. Rev. B 55, (1996) 9160

[Schweiss]

P. Schweiss, INFP Karlsruhe, private communication

[Shiohara]

Y. Shiohara, MRS fall meeting 1996 and private communication

7. Vortex Phase Diagrams of $REBa_2Cu_3O_{7-\delta}$

7.1 Introduction

It is now more then ten years ago that the discovery of the high temperature superconductors took place. At that time it was generally believed that there would be a revolution in the application of modern electronic technology and society by an increased practical use of superconducting appliances which could be operated by cooling only with the low-cost liquid nitrogen instead of the costly liquid helium. But so far no such revolution took place. What are the reasons ?

The answer lies partly in the complex chemistry and metallurgic problems which are peculiar to these oxide compounds, being brittle and chemically highly reactive, but partly also in the physics of these new compounds:

In a classical type II superconductor like Nb_3Sn the magnetic field penetrates into the superconductor (for fields above H_{c1}) in the form of a regular lattice consisting of small filaments, each one containing one quantum of magnetic flux Φ_0. In this so-called mixed state, an applied current would create dissipation, provided the lattice is allowed to flow. In the case of a flowing vortex lattice the moving vortices dissipate some of the energy in the current, thus losing the property of zero resistance. However, flux line lattice of classical superconductors is relatively stiff and the introduction of a few pinning centers for the vortices is already sufficient to pin the lattice down and hold it in place - much like a few pins would pin down a carpet.

In contrast to this behaviour the new class of high T_c superconductors misbehave in a way that the mixed state of these superconductors is divided up into different phase fields and generally the vortices which enter a superconductor first form a liquid rather than a lattice. A liquid, however, has no stiffness and can not be pinned down by just adding a few nails to fix the carpet, because there is no carpet. Thus the high T_c superconductors in the vortex liquid state do not show zero resistance because in the liquid state the vortices will flow if a current is applied. Only upon further cooling the liquid eventually freezes, then forming a lattice bringing back the feature of zero resistance. At low temperatures, the vortex lattice is a solid and thus the critical currents of the new class of superconductors are high, but if the temperature is raised above the temperature where his lattice melts the critical currents drop drastically. The melting line for Bi (2212) has been found [Zeldov] to join the

superconducting transition from 90 K, 0 T to a critical point at 37.8 K , 38 mT. (Fig.7.1) This is the reason why the technical application of this compound is actually limited.

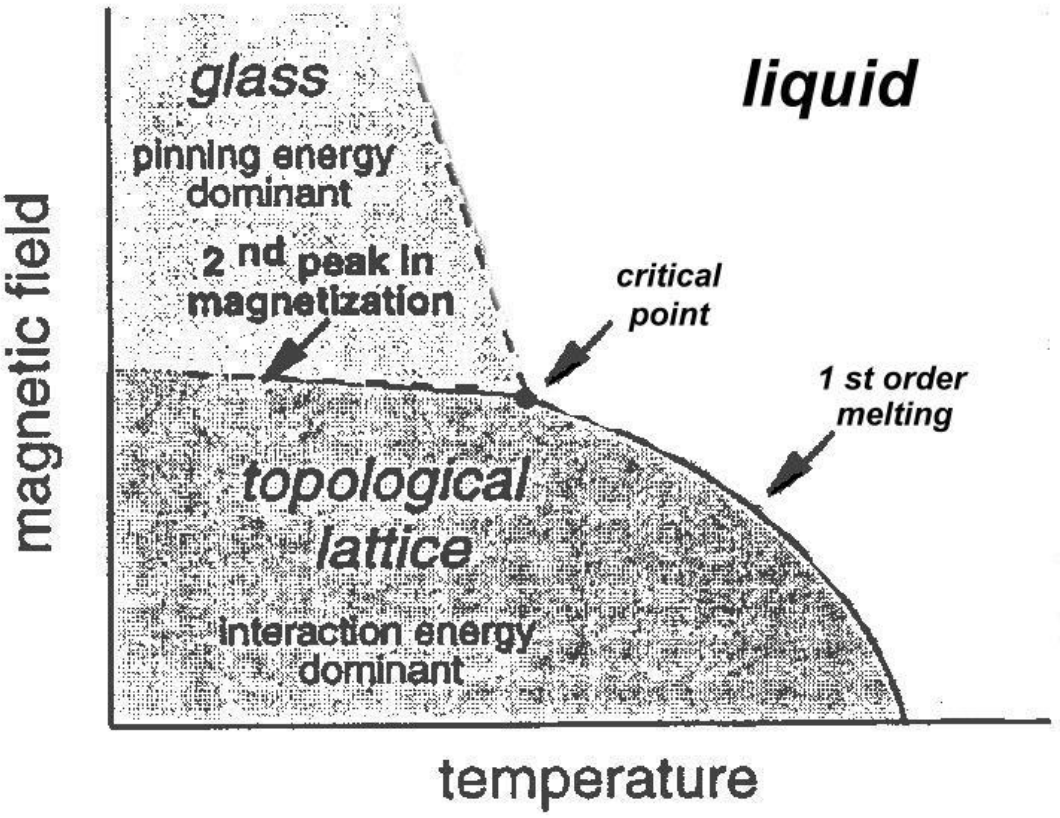

Fig 7.1 Schematic representation of the phase diagram of Bi-2212. The first order melting line, the line of irreversible second peaks in the magnetisation and the critical point is indicated. Adapted from [Crabtree]

In $YBa_2Cu_3O_{7-\delta}$ the situation is somewhat better due to the much higher melting fields. While in Bi-based superconductors the phase diagram studies are mainly performed by resistance, magnetisation and neutron diffraction experiments the much higher melting fields make the phase transitions accessible to high resolution specific heat measurements. It is the definitive proof for the transition from the vortex liquid to the vortex solid that a first order transition can be detected in specific heat measurements. From these experiments the vortex phase diagrams can be constructed – as we will see again these vortex phase diagrams are pretty much sample dependent and the influence of pinning by twin boundaries as well as the fishtail effect will be discussed with respect to some of the proposed phase diagrams from literature.

7.2 Detection of vortex lattice melting by specific heat

While most of the literature of vortex phase diagrams is based on measurements of resistivity and magnetisation the much higher density of the melting fields in $YBa_2Cu_3O_{7-\delta}$ allows the direct observation of the melting transition in specific heat measurements. Even though this was theoretically already clear since the first resistance and magnetisation experiments it took some more time to observe this transition in the specific heat. This has to do with the fact that if the vortex system is dominated by pinning on defects no intrinsic lattice will form and thus no specific heat peaks can be detected. Resistivity measurements and magnetisation measurements seem to be a bit less sensitive to pinning in respect with detection of the melting of the vortex lattice, however they are also less conclusive.

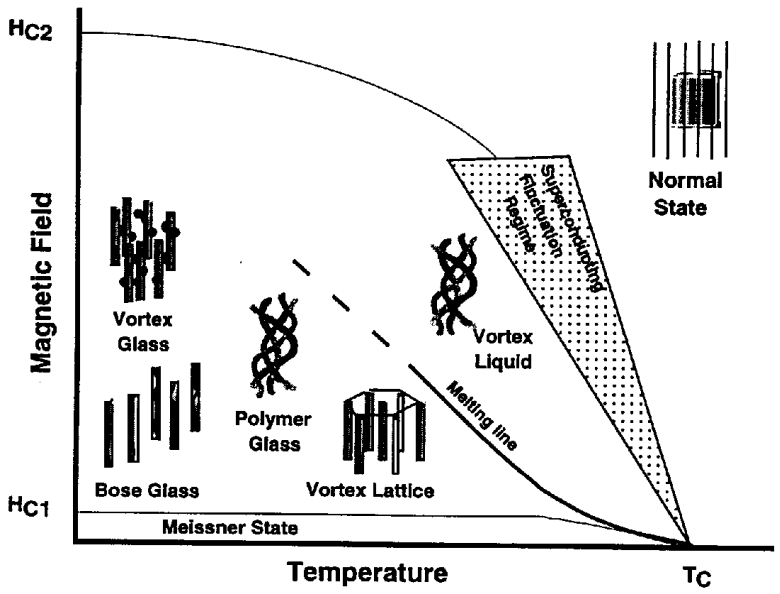

Fig. 7.2 The phase diagram of vortex matter, showing some of the proposed and established liquid, glassy and lattice phases and the transitions between them. Adapted from [Crabtree]

Vortex phase diagrams are subtle and many phases have been proposed being present below the melting line (see Fig 7.2), mostly in analogy with the proposed phase diagram of Bi-2212. While the fact of vortex lattice melting itself has been well established due to the specific heat measurements by different authors [Schilling, Roulin] it stayed unclear whether some of the proposed phases present in the solid are intrinsic or whether they are a result of microstructure. Especially the dashed line in Fig. 7.1 separating the vortex lattice from a

vortex glass has been and is still a subject of discussion. The existence or non-existence of such a line is equivalent with the presence of the so-called critical point on the melting line of $YBa_2Cu_3O_{7-\delta}$. For field values above the critical point the vortex liquid is then believed to transform into a vortex glass rather than a lattice. In that case the transition should then be of second order. There has been some support for the existence of such a point due to the fact that in the first measurements showing the first order transition in specific heat in optimally doped $YBa_2Cu_3O_{7-\delta}$ the peaks indicating the latent heat due to melting vanished at around 10 T and were not detectable above this field [Schilling]. Fig. 7.3

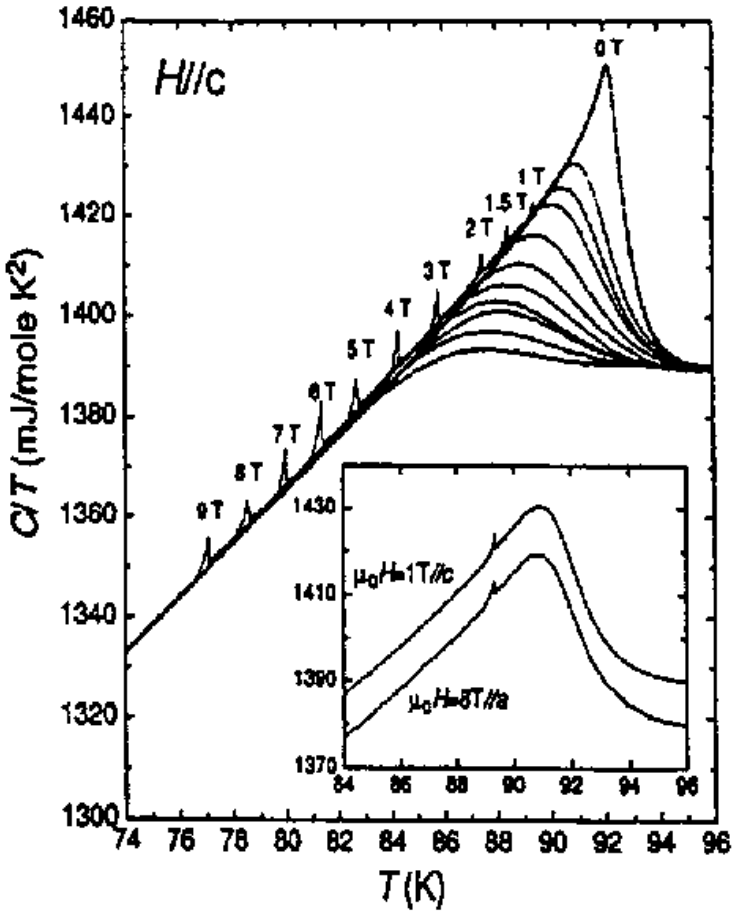

Fig. 7.3 Total specific heat of an untwinned $YBa_2Cu_3O_{7-\delta}$ crystals showing the peaks due to vortex lattice melting at the indicated fields [Schilling]

As mentioned before the existence of such a critical point on the melting line should be related to a line inside the phase diagram separating the vortex lattice from the vortex glass and some signature in magnetisation measurements should be found when crossing this phase boundary. The only signature that has been found there , however, which has been

interpreted as a signature of this phase transition is the broad fishtail effect in the irreversible magnetisation of the $YBa_2Cu_3O_{7-\delta}$ - the subject of chapter 6 and 7. Measurements of the irrversible magnetisation of $YBa_2Cu_3O_{7-\delta}$ single crystals in high field magnetic fields up to 28 T [Nishizaki] revealed a somewhat pathologic fishtail effect with a re-entrant fishtail peak at around 11-13 T. (Fig 7.4)

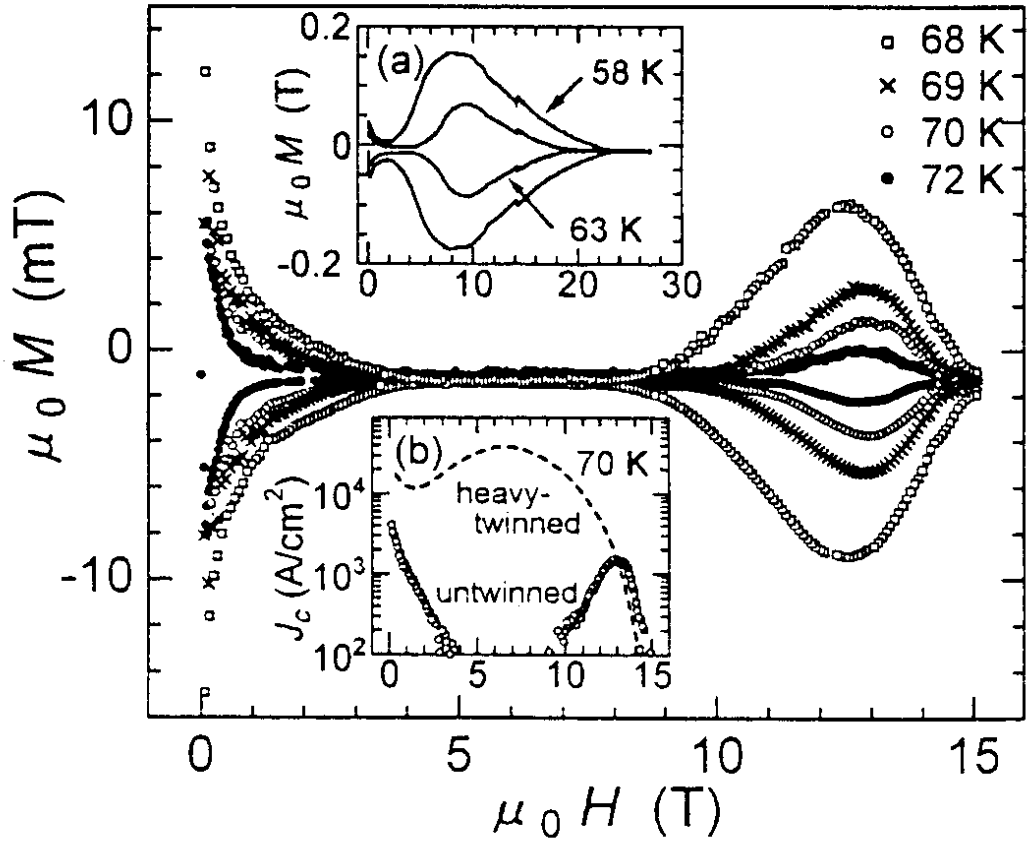

Fig. 7.4 Magnetisation curves of an untwinned $YBa_2Cu_3O_{7-\delta}$ single crystal at various temperatures [Nishizaki]

From this behaviour Nishizaki et al. [Nishizaki] concluded that this unusual fishtail peak should be the signature of the phase transition between the vortex solid and the vortex glass. Accordingly they constructed their tentative phase diagram (Fig.7.5) and attributed the peak maxima of the irreversible magnetisation to the transition from the lattice to the glassy state of the vortex system. Note that the inset of Fig. 7.4 shows the differences between a so-called heavy twinned and an untwinned sample, whole all the measurements of chapter 6 and 7 were done on twinned single crystals with the typical twin boundary spacing of 1 μm. Those measurements did not show an fishtail effect, thus the differences shown in the inset

of Fig. 7.4 are rather due to ohter effects than twins, especially since a typical average twin boundary spacing should correspond to matching fields in the region of a few tenth of Gauss.

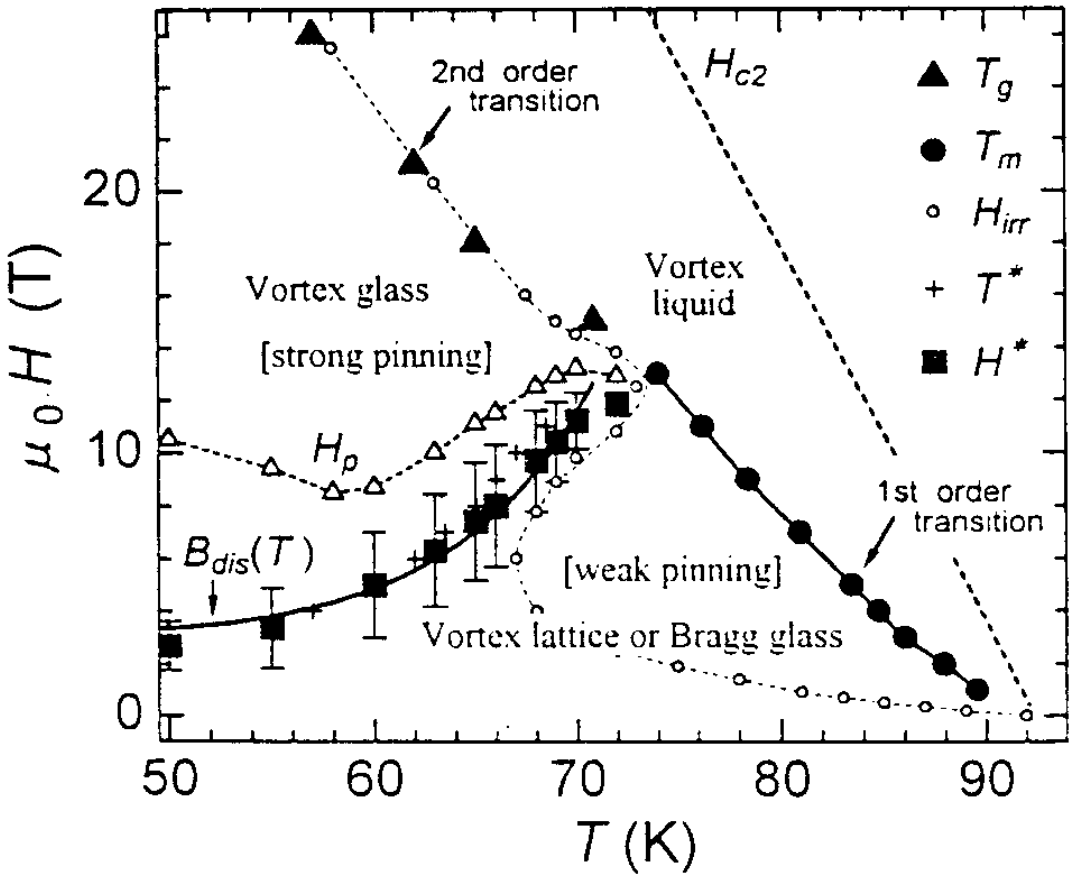

Fig.7.5 Vortex phase diagram as proposed by Nishizaki et al. [Nishizaki]. The line (H_p) separating the vortex lattice from a vortex glass is determined by the maxima of the fishtail anomaly deduced from Fig.7.4 and terminates at the multicritical point on the melting line

As we see from Fig. 7.5 the vortex phase diagram of Nishizaki et al. for $YBa_2Cu_3O_{7-\delta}$ shows some similarity with the phase diagram of Bi-2212. The critical point would, according to this diagram, lies at around 70 K, 11 T and for higher fields the liquid would transform into a glass upon cooling making the transition to one of second order with no latent heat involved. The line separating the vortex glass from the vortex lattice is determined by the maxima of the fishtail anomaly deduced from Fig.7.4 and terminates at the critical point on the melting line.

According to chapter 5 and 6, however, there is no fishtail anomaly in a really clean system and even though the measurements of Nishizaki et al. [Nishizaki] coincide with the results of Schilling [Schilling] obtained by specific heat measurements, it is questionable from that

point of view whether this proposed phase diagram is a result of the microstructure or is of intrinsic nature. Further support for questioning the phase diagram given by Nishizaki et al. [Nishizaki] came from detection of specific heat peaks on the melting line in $BaZrO_3$ grown samples [Roulin, Junod], that had received the oxygenation to bring them to a state of $YBa_2Cu_3O_{7.0}$ as described in chapter 6.

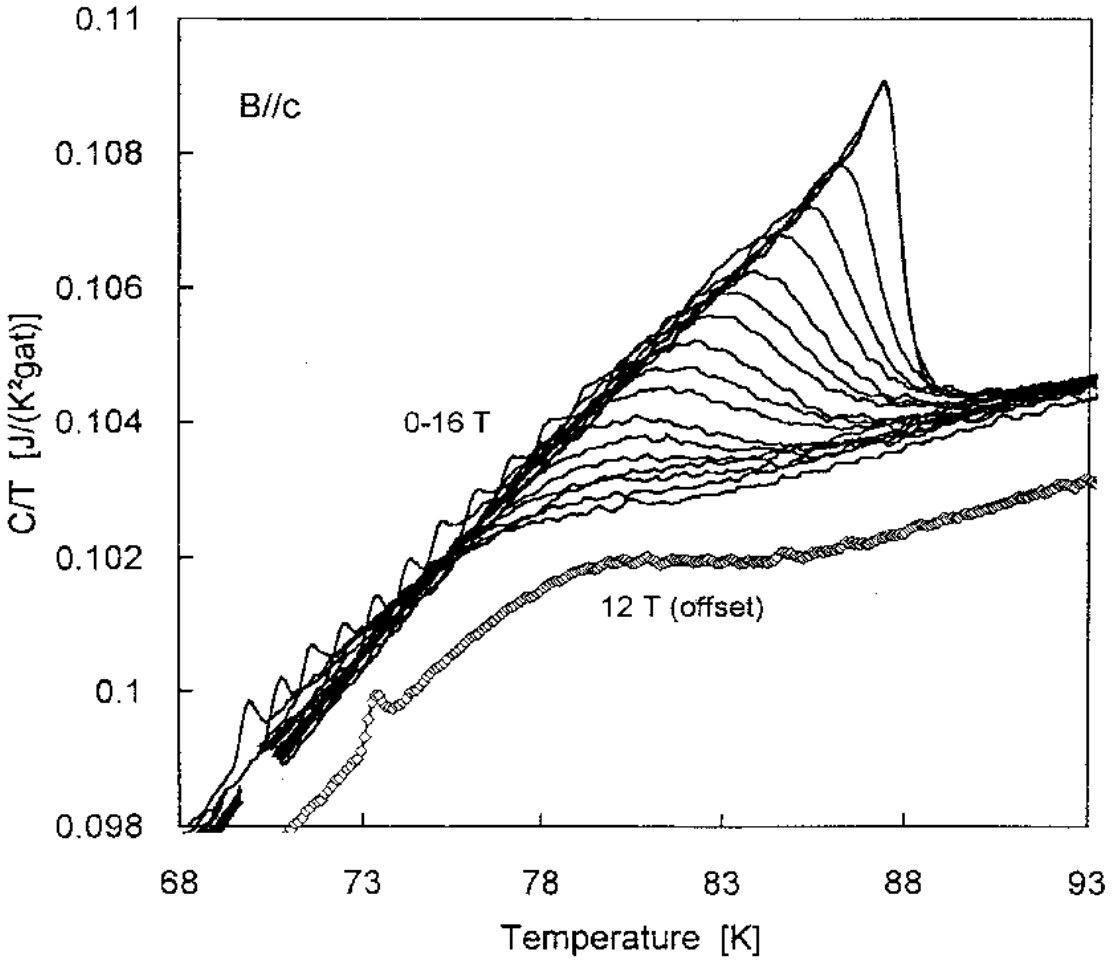

Fig. 7.6 Total specific C/T heat of a $YBa_2Cu_3O_{7.0}$ crystal versus temperature for B|| c. B= 0, 1,2,3,....16 T. Adapted from [Junod]

As one can see in Fig. 7.6 the small peak in the specific heat curves indicating first order like melting of the vortex lattice persists up to at least 16 T, which was the highest available field at that time. Thus, for those samples which had received the high pressure oxygenation to suppress the magnetic fishtail effect no critical point has been detected in those measurements at least up to 16 T. It has been shown by a subsequent study [Roulin98, RoulinDiss] that gradually re-establishing the fishtail effect by increasing the oxygen deficiency and allowing clustering of the oxygen vacancies the same sample shown in

Fig.7.6 then shows a terminating endpoint on the melting line – a critical point. The presence or absence of a critical point is intimately related to the presence of a magnetic fishtail effect, which hampers the formation of an intrinsic vortex lattice due to strong pinning. However, since we have seen in chapter 5 that even for optimally doped samples the fishtail effect can be suppressed by uniform distribution of the oxygen vacancies, it is not justified considering the phase diagrams obtained from measurements on samples with magnetic fishtail effect being intrinsic, not even for oxygen deficient $YBa_2Cu_3O_{7-\delta}$. The proposed phase diagrams rather represent the situation for a particular sample with its individual microstructural imperfection.

7. 3 High Field Studies on $YBa_2Cu_3O_{7.0}$

Since$YBa_2Cu_3O_{7.0}$ represents the 123 - structure without disorder, it should exhibit the intrinsic properties. Therefore the measurements of the irreversible magnetisation and the specific heat at fields higher than 16 T (the highest fields available at the DPMC in Geneva) were performed in collaboration with the group of Christophe Marcenat (DRFMC\SPSMS\LCP Grenoble France) for the specific heat measurements and with the group of Kazuto Hirata, National Research Institute for Metals in Tsukuba, JAPAN for the high field magnetisation data.

As discussedbefore the crystals used by Nishizaki et al. [Nishizaki] show an anomalous fishtail behaviour or as they refer to a second peak in the magnetisation at around 10 – 15 T. Even though it could already be argued that since we observed first order like melting of the vortex lattice up to 16 T, we should not have such a peak, there was no definitive proof for the absence of this peak in our samples. For that reason a fully oxygenated $YBa_2Cu_3O_{7.0}$ crystal was measured at various temperatures in fields up to 28 T, actually with the same equipment used by Nishizaki et al. [Nishizaki]. Fig. 7.7 shows the magnetisation curve for such a crystal at 64 K, a temperature where in the measurements of Nishizaki et al. a prominent fishtail effect has been observed at around 10 T (see inset in Fig. 7.4). Obviously no anomaly can be detected in our fully oxygenated crystals as one already could suspect for the results of the specific heat measurements. The anomalies obtained by Nishizaki are most likely do to finely dispersed small oxygen vacancy clusters; their fine dispersion being probably favoured by a small impurity content of Ti present in these crystals which is

introduced due to crucibles they use for crystal growth. These measurements again show that the anomalies are not due to phase transitions in the vortex system but a result of microstructure. Especially the line separating the vortex lattice region from the vortex glass region is not intrinsic and the drawing of this line, which has been introduced because of the similarity of this system with the phase diagram of Bi-2212, seems a bit arbitrary.

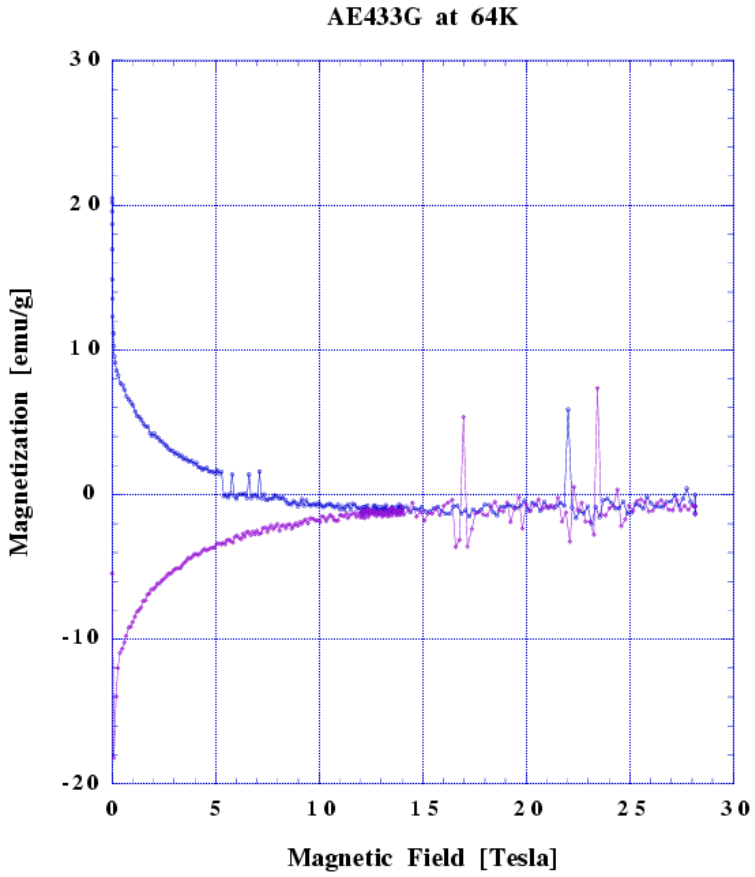

Fig.7.7 High field magnetisation data of a fully oxygenated twinned single crystal of $YBa_2Cu_3O_{7.0}$ in fields up to 12 T. The equipment for the measurement is the same than used by Nishizaki et al. [Nishizaki]. Measured by Hirata Kazuto [Hirata, ErbAPS99]

To further clarify whether there is a critical point on the melting line of the clean disorder free system and to which field the vortex lattice persists measurements of the specific heat were performed in very high fields up to 28 T. Unlike the specific heat measurements in Geneva which were performed using a quasi-adiabatic calorimeter, the measurements in the rather noisy environment of very high fields were obtained by using an ac-calorimeter which

yields less noisy signals and which is especially capable of detecting the relative small latent heat released during freezing of the vortex liquid [Bouquet]. Fig. 7.8 shows the results of these specific heat measurements obtained for the disorder free crystals. Specific heat peaks were detected up to the highest available fields revealing that no terminating end point for the first order transition can be detected up to 28 T. The amplitude of the melting peak generally grows upon increasing magnetic field up to half the maximum fields at which first order transitions can still be detected [Bouquet]. Therefore, since the melting peaks in Fig 7.8 grow at least until 24 T, no critical endpoint should be expected, at least up to about 50 T, and the 3 D vortex lattice should persist up to such values. At values around 50-60 T then a crossover may occur due to the crossover of the 3 D vortex lattice to a 2 D disordered solid, similar to the case of the Bi-2212 compound [Zeldov].

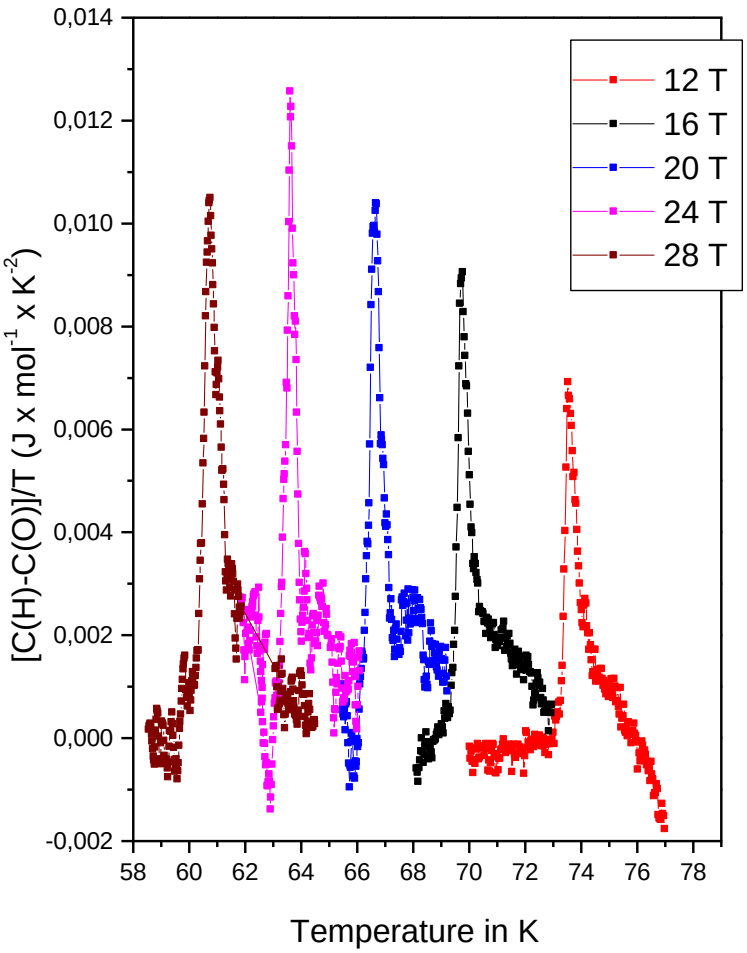

Fig.7.8 Specific heat peaks upon vortex lattice melting obtained in $YBa_2Cu_3O_{7.0}$. For clarity the zero field data its subtracted from the field data

Summarising the data obtained from measurements of the specific heat on different crystals with different oxygen content and pinning properties (oxygen cluster formation was not suppressed for those samples) one may construct the phase diagram shown in Fig. 7.9.

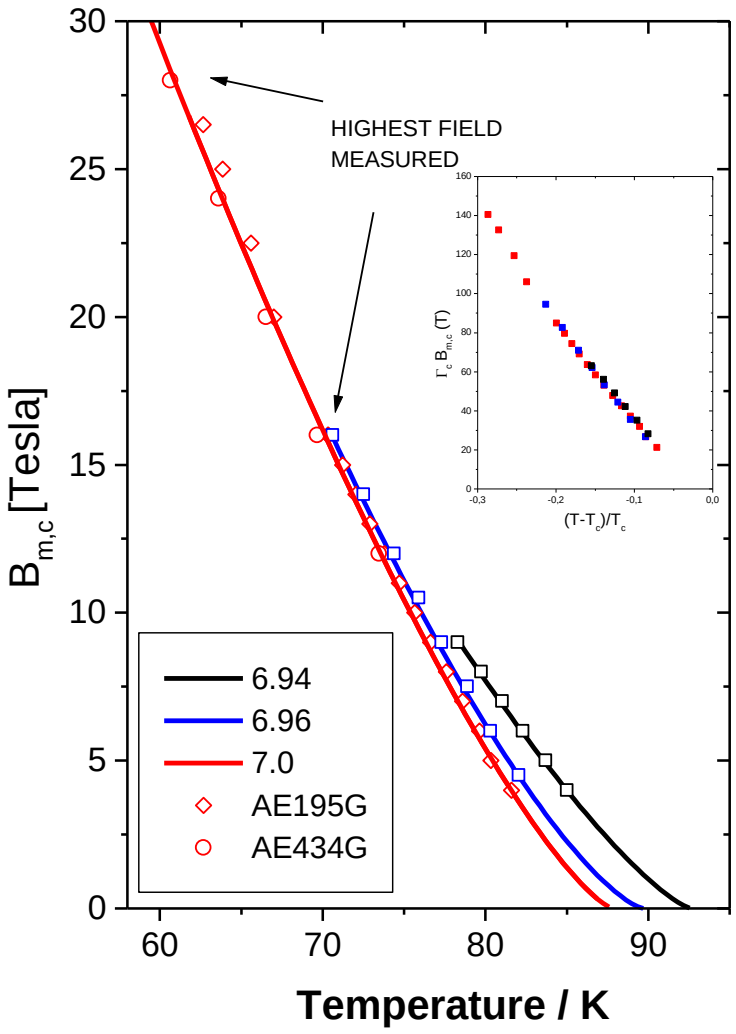

Fig. 7.9 B-T phase diagram for different crystals of $YBa_2Cu_3O_{7-\delta}$. Points represent the fields at which first order like melting has been detected. Colours stand for different oxygen content (6.94, 6.96, and 7.0 respectively)

For the oxygen contents of 6.96 and 7.0 no critical point has been detected up to the highest measured fields(16 and 28 T respectively), however, the sample with an oxygen concentration of 6.94 which shows an magnetic fishtail shows such a point at around 8 T, 78 K. It will be the subject of further study whether such a critical point is present for the same oxygen concentrations when the fishtail is suppressed.

Another feature which is interesting is that no first order like melting could be detected below about 4 T for all our twinned samples. This stands in contrast with the measurements of Schilling et al. [Schilling] on untwinned crystals in which the first order transition could be followed down to the lowest fields and raises the question which will be briefly discussed in the next paragraph.

7.4 Influence of twin boundaries on pinning of vortices

Since single crystals of 123-compounds are normally twinned after synthesis with an average twin spacing of about 1μm. It was not very clear whether twin boundaries play an important role in the pinning of vortices or if they may even be responsible for the fishtail effect (see for instance inset in Fig. 7.4). Charging from the average spacing of the twin boundaries the corresponding matching fields however seem to be far to small (eg. some mT) to explain this effect. However, it has been seen by imaging the vortices on a twin boundary [Maggio-Aprile] that at least at low temperatures the twin boundaries do pin vortices (Fig. 7.10).

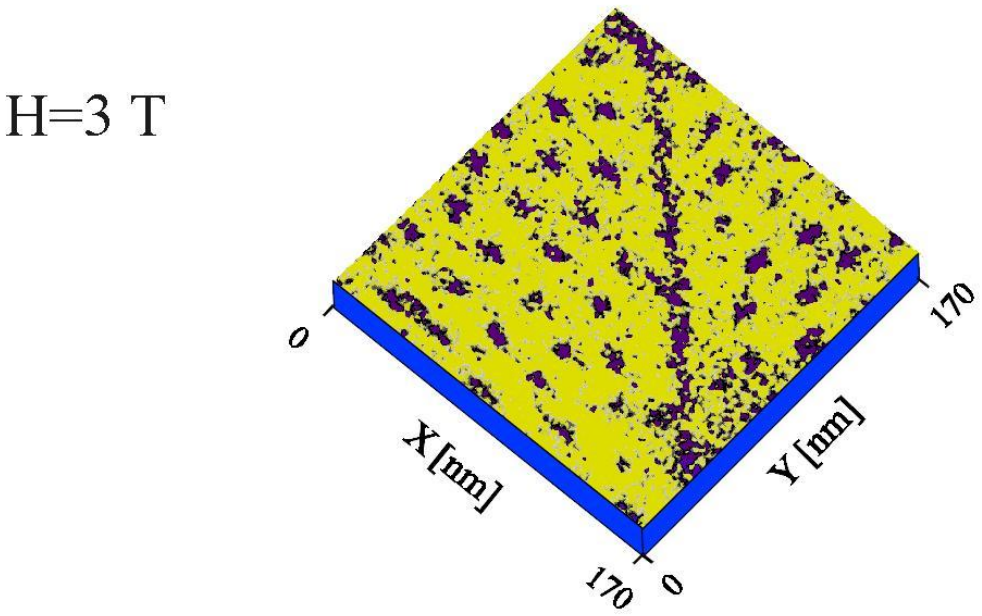

Fig.7.10 Spectroscopic Images of the vortex lattice on the (001) YBCO single crystal surface at T=4.2 K The black regions represent the vortices. On the twin boundary a high density of vortices can be found. Adapted from [Maggio-Aprile]

Moreover it has been seen from these measurements that the twin boundaries are even preferential sites for the vortices which become occupied first when increasing the magnetic field and that only at higher fields the vortices, when all the twin-boundaries all occupied the vortices go into the twin-free region between boundaries. There is further support for this interpretation from magnetic force microscopy (MFM) measurement performed at the University of Basel, Switzerland [Stiefel] in very low fields ranging from 2 mT to about 0.5 T. Fig. 7.11 shows such a MFM -measurement at a field of 2 mT. The bright spots represent the vortices, which are perfectly aligned with the direction of the twin-boundaries proving that the first positions being occupied by vortices are the twin boundaries.

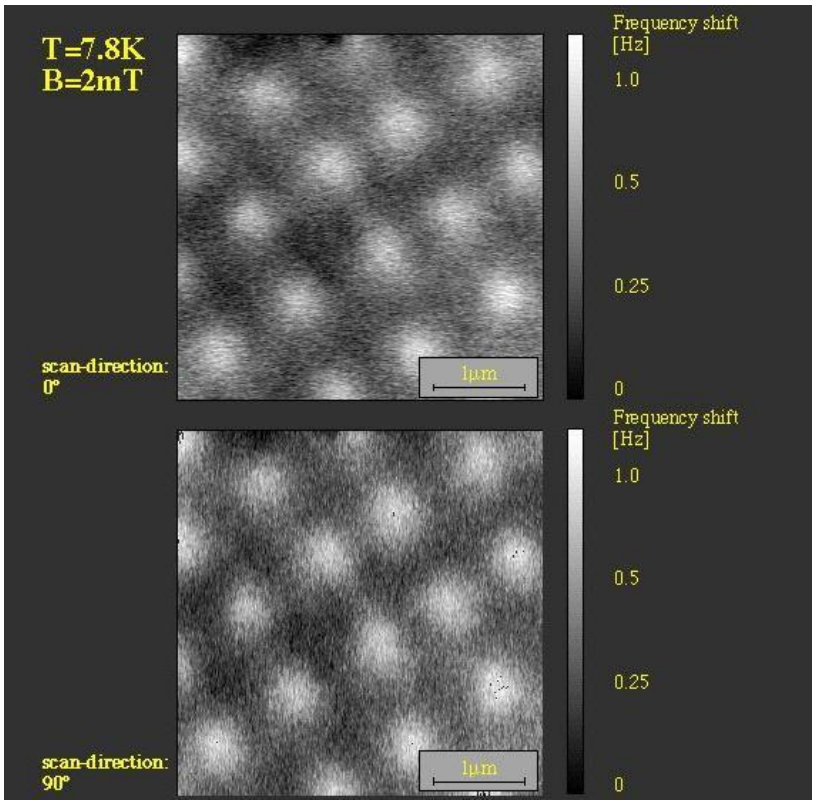

Fig. 7.11 MFM -measurement at a field of 2 mT. The bright spots represent the vortices, which are perfectly aligned with the direction of the twin-boundaries [Stiefel]

In increasing magnetic fields the twin boundaries gradually fill up with vortices, increasing first the density of vortices on the twin boundary and then occupying sites in between twin boundaries, however still perfectly aligned with the twins. Fig. 7.12 shows this gradual filling of twin boundaries (marked s1,s2...) and the subsequent occupation of the twin free regions in between, which is however still influenced of the twins. Only when the interaction between the vortices inside the single domains becomes high, e.g. when their distance becomes very small at higher fields, we can expect that the intrinsic vortex lattice forms.

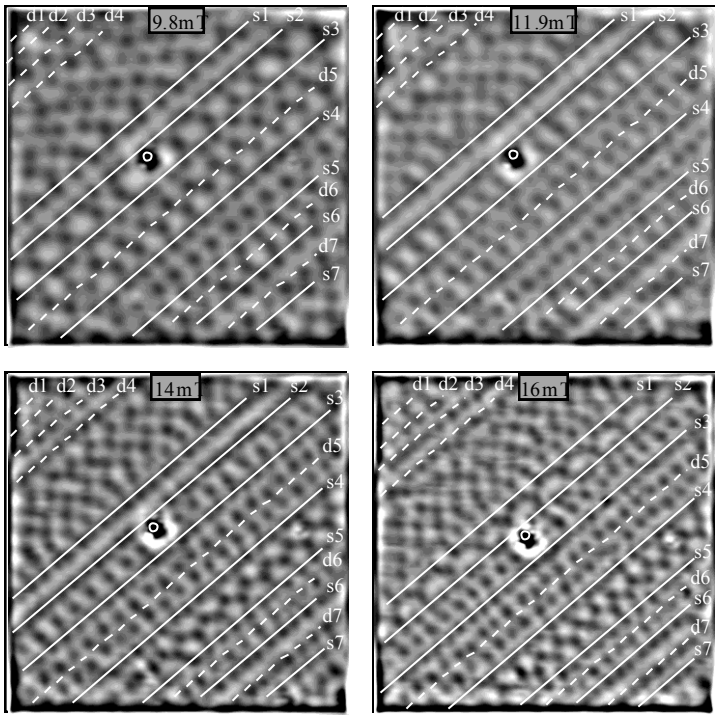

Fig. 7.12 Gradual filling of the twin boundaries (s1, s2....) with vortices (black dots) on increasing magnetic field. The additional vortices which go into the twin free regions are still lined up in the directions of the twin boundaries for those low fields. Area 6x6 μm^2. Adapted from [Stiefel]

Thus, for low fields there is no intrinsic lattice formed in twinned crystals, which explains why no sign of vortex lattice melting can be detected in specific heat measurements in fields below 3-4 T. Similar behaviour has been found [Crabtree] for crystals which have been irradiated with heavy ions at an equivalent dose of 20 G, also in that case the lower detection limit for first order melting of the vortex lattice is shifted to a value of about 4 T.

7.5 Melting of the vortex lattice in $DyBa_2Cu_3O_{7-\delta}$ and $EuBa_2Cu_3O_{7-\delta}$

The second compound in which the melting of the vortex lattice has been observed experimentally by specific heat measurements is the compound $DyBa_2Cu_3O_{7-\delta}$ [Revaz]. Dy-123 as well as the Er-123 is, beside from the magnetic moment of the central atom, not much different compared to Y-123, both in respect to T_c versus delta (Fig.6.6) as well as with respect to the disorder on the metal sub-lattice. Due to ion sizes similar to Y a solid solution or spinodal decomposition is unlikely to occur.

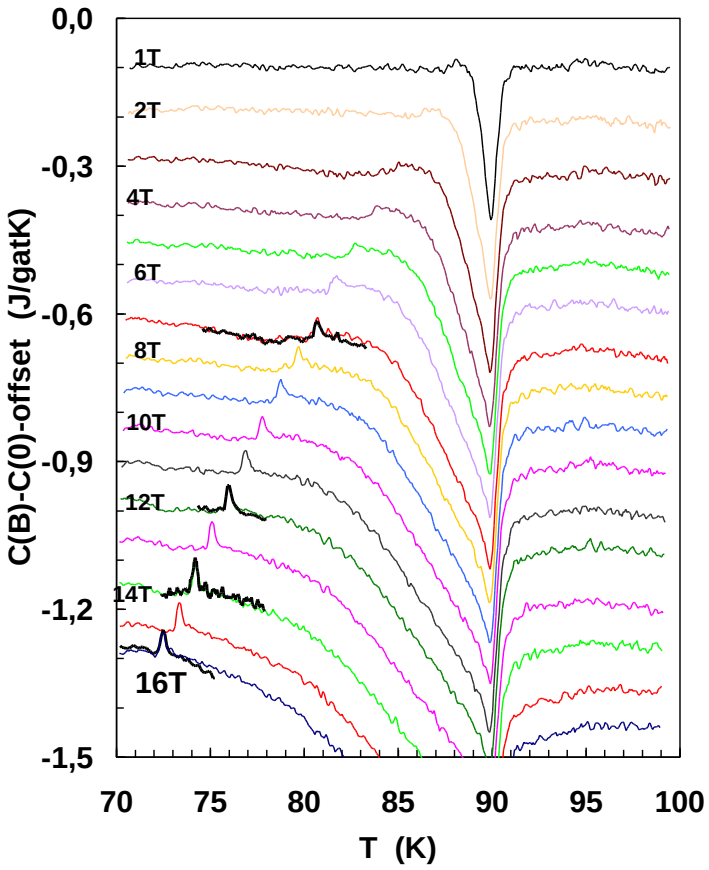

Fig.7.13 Specific heat peaks upon the melting of the vortex lattice in $DyBa_2Cu_3O_{7.0}$

Thus, from the point of disorder the finding of a calorimetric signature of melting of the vortex lattice could be expected assuming that the magnetic moment of the Dy ion does not interfere with the vortex matter. The experimental finding reproduces completely the case of $YBa_2Cu_3O_{7-\delta}$ except for the fact that T_c of the Dy-123 compound is somewhat higher for the

fully oxygenated state. No critical point is observed up to the highest applied fields (16 T). The situation changes if disorder increases for the bigger light rare earth 123 compounds. For the $EuBa_2Cu_3O_{7.0}$, the third compound where ever a thermal signature of melting has been detected [ErbAPS99], the critical point lies somewhere in the region of 11-12 T. Additionally the melting entropy is smaller when compared to $DyBa_2Cu_3O_{7.0}$ or $YBa_2Cu_3O_{7-\delta}$, which basically means that less vortices contribute to the lattice, as a result of increased pinning due to inhomogeinities of the metal sub-lattice.

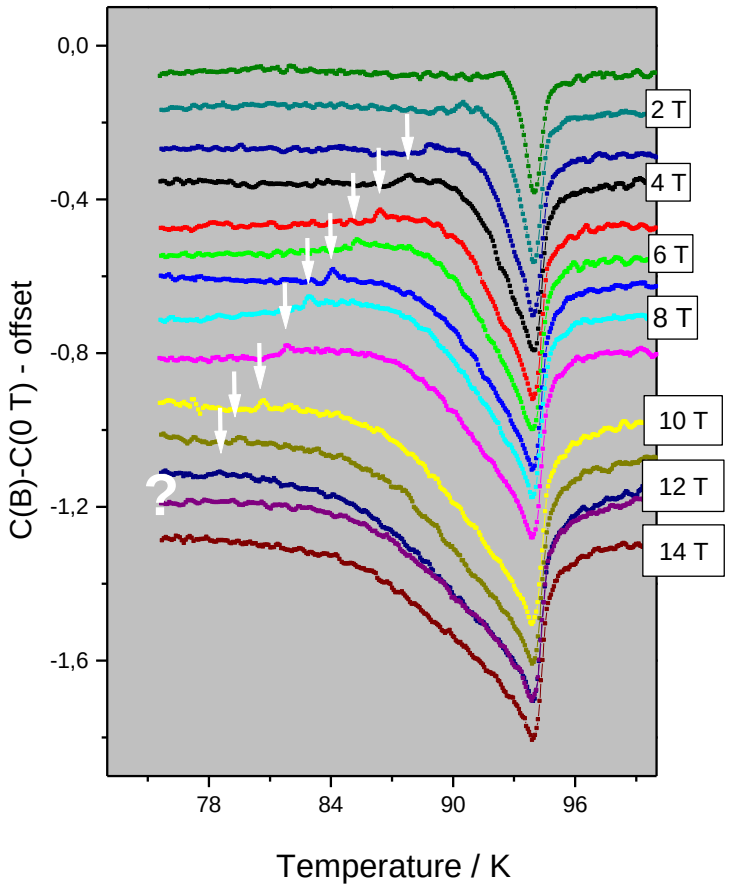

Fig.7.14 Specific heat peaks upon the melting of the vortex lattice in $EuBa_2Cu_3O_{7.0}$. The signature of melting vanishes at around 11-12 T.

Such disorder in the metal sub-lattice can be expected for the Eu-123 system as explained in chapter 3 and 6 and becomes even more pronounced for the lighter Nd-123 compound. For Nd-123 no vortex lattice melting has been observed so far even though we tried to suppress metallic disorder.

References:

[Zeldov]

E. Zeldov et al. Nature 375 (1995) 373

[Crabtree]

G. W. Crabtree et al. Proc. of the NATO Advanced Study Institute on the Physics and Material Science of Vortex States, Flux Pinning and Dynamics Kusadasi, Turkey (Aug.1998) Kluwer Academic Publisher, Sam Bose and Ram Kossowski, eds.

[Schilling]

A. Schilling et al. Nature 382 (1996) 791 and A. Schilling et al. Phys. Rev. Lett. 78 (1997) 4833

[Nishizaki]

T. Nishizaki et al. , Phys. Rev. B 58 (1998) 11169

[Roulin]

M. Roulin, A. Junod, A. Erb, E. Walker, J. Low Temp. Phys. 105 (1996) 1099

[Junod]

A. Junod, M. Roulin, J.-Y. Genoud, B. Revaz, A. Erb, E. Walker, Physica C 275 (1997) 245

[Hirata]

Kazuto Hirata et al. , unpublished

[ErbAPS99]

A. Erb, M. Roulin, A. Junod, B. Revaz, C. Marcenat, F. Bouquet, R. Calemczuk, K. Hirata, H. Suzuki, H. Abe, Spring meeting of the American Physical Soc. Atlanta 1999-04-22

[Roulin98]

M. Roulin, A. Junod, A. Erb, E. Walker, Phys. Rev. Lett. 80 (1998) 1722

[RoulinDiss]

Marlyse Roulin, Thesis 2989 (1998), University of Geneva, Switzerland

[Bouquet]

F. Bouquet, C. Marcenat, R. Calemczuk, A. Erb, A. Junod, M. Roulin, U. Welp, W. K. Kwok, G. W. Crabtree, N.E. Phillips, R. A. Fisher, A. Schilling

Proc. of the NATO Advanced Study Institute on the Physics and Material Science of Vortex States, Flux Pinning and Dynamics Kusadasi, Turkey (Aug.1998) Kluwer Academic Publisher, Sam Bose and Ram Kossowski, eds.

[Maggio-Aprile]

I. Maggio-Aprile, Ch. Renner, A. Erb, E. Walker and O. Fischer , Nature 390 (1997) 487

[Stiefel]

Bruno Stiefel, Thesis (1998), University of Basel, Switzerland

[Revaz]

Bermard Revaz, Alain Junod and Andreas Erb, Phys. Rev. B 58 (1998) 11153

8. Different channels for hole doping of the CuO planes in $REBa_2Cu_3O_{7-\delta}$; Ba-site occupation, spinodal decomposition, oxygenation problems and superconductivity in the $PrBa_2Cu_3O_{7-\delta}$ system

8.1 T_c versus annealing temperature for the different $REBa_2Cu_3O_{7-\delta}$

One of the somewhat puzzling results obtained in the present investigation was the dependence of T_c versus δ or T_c vs. annealing temperature [Erb97] (Fig 3.13) for different crystals of RE-123 grown in air and oxygenated in 1 bar of flowing oxygen. For the convenience of the reader the figure is reproduced here once again (Fig. 8.1) and the values for a $YBa_2Cu_3O_{7-\delta}$ single crystal doped with 7.5 % Ca on the Y site are included.

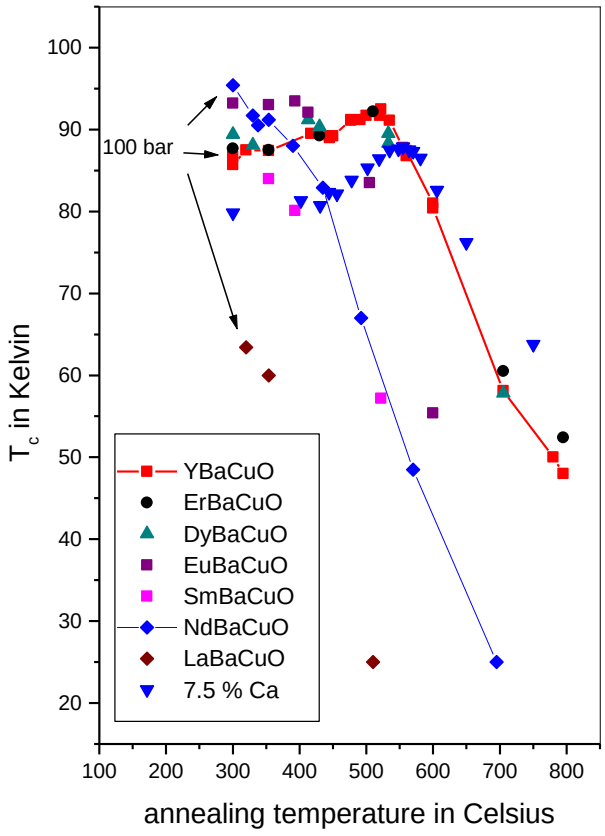

Fig. 8.1 T_c versus anealing temperature for the different RE-123 compounds

For the heavier central atom 123 compounds like Er-123 the curve of Tc does not differ from the one for Y-123, which is not too astonishing since there should be no solid solution for this compound (see also chapter 6.2). For the Dy-123 compound the curve is already slightly

shifted to lower temperatures and for the Eu–123 the shift to lower temperatures already equals about 100 °C. Following up are the Nd–123 and the Sm-123, where this shift is already 200 °C and the La –123 where the curve is shifted 400 °C to lower temperatures. To explain this behaviour, the generic phase diagram proposed by Tallon [Tallon2] is used, as well as the analogy found in the case of Ca-doped Y-123, where the Ca^{2+} substitutes the RE site and thus leads to additional hole doping of the CuO planes. This situation is sketched in Fig. 8.2 (red curve) : Additional hole doping leads to a shift of the T_c vs. delta (or annealing temperature, which is equivalent) to the right - the reason why Ca – doped YBCO can be driven much more over-doped by oxygenation.

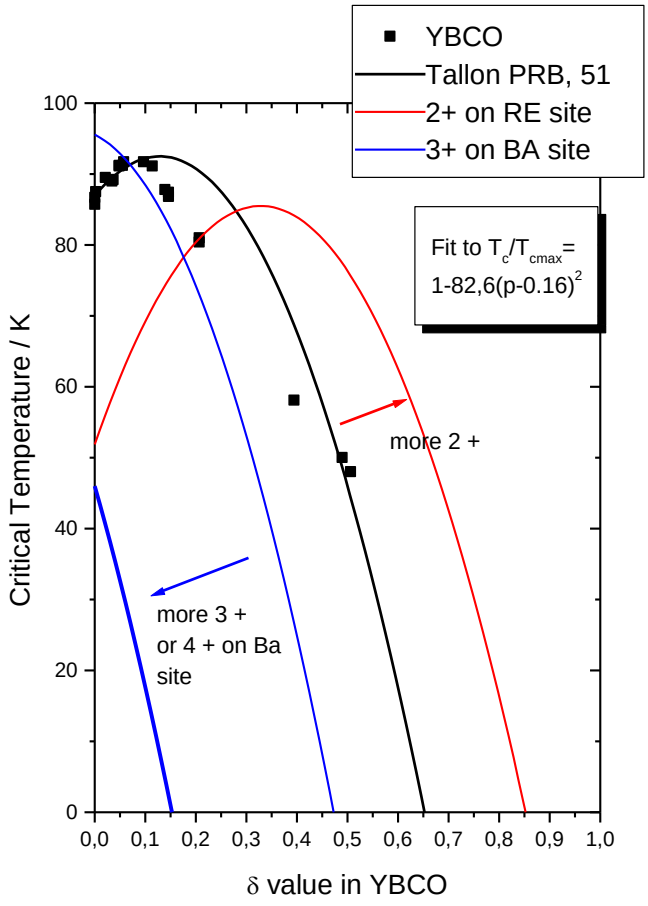

Fig. 8.2 T_c versus δ for differently doped 123-compounds with 2 different channels for hole doping in $REBa_2Cu_3O_{7-\delta}$: 1) oxygen doping , 2) doping by RE site substitutions; Points represent experimental data on YBCO, black curve represents the equation given by Tallon et al. [Tallon2]

On the contrary the formation of a solid solution of the form $RE_{1+x}Ba_{2-x}Cu_3O_{7-\delta}$ results in a doping with 3^+ RE atoms on a Ba-site and, as suggested above, will have the opposite effect: The T_c versus delta curves are increasingly shifted to the left hand side (blue line) and for higher RE - doping levels the superconductivity is limited to the highest oxygen (bold blue line) doping region. Fig. 8.2 represents well the situation we find in Fig. 8.1, so that the reason for the shift in the T_c versus delta curves for the different RE -123 may be attributed to the formation of solid solution crystals for the light rare earth elements. As shown in Fig. 8.1 the shift increases with decreasing atomic number, thus implying that the effect will be most pronounced for the lightest element and that superconductivity might eventually be completely suppressed by this mechanism if the RE^{3+} doping of the Ba site is sufficiently high – the superconducting region of the phase diagram is than not any longer accessible by any oxygen doping. The detection of the surplus of RE^{3+} in these solid solution crystals, however, posses some experimental problems, since overlapping of the characteristic lines of Ba and Nd as well as for Eu and Ba hampers the use of EDX measurements. Some of the Nd-123 samples have been chemically analysed by Atomic Absorption Spectroscopy (a destructive method) and the Nd/Ba has been found to be 1/1.73 [Wendl], from which one calculates on a stoichiometry of about $Nd_{1.25}Ba_{1.75}Cu_3O_{7-\delta}$. It is noteworthy that the results of EDX measurements on the same samples showed no off-stoichiometric composition, probably due to the uncertainty arising from the overlap of the characteristic lines used for standardless analysis. From this result one can calculate on a shift of the effective oxygen doping of the CuO-planes by 0.125, assuming that every RE^{3+} requires half an oxygen for charge neutrality. Thus the calibration for δ is shifted by half the value of the off-stoichiometry. In that sense $RE_{1+x}Ba_{2-x}Cu_3O_{7-\delta}$ has to be compared with $YBa_2Cu_3O_{7-\delta-x/2}$, or in the present case the $Nd_{1.25}Ba_{1.75}Cu_3O_{7.0}$ would have to be compared with $YBa_2Cu_3O_{6.875}$, which means almost optimal doping. Further support for this interpretation comes from the measurements of the thermal expansion coefficients in the c-direction of such crystals and the pressure dependencies deduced from them [Meingast]. In Y-123 the pressure dependence dT_c/dp_c for uniaxial pressure along the c direction is positive underdoped samples, turns to zero at optimal doping, and is negative for overdoping [Kraut]. For Nd-samples used in this study the measured dT_c/dp_c is small but still positive as one would expect of a Y-123 sample with a oxygen concentration of 6.875. It also means that the Nd-123 system, even at highest possible oxygen content, has not yet reached optimal doping and $T_{c,max}$ under pressure could be expected to be around 98 K. Also the anisotropy of the thermal expansion coefficients along the a/b- and c-direction speaks in favour for the scenario proposed above.

When measuring the thermal expansion coefficient in Y-123 samples one finds a big difference in the thermal expansion for the a/b- (twinned crystal) and the c-direction. This anisotropy is largely reduced for the Nd-123 crystal (Fig. 8.3). By replacing the Ba-ion with Nd , however, the 3 superposed blocks of the 123 structure become more similar to each other and the structure more isotropic.

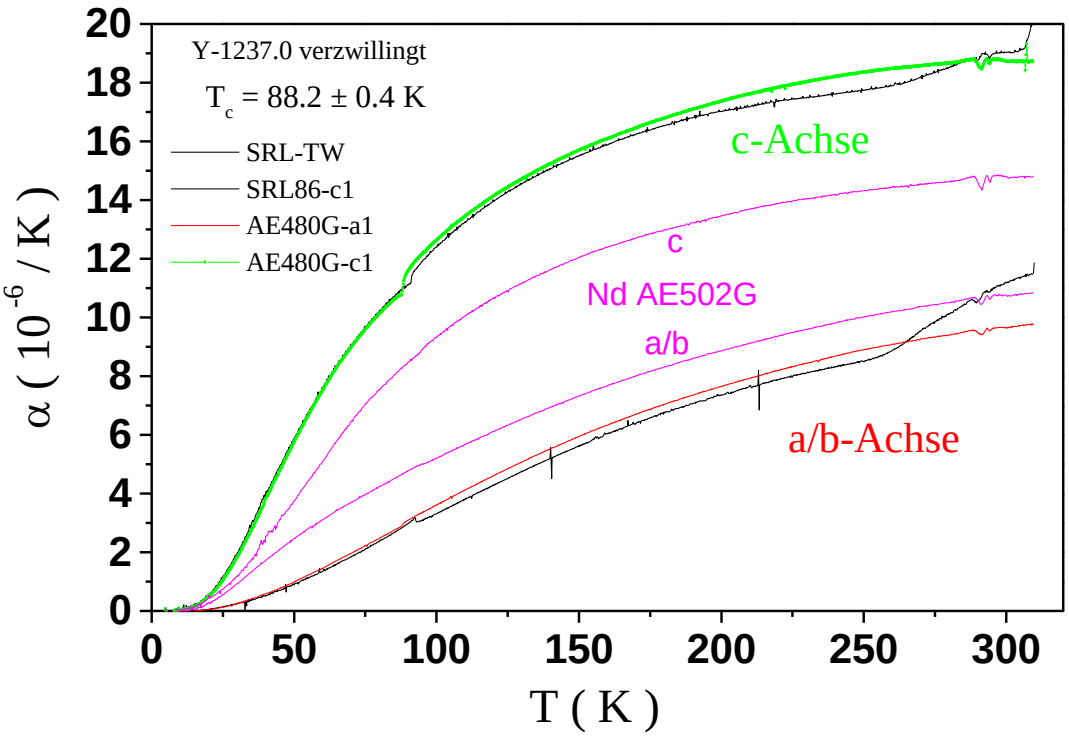

Fig. 8.3 Thermal expansion coefficient for different crystals of Y-123 (black line: near optimally doped, green: overdoped c-direction, red : overdoped a/b-direction) and Nd-123 (margenta).

For an overdoped Eu-123 crystal the anisotropy has been found [Meingast] to lie in between the Nd-123 and the Y-123 value, in agreement with the less pronounced Ba site occupation in this Eu-123.

Before ending this paragraph, it should be noted that the suppression of T_c by Al and the shift of the curves of T_c versus annealing temperature for Au doped Y-123 crystals can be described in terms of the proposed model of a second doping channel (Fig. 8.2) as well. Both the aluminium and the gold are 3^+ elements, which substitute mainly on the 2^+ copper chain site. We have, thus a mechanism similar to that proposed in Fig. 8.2, where we place 3^+ RE atoms on the 2^+ Ba site, changing the effective doping of the CuO planes. Within this

framework the observed lower annealing temperatures at which a maximum in T_c is observed for both the Au doped crystals and the crystals slightly contaminated with Al can be easily explained.

8.2 . Superconductivity in $PrBa_2Cu_3O_{7-\delta}$

8.2.1 Introduction

Among the RE - 123 compounds, which can actually be synthesised, $PrBa_2Cu_3O_{7-\delta}$ is the only one which does normally not show superconductivity. It is this exception that made $PrBa_2Cu_3O_{7-\delta}$ one of the more intensively studied materials among the 123 - compounds. Even though the Fermi surface for the CuO chains was found to be similar to that of $YBa_2Cu_3O_{7-\delta}$ [Hoffmann], the samples do not turn superconducting and it was generally accepted that $PrBa_2Cu_3O_{7-\delta}$ is an intrinsic insulator due to 4-f hybridisation – as described by the model of Fehrenbacher and Rice [Fehrenbacher]. Recently, however, there were first reports about superconducting bulk samples [Zhou, Oka, Zou], leading to a renaissance of the subject.

It is due to reports of Blackstead and Dow [Blackstead95,Blackstead96,Blackstead95a], who were the first reporting superconductivity in $PrBa_2Cu_3O_{7-\delta}$ thin films, that the interest in this compound never completely vanished but led to the reports of bulk superconductivity. The occurrence of these samples led to an immediate controversial discussion about the origin of superconductivity in these samples and different models and scenarios have been proposed to explain why those samples are superconducting. Most of those scenarios question the sample quality and perfection, thus explaining superconductivity as an artefact due to inadequate sample preparation and, most important, saving the generally accepted opinion of $PrBa_2Cu_3O_{7-\delta}$ being an intrinsic insulator. It is the goal of this paragraph to discuss why the different mechanisms of disorder, which were mentioned in the former chapters may be responsible for the absence of superconductivity in most samples. By avoiding the sources of disorder for one can, however, synthesise superconducting $PrBa_2Cu_3O_{7-\delta}$. From the oxygen doping dependence one may conclude that the perfect $PrBa_2Cu_3O_{7-\delta}$ without the different sorts of disorder is an intrinsic superconductor, but it is a meta-stable compound.

8.2.2 Problems arising during growth and synthesis of $PrBa_2Cu_3O_{7-\delta}$

As proposed in paragraph 8.1 a solid solution of the type $RE_{1+x}Ba_{2-x}Cu_3O_{7-\delta}$ will change the effective doping of the CuO-planes. We should now keep in mind that the Praseodymium has 2 different oxygenation states, namely Pr^{3+} and Pr^{4+}. At room temperature and ambient oxygen partial pressure both of these valences are present, while at high temperature where the synthesis of the 123 phase takes places the Pr^{4+} is unstable, thus, during synthesis only Pr^{3+} is present and the phase relationships during growth are similar to those for the other light rare earth elements. This, however, also leads to the formation of a solid solution in the Pr – 123 compound and thus to a decrease in the number of holes in the resulting compound. Since Praseodymium can also be 4- valent at low temperature (the stable form at room temperature is a mixture labelled Pr_6O_{11} , thus 2/3 of the Pr is in the highly oxidised Pr^{4+} state) this doping may be even more effective in the case of Praseodymium-123 than it is for the La, Nd or Sm-123, in a way that the Pr doping shifts the curve in Fig 8.2 that far to the right, that even for the highest possible oxygenation state a sufficiently high hole doping of the CuO planes to produce superconductivity can not be obtained. It is probably for that reason that crystals or ceramic samples synthesised in high or ambient oxygen partial pressures do not show superconductivity, but the reported [Zhou, Oka, Zou] superconducting samples all have been synthesised at oxygen partial pressures as low 0.001 bar, which have been reported to supress the formation of solid solutions of the type $RE_{1+x}Ba_{2-x}Cu_3O_7$.

As explained in chapter 6 there is good evidence from the studies of the magnetic fishtail effect in the Nd –123 system that a so-called spinodal decomposition leads to a further complication in the sample preparation of homogeneous light rare earth element 123-compounds even in the case were an overall off-stoichiomerty of the type mentioned above can be avoided.

In chapter 6 it was also shown that this spinodal decomposition can be avoided or largely reduced by quenching the samples from a temperature above 700 °C down to room temperature after synthesis. In that case the spinodal decomposition does not occur because it is kinetically hindered. Due to the similarity of the Nd and Pr system, it is proposed here that such a spinodal decomposition should also take place in the Pr- system, which provides us with with source of suppression for superconductivity in the Pr-123. Following the arguments raised in chapter 6 one can see from Fig. 6.3 that most of the material is indeed off-stoichiometric and therefore not superconducting. There are, however, some regions, e.g. the nodes, were the 123 stoichiometry is retained and which should therefore show superconductivity or at least metallic behaviour. Some observations from literature may

actually support such an idea here as well: Measurements of the optical reflectivity of fully oxygenated PrBCO still show some free charge carriers [Widder], however, the resistive measurements showed isolating behaviour. The same may be true for the thin films in Blackstead‘s original report [Blackstead95a] were no macroscopic but most probably local superconducting regions were reported. In the scenario given above superconductivity could exist locally, without being necessarily percolated, explaining the lack of zero resistivity for most samples. Also, the resistivity measurements in the report of Zou et al. [5] show an non-uniform behaviour for different pieces of their crystals, some of them show an semiconductor like increase upon cooling before actually turning superconductive, others exhibiting this increase only without turning superconductive.

For the preparation of superconducting $PrBa_2Cu_3O_{7-\delta}$ the spinodal decomposition should thus be avoided by subsequent quenching after the synthesis which leads us to the next problem:

Even if we achieved to suppress the disorder, the sample than will show no superconductivity because the necessary oxygen doping has not yet been performed and the oxygen content of the sample should be around 6.0. Now the problem arises that one has to oxygenate the sample at a temperature sufficiently high to allow oxygen diffusion but low enough that the metals atoms are not mobile. Here, most probably also the annealing time may play a role. Thus, following the scenarios of disorder formation in the light rare earth 123-compounds the last step of oxygenation is again a crucial point in the preparation of a superconducting Pr-123 sample.

To test this scenario several crystal growth experiments have been performed. Because of the reasons given above the growth experiments were performed at very low oxygen partial pressure (0.002 – 1 % O_2 in Ar , flowing atmosphere) with high purity (99.999 at. %) initial materials. After growth the batch was quenched to room temperature.

Using an atmosphere of 0.002 % O_2 some small crystallites were found, mixed with flux and parasitic phases like $PrBaO_3$. Some of these crystallites, together with the other phases, were oxygenated at 330 °C for 48 h in 100 bar of oxygen.

The crystallites were measured in a commercial Squid magnetometer (Quantum Design MPSR), both in zero field and field cooled mode, clearly showing bulk superconductivity at 90 K with a Meissner effect. The inset shows the whole temperature range from 0 to 110 K and one can observe an upturn at around 15 K originating from magnetic ordering of the impurity phase $PrBaO_3$. As stated above the sample consisted of a conglomerate of different phases nevertheless we see superconductivity at 90 K.

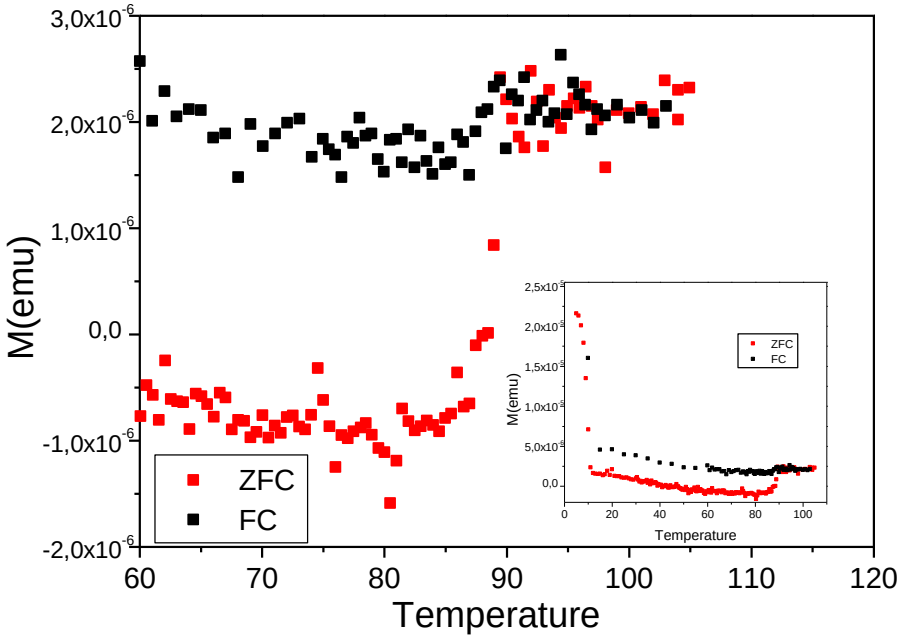

Fig. 8.4 Superconductivity in a $PrBa_2Cu_3O_{7-\delta}$ sample

Unlike crystal growth in air, which always yields nice looking but not superconducting $PrBa_2Cu_3O_{7-\delta}$ crystals, the synthesis or crystal growth of superconducting $PrBa_2Cu_3O_{7-\delta}$ is, as already stated in several other reports, not reproducible and one has to find some pieces of the batch which do show superconductivity. Moreover, superconductivity seems not to be stable over a longer period of time. The sample was re-measured after 2 month and did not any longer show superconductivity. This should not be too surprising, because it is clear that the $PrBa_2Cu_3O_{7-\delta}$ without the different sorts of disorder is a meta-stable compound; a sample which is brought down to room temperature in thermodynamic equilibrium conditions does show the different sorts of disorder, that do destroy superconductivity.

8.3 Discussion

Several scenarios have been proposed to explain the absence or presence of superconductivity in $PrBa_2Cu_3O_{7-\delta}$. The problem with a definite test of these scenarios is that in the most cases the samples available are not $PrBa_2Cu_3O_{7-\delta}$, but rather samples with either metallic impurities from synthesis, microstructural disorders originating from the formation of solid solutions and spinodal decompositions or both. Nevertheless some of the proposed scenarios are discussed

here since even with the now available information some of those scenarios may be excluded from further discussion.

In a pre-print by Pieper et al. [Pieper] based on NMR studies on non-superconducting $Pr_{1+x}Ba_{2-x}Cu_3O_{7-\delta}$ the presence of superconductivity was suspected to be due to an partial substitution of the RE site by the 2^+ Ba-ion and thus to a situation similar to the one in Ca-doped Y-123 represented in Fig. 8.2 by the red curve. They propose that the necessary hole doping of the CuO- planes is then solely achieved by the Ba and the RE-site. There are some mayor problems with this interpretation.

The reported c-axis lattice constants [5] for superconducting samples fall on one line with the series of the other RE elements, while the non-superconducting ones lie under this line. This suggest, however, more the mechanism of a partial occupation of the Ba site by Pr being responsible for the suppression of superconductivity in $PrBa_2Cu_3O_{7-\delta}$. The partial occupation of the Ba site by the smaller sized Pr atom should lead to a somewhat decreased c-axis for the non-superconducting samples, while the absence of such a substitution should lead to a bigger c-axis, both in agreement with the experimental finding.. Following the proposal of Pieper et al. assuming an RE-site occupation by the big Ba atom on the rare earth site then the c-axis of the superconducting samples should be even bigger than the trend given by the series of the rare earth elements and the non-superconducting should match this tendency, which is not the case. Moreover and perhaps even more striking is that with our oxygenation treatment, which yields T_c values around 90 K for YBCO, we find 90 K for our Pr-123 sample as well. Coming back to Fig. 8.2 this means nothing else than if the Pr-samples are stoichiometric the oxygen dependence is the same for Pr-123 and Y-123, while in the scenario of Ba substituting on the RE site, a T_c of 90 K for this oxygen doping would be rather coincidental.

On the other hand, the scenario of two different doping channels does explain the absence of superconductivity for $Pr_{1+x}Ba_{2-x}Cu_3O_7$. This scenario should hold without further implications like for instance the opinion raised by Blackstead and Dow that the superconductivity resides in the CuO chains rather than in the CuO planes. Their main argument for this statement was in fact that a Nd or Pr substitution on the Ba site does destroy superconductivity, while the presence of Nd or Pr at the RE site does not. They argue that superconductivity is destroyed by magnetic pair breaking if the magnetic ions Pr or Nd are placed near the chains (a Ba site substitution), while they do not act pair breaking if they reside on the more distant RE site. Thus, they conclude, superconductivity should be located in the chains rather than the planes. However, my experimental finding is different (see Fig. 8.1 and Fig. 8.3). A Nd- or Pr-occupation of the Ba-site only changes the effective doping of the CuO planes, which has to

be compensated by stronger oxygen doping. By changing the oxygen content from 6.9 to 7.0 the superconductivity in a Nd-123 crystal can be raised to values above 90 (see Fig 8.1), without changing the Ba site occupancy by Nd. The magnetic pair breaking of the Nd-ion should not be changed by changing the oxygen content, while the effective doping of the planes is changed - bringing back the superconductivity to the CuO planes.

It is the merit of Blackstead and Dow that the possibility of superconductivity in $Pr_1Ba_2Cu_3O_7$ has not been abandoned, however, placing the superconductivity in the CuO chains upon the Pr results only, seems to be questionable.

References:

[Erb97]

A. Erb et al., Physica C 282-284 (1997) 89

[Tallon2]

J. L. Tallon, C. Bernard, H. Skaked, R. L. Hitterman and J. D. Jorgensen, Phys. Rev. B 51 (1995) 12911

[Wendl]

W. Wendl, Kristall-und Materiallabor, University Karlsruhe Germany, private communication

[Meingast]

C. Meingast, INFP, Forschungszentrum Karlsruhe , private communication

[Kraut]

O. Kraut, C. Meingast, G. Bräuchle,H. Claus, A. Erb, G. Müller-Vogt, Physica C 205 (1993) 139

[Hoffmann]

L. Hoffmann, A.A. Manuel, M. Peter, E. Walker, M. Gauthier, A. Shukla, B. Barbiellini, S. Massidda, S. Adam, G.Adam, W.N. Hardy, Ruixing Liang, Phys. Rev. Lett. **71**, 4047 (1993)

[Fehrenbacher]

R. Fehrenbacher and T. M. Rice, Phys. Rev. Lett. 70, 3471 (93)

[Zhou]

Z. Zhou, K. Oka, T. Ito, Y. Nishihara, Jap. J. of Applied Physics 36 (1997) L18

[Oka]

K. Oka, Z. Zou, J. Ye, Physica C 300 (1998) 200

[Zou]

Z. Zou, J. Ye, K. Oka, Y. Nishihara, Phys. Rev. Lett. 80 (1998) 1047

[Blackstead95]

H. A. Blackstead and John D. Dow, Phys Rev B, 51, 11830 (1995)

[Blackstead96]

H. A. Blackstead, J. D. Dow , D. B. Chrisey, J. S. Horwitz, M. A. Black, P.J., McGinn, A. E. Klunzinger, D. B. Pulling, Phys. Rev. B 54 (1996) 6122

[Blackstead95a]

H. A. Blackstead, D. B. Chrisey, J. D. Dow , J. S. Horwitz, A. E. Klunzinger, D. B. Pulling, Physics Letters A 20, 109 - 112 (95)

[Widder]

K. Widder, M. Merz, D. Berner, J. Münzel, H.P. Geserich, A. Erb, R. Flükiger, W. Widder, H. F. Braun, Physica C 264, (1996) 11

[Pieper]

M. W. Pieper, F. Wiekhorst, T. Wolf, preprint cond-mat/9803336

Carrier doping in Pr_{1+x}Ba_{2-x}Cu_3O_7 studied by NMR

9. Summary, Conclusions and Outlook

When dealing with research in the high T_c superconductors and especially with $YBa_2Cu_3O_{7-\delta}$ one of the problems one has to face is that the large number of reports about these compounds makes it nearly impossible to keep track of all the developments. As well, the diversification of the field has developed and the many of the research teams working in the field have dedicated their work and attention to a small sub-field in the really huge amount of work being done since the discovery of high T_c superconductors.

It may be due to this fact, that some of the old and early ideas, which have been proven to be wrong in the meantime, still persist in the mind of many people in the community. It is thus difficult to come up with new ideas, which emerge somewhat above the average of the constant flow of new and sometimes old information, to gain attention from all sides and to overthrow “generally accepted” opinions.

It is the strongest point of the work in presented this summary, which in fact can only be a snapshot of the things that are still going on and thus can never be written at a good time, that it gained international attention and that in many parts it is now the “generally accepted opinion” – we will see how long this will last.

The strongest impact came from a new motto: “We have to make better samples !” and not only to assure everyone that the samples are already “high quality single crystals" – a term used nearly in every publication. In most cases this term is used unjustified and in the last years a growing number of well-known scientists have realised and criticised the use of this term, when basically no information about the sample was available, since no characterisation had been performed. By a detailed study of the processes going on during the synthesis of samples and by the interaction of the samples with the crucibles a really new idea was born and, in difference with some other ideas or suggestions which have never been put to a test, turned into a reality : The development of a really inert crucible material for the synthesis of the 123- compounds.

As a matter of fact this new development was recognised as being something substantial surprisingly fast and the crystals that came from growth experiments using this new crucible material $BaZrO_3$ gained attention. The term $BaZrO_3$ –grown single crystals became a new synonym for really clean crystals and a new quality standard, partly because the purity of the crystals has been increased by 1 –2 orders of magnitude compared to the earlier “canonical”

crystals originating from the widely used ZrO_2 crucibles, but also by a series of new results obtained on the these new $BaZrO_3$ grown crystals. In the meantime the production of single crystals in $BaZrO_3$ crucibles has been reproduced by the same group which produced the formerly "canonical" crystals. This group is now stating that the earlier crystals perhaps weren't that "canonical" after all, which is the best confirmation of the presented results.

Without the new results in physics the impact of these new crystals would, however, have been less significant. One very important and also early result, which strongly supported both the crystals and its manufacturer, was the imaging of vortices on such single crystals by Scanning Tunnelling Spectroscopy, an experiment which has been unsuccessfully tried often until the new crystals were available. It was an especially favourable situation that these experiments were performed in the same department and there was and is a steady flow of information in both directions.

Beside this situation the investigations on the so-called fishtail anomaly have been – once the crystal growth was in a state where it could be considered as being routine and very reproducible – the central part of this work. With the new crystals we were in the situation with oxygen, being the only parameter left that can produce a microstructural inhomogeneity. Such microstructural inhomogeneities have been proposed earlier as being at the origin of this anomaly in the irreversible magnetisation of the 123-compounds, but it was never possible to really prove this, since residual metallic impurities could not been controlled in earlier samples and thus obscured the investigations in that field. By changing the spatial distribution of the oxygen vacancies present in optimally doped samples of $YBa_2Cu_3O_{7-\delta}$ it has been shown that the anomaly in the magnetisation curves is due to field induced pinning in small oxygen deficient precipitates and that the anomaly is absent if one avoids the formation of those. In fully oxygenated $YBa_2Cu_3O_7$ the fishtail is intrinsically absent.

To allow this study an earlier study on oxygen diffusion coefficients in $YBa_2Cu_3O_{7-\delta}$ which gave reliable numbers for the mobility of oxygen in the $YBa_2Cu_3O_{7-\delta}$ structure was essential. Not only that it allows to calculate the time that is needed to homogeneously oxygenate the crystals, but also it allows estimations of how fast the precipitations provoking the fishtail effect occur in $YBa_2Cu_3O_{7-\delta}$. It also ruled out speculations of surface barriers hampering oxygenation that have been proposed to explain different in- and out diffusion of oxygen.

Having understood that it is possible to use magnetisation measurements as a probe for local inhomogeinities the studies were expanded into the more complicated structure of the rare

earth 123–compounds, where additional disorder arises from the metal sub-lattice. Again here eliminating the disorder leads to the absence of anomalies in the magnetisation curves and the formation mechanism of the precipitates could be studied.

Understanding this formation mechanism is important for technical applications ever will be of these compounds, since the control of the disorder gives rise to tailored samples for such applications. Already here some questions and solutions have been proposed to overcome principal problems of oxygenation for the light rare earth 123-compounds.

Very closely connected with the disorder and fishtail studies is the fundamental research on vortex phase diagrams. By elimination the disorder to the highest possible degree the intrinsic phase diagrams of vortex matter in the 123 –compounds could be studied. As long as disorder exists in the samples the measured phase diagrams often represent just the situation of the vortex matter for a individual sample with its individual degree of imperfection. The finding of first order transitions upon melting of the vortex lattice and the absence of the fishtail in magnetic fields up to 28 T brought clarification into this long investigated field. On the other hand, the specific heat measurements concerning melting of vortex matter also turned out to serve as a probe for disorder in those compounds, perhaps even more sensitive than the magnetisation measurements are. Complementary measurements using STS and MFM shed light on the influence of twins on pinning of vortices.

With the different informations about the most probable mechanisms for disorder formation in the 123 compound at hand then the synthesis of superconducting $PrBa_2Cu_3O_{7-\delta}$ has been performed - a compound which has been believed to be an intrinsic non-superconductor for nearly 10 years. Even though the experiments suffer from lack of reproducibility, due to the fact that the superconducting state of $PrBa_2Cu_3O_{7-\delta}$ is meta-stable, a convincing and plausible scenario for the presence and absence of superconductivity in the $PrBa_2Cu_3O_{7-\delta}$ can be proposed . This scenario also explains the shift of T_c versus delta for the different rare earth 123 –compounds and the influence of metallic impurities on the relationship.

In conclusion a big series of experiments have emerged from the development of the crucible material $BaZrO_3$, being the basis of all. The last 5 years were full of work and excitement about the newest results and full of international recognition not only for my work but also for the work of other people working in the DPMC at the University of Geneva. We all profited from each others work and for this I am very grateful – it was a great team.

For the future I think that there are still more interesting experiments to do on these crystals and that knowledge of "materials art" should be expanded to other compounds. A big part of this work was dedicated to the complex chemistry of the superconducting oxides which we begin to understand better now. The new samples gave clear insight in some of the intrinsic properties and having understood those one can develop strategies to overcome some of the basic problems for the application of high T_c superconductors.

Based on the further development of material science in this field it is expected to produce in near future long conductors of $YBa_2Cu_3O_{7-\delta}$ in a competitive manner. At that moment large scale applications will undoubtedly be possible and high T_c superconductivity may enter into daily life.

At the end of every such work there should be a place to thank some people.

First of all I want to thank the 3 professors who agreed to read and correct this work, namely Prof. R. Flükiger, Prof. H. Bill and Prof. ∅. Fischer.

When it comes to the collaborations and the acknowledgements one is in the difficult situation that one may forget someone, unintended or not.
In my case this is much more the case than normal, because there were so many people I had the pleasure to work with in the last 5 years in Geneva, Karlsruhe, Boston, Grenoble, Groningen, Munich, Zürich, Basel and elsewhere. I benefited a lot from these collaborations and want to express my honest gratitude to all of these people.

What I want to mention specially was the spirit among the co-workers at the DPMC of "being a team", which I experienced often and which can not be taken for granted.
It will definitively stay in my memory.